June 2020

Electrospun Nanofibrous Membrane Based Glucose Sensor with Integration of Potentiostat Circuit

Kavyashree Puttananjegowda
University of South Florida

Electrospun Nanofibrous Membrane Based Glucose Sensor

with Integration of Potentiostat Circuit

by

Kavyashree Puttananjegowda

A dissertation submitted in partial fulfillment
of the requirements for the degree of
Doctor of Philosophy
Department of Electrical Engineering
College of Engineering
University of South Florida

Co-Major Professor: Sylvia Thomas, Ph.D.
Co-Major Professor: Arash Takshi, Ph.D.
Nasir Ghani, Ph.D.
Norma Alcantar, Ph.D.
Shamima Afroz, Ph.D.

Date of Approval:
June 12, 2020

Keywords: CMOS, TIA, ENFM, SCTF, Silicon Carbide Nanoparticles, Conductive Polymer,
Low-power, Low-noise

Dedication

To my parents and my sister for their unconditional love, and motivation; to my teachers, mentors, and guides for their encouragement and support.

Acknowledgments

I am thankful to my research team members in AMBIR (Advanced Materials Bio and Integration Research) laboratory and the Bio-Organic Electronics laboratory, this dissertation wouldn't have be possible without their support and collaboration. It was my pleasure to have Dr. Sylvia W Thomas and Dr. Arash Takshi as my research advisors, who guided me to present this research to the world with the goal that mankind can benefit from my research work.

I would like to thank Dr. Nasir Ghani, Dr. Norma Alcantar, and Dr. Shamima Afroz for being a part of my dissertation committee and also investing their significant time to read the dissertation and agreeing to join my defense presentation. I am also thankful to the members of NREC who helped me to conduct the research effectively.

I am extremely lucky to be encircled by a lot of good, friendly, present and past lab-mates, who are consistently there to support me and I'm honestly grateful to all of them for their valuable suggestions, discussions and co-operation while conducting the experiments in the lab.

I want to thank my family members, they have been inspiring, supporting and persistent during my time of study. Specifically I am very much grateful to my dad who trusted and allowed me to pursue my dreams. I'm also thankful to my friends, they helped me particularly in my initial and difficult days in US. Finally I want to thank God who is always be with me and motivating to achieve my goals.

Table of Contents

List of Tables

List of Figures

Abstract

Although wearable and portable biomedical devices are the pillar of modern and smart societies, a large portion the device infrastructure is still under development, operates with poor monitoring and automation, and lacks sufficient communication among components. Moreover, demand for wearable bio-medical devices is expected to increase in the coming years. This situation presents a unique opportunity for electrical engineers to design novel strategies that allow point-of-care diagnostics to satisfy the increasing demand of wearable bio-medical devices. For example, in the medical field there is a rising diabetic population base, high demand for miniature and low-power diagnostic devices, and the need for rapid technological advancements driving the market growth. Among biosensors, glucose sensors have the largest market presence due to the increasing population of diabetic patients and the rising need for point-of-care diagnostics and detection. Glucose sensors are used to measure the glucose concentration in blood of a patient and are an important part of managing diabetes mellitus. However, to be truly beneficial, the glucose sensor must be able to function properly over a long time period. The critical issues of a glucose sensor are limits in the device longevity, power consumption, sensitivity and biocompatibility.

This continuous glucose monitoring system needs to be power efficient, compact, portable, sensitive, and have a linear response for targeted levels. This research focuses on three main components, each of which addresses a challenge central to the future 1) Fabrication and characterization of spin-coated-thin-film (SCTF) and electrospun nanofibrous membrane (ENFM) based electrochemical enzymatic glucose sensors; 2) Design and simulation of a proposed low-

power, low-noise transimpedance amplifier (TIA) and voltage control unit (VCU) for glucose sensing system; and 3) Integration of proposed chronoamperometric potentiostat (TIA and VCU) with glucose sensors to use it later for implantable bio-medical devices and In-vivo applications. Electrochemical enzymatic biosensors have become popular for point-of-care monitoring of glucose levels in the blood. The sensitivity, limit of detection and durability of these biosensors can be significantly enhanced by the utilization of nanostructures in sensor fabrication. More specifically, a conductive polymer (CP) PEDOT:PSS based electrospun-nanofibrous-membrane (ENFM) can increase sensitivity, provide larger surface-to-volume catalyst loading, and create platform for effective enzyme binding. ENFMs are easily fabricated, cost effective, and can be tailored to detect a wide range of biochemical reactions with the appropriate materials and functionalization.

This work represents an integrated glucose monitoring system with a complementary metal oxide semiconductor (CMOS) based low-power, low-noise chronoamperometric potentiostat and electrochemical enzymatic ENFM based glucose sensor. The sensing circuitry can detect electrochemical current ranging from nanoamps to microamps from the ENFM glucose sensor. The proposed chronoamperometric potentiostat was implemented in 180 nm CMOS process using multi-stage difference-differential telescopic cascode operational amplifier configuration. The configuration achieves low-noise, high gain, stability and a low-power. The integration of ENFM glucose sensor with chronoamperometric potentiostat provides the basis for future wearable and portable biosensors.

Chapter 1: Introduction

With the rapid growth of ultra-low power devices for biomedical, military, and space applications on the rise, there is a large market need in the field of sensor technology, valued at USD 15.6 billion in 2016 and expected to grow at a CAGR of 7.9% over the next forecast period ending in 2026 [1-2]. For example, in the medical field there is 1) a rising diabetic population base, 2) a high demand for miniature and low-power diagnostic devices, and 3) a need for rapid technological advancements driving this market growth. Among biosensors, glucose sensors have the largest market presence due to the increasing population of diabetic patients and the rising need for point-of-care diagnostics and detection [3-7].

Approximately 285 million people suffer from some form of diabetes. This number is expected to increase to 700 million by 2045, and an estimated 4 million deaths will be due to diabetes worldwide [8]. This global disease impacts a large number of people and can adversely effect the biological system. One way to investigate this issue is to monitor the disease and more specifically, the glucose level in a person's blood. The monitoring and sensing of glucose (sugar) levels in the blood is very important for people with diabetes. More specifically, diabetes is a disorder associated with an insufficiency of insulin secretion, and a large number of people around the world suffer from this disorder, which can result in damages to eyes, kidneys, nerves and even death. One of the most common methods to detect the diabetes is to monitor the levels of glucose in the blood stream using glucose sensors [9-10]. In addition, these glucose sensors require very highly sensitive and selective current readout circuitry because of its small size and low power

requirements. Particularly for diabetic patients, the large scale impact of these glucose sensors will be the preservation of thousands of lives due to timely treatment and monitoring of their health conditions. Efficient, cost effective, low power blood glucose sensing and monitoring systems will extend the life of diabetic patients globally.

1.1 Objectives

The main objectives of this research work is focused 1) the feasibility of electrospinning conductive polymers to produce enzymatic surfaces for glucose sensing applications, in comparison to a thin film of the same conductive polymer as the sensing surface and 2) the integration of ENFM based glucose sensor with a proposed CMOS based potentiostat circuit designed based on a multi-stage difference-differential telescopic cascode operational amplifier configuration. The simulation results confirm that the potentiostat circuit achieves competitive performance in terms of low-noise, high gain, increased linearity and stability with a significantly lower-power compared to the prior state-of-the-art potentiostats. The ENFM based glucose sensor provides enhanced sensitivity, better limit of detection (LOD), good stability, durability, and fast response time, of reliable results for glucose detection. The aim is to provide researchers and industry with more information regarding nanostructured conductive polymers in the fabrication of glucose sensors and it's integration with the current readout circuit. Due to the low cost fabrication method and the enhanced durability of an ENFM based glucose sensor response and a proposed potentiostat circuit, this work is practical and novel solution for implantable and continuous glucose monitoring systems, hence becoming a potential candidate for future biosensing applications.

1.2 Organization

This dissertation work is organized by chapters. Chapter 2 introduces the fabrication process, morphological and electrochemical characterization of spin-coated-thin-film (SCTF) and an electrospun-nanofibrous-membrane (ENFM) based glucose sensor. It also presents the literature review on various electrospun nanofibrous membrane based glucose sensors using composites of carbon nanotubes, carbon nanofibers, conductive nanoparticles and conductive polymers.

Chapter 3 introduces the fabrication process of a conductive polymer (CP) PEDOT:PSS based electrospun–nanofibrous-membrane (ENFM) embedded with silicon carbide nanoparticles (SiCNPs) and the comparative analysis, morphological and electrochemical characterization of a SiCNPs-ENFM and SiCNPs-SCTF based glucose sensors.

In Chapter 4 the literature review on various transimpedance amplifier (TIA) circuit configurations and a novel design of a low-noise, low-power TIA is presented for a continuous blood glucose monitoring system for wearable devices. The proposed multi-stage cascode common source (MSCCS) TIA circuit is designed and implemented in a 180 nm CMOS technology.

Chapter 5 represents the literature review on the various architectures of potentiostat circuits for glucose monitoring systems. The proposed chronoamperometric potentiostat was implemented and simulated using a multi-stage difference-differential telescopic cascode operational amplifier configuration. Finally, Chapter 6 concludes the dissertation and also suggests the potential future work.

Chapter 2: Electrospun Nanofibrous Membrane Based Glucose Sensor

2.1   Introduction

Biosensing has capitalized on the excellent characteristics and properties of nanostructures for detecting glucose levels in diabetic patients. In glucose sensing systems, the fabrication of a suitable matrix for immobilizing glucose oxidase (GO_x) has become more interesting for the application of nanofibers in enzymatic electrochemical biosensors [11-13]. These nanofiber based electrochemical biosensors are superior in manufacturability and performance due to low cost, diversity of materials, ease of miniaturization, response time, durability, and structure versatility. This chapter highlights the latest material integration of various nanofibrous composite membranes of carbon nanotubes, carbon nanofibers, conductive nanoparticles and conductive polymers that [1]provide large matrix-like, porous surfaces to enhance the immobilization of enzymes, for the fabrication of glucose biosensors [14-20]. This chapter presents a comparative electrochemical and morphological analysis of spin-coated thin film (SCTF) and electrospun-nanofibrous-membrane (ENFM) based glucose sensor using a conductive polymer. The fabrication of sensing electrodes was completed by the immobilization of glucose oxidase (GO_x) enzyme onto the conductive

K. Puttananjegowda, A. Takshi, S. Thomas, "Electrospun Nanofibrous Membrane based Electrochemical Glucose Sensor", IEEE Sensors Lett., vol. 4, no.2, pp. 1-4, 2020.
K. Puttananjegowda, A. Takshi, S. Thomas, "Electrospun Nanofibrous Structures for Electrochemical Enzymatic Glucose Biosensing: A Perspective", J. Electrochem. Soc., vol. 167, no. 3, pp. 1-6, 2020.
S. Thomas, R. Khan, K. Puttananjegowda, W. Serrano-Garcia, "Conductive polymers andmetal oxide polymericcomposites fornanostructures andnanodevices", Advances in Nanostructured Materials and Nanopatterning Technologies, pp. 243-271, 2020.

polymer, poly(3,4-ethylenedioxythiophene):poly(styrene sulfonate) (PEDOT:PSS), electrospun composite membrane and PEDOT: PSS thin film, which was spin-coated onto gold electrode. The ENFM and SCTF based glucose sensors were characterized for morphology by using transmission electron microscopy (TEM), scanning electron microscopy (SEM), atomic force microscopy (AFM) and for electrochemical activity by using chronoamperometry (CA), electrochemical impedance spectroscopy (EIS) and cyclic voltammetry (CV) methods. The electrochemical analysis results demonstrated that the ENFM based glucose sensor provides reliable results of enhanced sensitivity, good stability, reasonable repeatability, durability, and quick response time for glucose detection compared to SCTF based sensing electrodes.

The remainder of chapter 2 is arranged as follows: A review of the proposed ENFM based glucose sensor and literature review of nanofibrous sensors is provided in Section 2.2; Sensor fabrication procedures are discussed in Section 2.3; Sensor characterization is presented in Section 2.4; Experimental results were explained in Section 2.5 and performance comparison was discussed in Section 2.6.

2.2   Literature Review

Many people around the world suffer from diabetes, which can result in damages to eyes, kidneys, nerves, gangrene, subsequent amputation and even death [21]. Approximately 285 million people suffer from diabetes, and this number is expected to increase to 430 million by 2030 [22-23]. The monitoring and sensing of glucose (sugar) levels in the blood is very important for people with diabetes [24]. The recent development of low-cost, highly sensitive, and highly stable electrochemical glucose biosensors has been given much attention due to promising results for point-of-care diagnoses and accurate monitoring of blood glucose levels in diabetic patients [25-27].

One important aspect in the fabrication of glucose sensors is the capability of keeping the glucose oxidase (GO_x) enzyme on the surface of the electrode to electrochemically detect the active species [28-30]. This has been accomplished by the use of suitable nanostructures for the immobilization of the enzyme. Among several configurations of nanostructures being used for glucose bio-sensing, electrospun nanofibrous structures are the most effective in achieving higher sensitivity, minimum limit of detection (LOD), better binding of enzyme with electrode, favorable porosity and thermal stability.
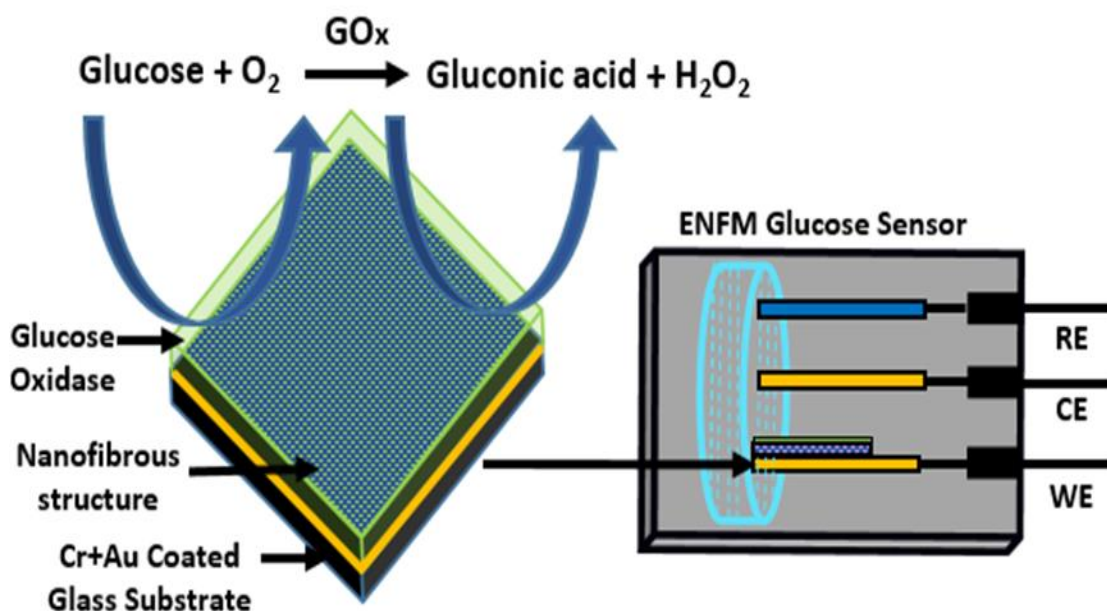
Figure 2.1 Representation of the nanofibrous structure based glucose sensor.

A nanofibrous structure-based glucose sensor is represented in Figure 2.1. Nanofibrous structures offer configuration and integration advantages due to structural dimensions on the order of nanometers, small size, high surface area, porosity, enhanced optical and electrical properties, more efficient enzyme to electrode electron-transfer, and the capability of enhancing additional catalytic reactions; all, of which, demonstrate significant benefits compared to macroscale materials [31-33]. Electrospun nanofibrous membranes are tunable in terms of dimension; cost

effective and safer in terms of fabrication; flexible in terms of orientation, scaling and bending; greener in terms of material processing; and versatile in terms of high surface-to-volume ratio [31,32,34-50]. It is advantageous to fabricate bead free nanofibers, which has less variability in the fiber morphology and favor reproducibility of the sensing surface [51]. Various nanofibrous composite structures, comprised of carbon nanotubes, carbon nanofibers, conductive nanoparticles, and conductive polymers, are suitable for the fabrication of glucose sensors due to the direct charge transfer process between GO_x and the surface of the electrode material, which effectively immobilizes the enzymes and promotes the electrochemical response [34-37]. Emphasis is placed on these composite structures due to the material conductivity, which in turn increases the sensitivity of the sensor. Researchers have begun to actively exploit these properties to improve the lifetime, efficiency, size, accuracy and usability of sensors for treating diabetes. Therefore, nanofibrous based glucose sensors are finally being considered for the initial stages of commercial and clinical implementation, which is predicted to offer better treatment in the future for diabetic patients.

Since the first reported GO_x enzymatic electrode in 1967 [38], electrochemical glucose sensor structures have evolved from thin film to 2D and 3D structures. By embedding 2D and 3D structures into electrospun nanofiber composites and using conductive polymers, researchers have been able to offer customized loading of enzymes, better binding of GO_x with the electrode and excellent ability to immobilize enzymes. Electrospun nanofibrous structures have a critical impact on glucose sensor reliability, surface sensitivity and real-time responsiveness for detecting changes in glucose levels [34, 39-42]. Enzyme based detection requires a stable and highly sensitive sensing electrode matrix. This matrix, fabricated by electrospinning, can have a dispersion or attachment of functional nanostructures in the polymeric solution and offers efficient binding of

functional particles. The nanofibrous matrix can also encapsulate or protect the enzymes from denaturation when exposed to changes in pH or temperature, leading to enhancements in sensing performance and long-term stability (addressing issues plaguing enzymatic sensors). In addition, nanofibrous membranes allow for increased stabilization of the enzymatic activity and limit leaching of enzyme molecules in the electrolyte solution. A favorable surface for effective enzyme loading is created, and direct electron-transfer between electrode and enzyme is facilitated using nanofibrous composites of carbon nanotubes, carbon nanofibers, conductive nanoparticles and conductive polymers.

2.2.1 Carbon Nanotube (CNT) Based Electrospun Nanofibers

Carbon nanotubes (multi and single-walled) have been discovered to promote catalytic behavior, electrical conductance and reduce immobilization matrix fouling [46, 43]. Multi-walled carbon nanotubes (MWCNTs) mixed with poly(acrylonitrile-co-acrylic acid) (PANCAA) based nanofibrous membranes (NFMs), were electrospun onto platinum (Pt) electrodes, which enhances the sensing activity and the lifetime of glucose sensor [44]. Nylon 6,6 nanofibers were electrospun and MWCNTs were incorporated and encapsulated with conducting polymer, (poly-4-(4,7-di(thiophen-2-yl)-1H-benzo[d]imidazol-2-yl)benzaldehyde) (PBIBA), to form a nanofibrous matrix. These nylon 6,6 nanofibers are bead free (Figure 2.2 (a)), which helps with the formation of a homogenous distribution of a nanofibrous membrane on the electrode surface and promotes good stability. It is highlighted that with an increase in CNTs, there is an increase in electron transfer and an increase in morphological porosity due to CNTs. The matrix has a high ratio of surface to volume coating of PBIBA, which enhanced the covalent loading of the GO_x (Figure 2.2 (b)) to the nanofibrous surface for effective immobilization [52]. Nitrogen-doped carbon nanotubes (NCNTs) were also presented as ideal carbon nanomaterials for immobilizing and

maintaining better electrochemical enzymatic activity [45]. For more timely point-of-care diagnosis of glucose levels, it will be encouraging for researchers to investigate nanofibers filled with single-walled carbon nanotubes (SWCNTs) to fabricate glucose biosensors. As a comparative, SWCNTs have been shown to have lower charge transfer resistance than MWCNTs, yielding a higher electron-transfer rate at the electrode-enzyme interface and better glucose detection [46].

2.2.2 Carbon Nanofiber (CNF) Based Electrospun Nanofibers

In considering CNFs, nitrogen-doped carbon nanofibers (NCNFs) were prepared by electrospinning polyacrylonitrile (PAN) nanofibers and conducting carbonization, as shown in Figure 2.2 (c) [47]. Incorporating nitrogen increases the electron-transfer rate and enhances oxygen reduction for a highly stable and quickly responsive glucose sensor. Due to the unique free-standing NCNF structure, the glucose sensor demonstrated enhanced stability and high sensitivity [47]. Highly dispersive nickel (Ni)/ cobaltous oxide (CoO) carbon nanofibers were fabricated by electrospinning and exhibited excellent sensitivity and catalytic activity for determining levels of glucose. The amount of surfactant had a significant impact on the material morphology, which further affected the current response sensitivity as glucose levels changed [46]. Another glucose sensor was fabricated based on hybrid nanostructures of palladium-helical carbon nanofibers (Pd-HCNFs), and immobilization of GO_x with nafion was conducted on glassy carbon electrodes (GCE). The resulting biosensor exhibited good sensitivity and responded to a wide range of changes in glucose levels [48]. Prussian blue (PB) nanofeatures were grown on carboxylic group-functionalized carbon nanofibers (FCNFs) to form low cost nanocomposites with good stability and selectivity. Results supported PB–FCNF biosensors being effectively applied for glucose measurements [49]. Therefore, the sensing performance and enzymatic glucose response of

9

electrospun carbon nanofibers will continue to improve as researchers investigate nanofiber-hybrids (incorporation of nanostructures, particularly nanoparticles).

2.2.3 Conductive Nanoparticles (CNP) Based Electrospun Nanofibers

Conductive nanoparticles have sensitive electrochemical properties based on their size, dispersion, atomic configuration, and level of conductivity. For high electrochemical activity to occur in functional materials, there needs to be a high dispersion of nanoparticles in the material, but there is a propensity for nanoparticles to aggregate, lowering the catalytic activity and reuse lifetime [34,37,50-54]. Therefore, there is a trade-off with the amount of nanoparticles that can be dispersed, in-situ or ex-situ, to the nanofibers via covalent bonding, adsorption, or encapsulation. A polymeric nanofiber matrix with nanoparticles tends to offer a stable support structure for the interface of the enzyme on a solid surface for immobilization. In recent fabrications of nanofibrous composite sensors, the nanoparticle of choice has been gold nanoparticles, where gold is one of the highly conductive materials at 4.10×10^7 S/m (20°C). A nanofibrous surface of a poly(vinyl alcohol) (PVA) and graphene oxide (GO_x) electrospun composite was coated with gold nanoparticles (AuNPs) and then exposed to a copper (Cu) nanoflower GO_x and horseradish per-oxidase [44]. The electrochemical analysis of the PVA/GO-AuNP-Cu-nanoflower nanofibrous glucose sensor was enhanced by the addition of AuNPs and Cu nanoflowers, which increased the overall conductivity of the sensing electrode. Poly(ethyleneimine) (PEI)/PVA/GO_x were electrospun on gold electrodes, and the surface of the nanofibers were post treated with AuNPs. The adhesion of gold electrodes with the nanofibrous membrane and the nanofiber water stability was improved by modifying the surface of the glucose sensor [54]. In another study, gold nanoparticles, poly(acrylonitrile) (PAN) electrospun nanofibers, and CNTs were used to fabricate a glucose sensor [47]. The PAN nanofibers were

decorated with gold nanoparticles, and carboxylated CNTs were further coated onto the nanofibers by electrophoretic deposition, which helped to facilitate direct electron transfer and the GO_x immobilization with this nanofibrous electrode surface [47]. Hence, the conductive properties of the glucose sensor electrode were significantly enhanced by decorating the nanofibers with gold nanoparticles and CNTs and thus the sensitivity of the sensor. The glucose biosensors exhibited good operational stability and repeatability with low LOD. It should also be noted that a dispersion of nanoparticles into nanofibers may have a mass transfer rate limit and are less likely to be recyclable (impacting sustainability), and the nanoparticles may tend to aggregate causing the sensor to lose detection functionality. Therefore, further exploration of conductive nanoparticles, as another alternative component of nanofibrous glucose sensing, is needed.

| (a) | (b) | (c) |
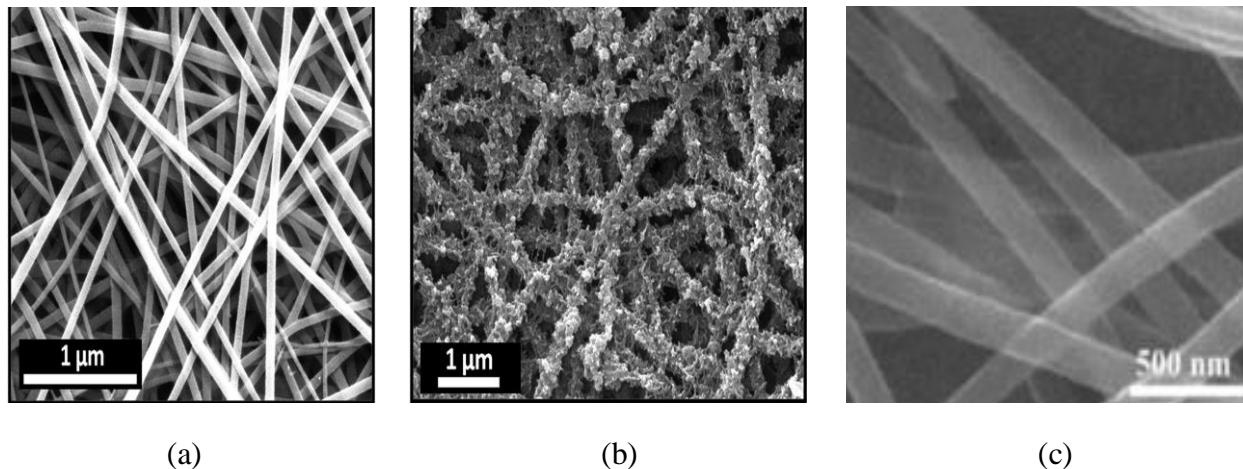
Figure 2.2 (a) Nylon 6,6/MWCNT nanofibers SEM image [52] (b) SEM image of PBIBA coated Nylon 6,6/MWCNTs nanofibers with GO_x [52] (c) NCNF SEM image [47]

2.2.4   Conductive Polymers (CP) Based Electrospun Nanofibers

In this section, we focus on sensing applications of conductive polymers (CP), where CPs impact reaction time, affectability, sensitivity, and selectivity, i.e. sensor innovation parameters. For biosensing, sufficient response times tend to be on the order of seconds for human reaction, and when investigating sensor, it is advantageous to focus on response times. Detecting parameters

of polymer-based sensors can include redox responses, chain entanglement changes, molecular adsorption and desorption, volume and weight changes, or charge mobility/screening. Leading CPs have intrinsic characteristics influencing high affectability and selectivity via qualities of low-temperature amalgamation and preparation, compound versatility, large surface area production, adaptability, and cost viability. Accordingly, the use of conducting polymers in sensor application has been aggressive, and these materials have subsequently been viewed as standout amongst polymers.

Different conducting polymers, including polyaniline (PANI), poly(3,4-ethylenedioxythiophene):poly(styrenesulfonate) (PEDOT:PSS), and polypyrrole (PPy) have been widely researched for biosensing. PPy and PANI nanowires provided connectivity of two terminals on a silicon wafer through an electrolyte channel when an electric potential was connected. Analyzing the electrochemical reaction of the nanowires can help gauge a biosensor response depending on these leading polymer nanomaterials. The parameters of the nanowires were dictated by the width of the channel and the separation between terminals. The embedded receptors into the polymer during electropolymerization, and an avidin protein was then entangled in the PPy nanowire, crafting the sensing of a biotin-conjugated DNA [51-55].

Conducting polymers continue to attract much attention in the development of amperometric glucose biosensors, because of the physical entrapment of glucose oxidase, GO_x, within their porous structure. Particularly, PEDOT: PSS has been studied widely, due to its higher enzyme immobilization capability, good electrical conductivity, better processability, excellent electrochemical stability, reliability, and biocompatibility [54-55].

One vital aspect in the development of amperometric biosensors is the capability of the enzymatic surface on the electrode to electrochemically detect the active species. Researchers have

accomplished this by using suitable substrates for the immobilization of the enzyme. This immobilization can be conducted in different ways, such as in the utilization of carbon–organic polymer composites, conductive salts, cross-linked polymers, conductive polymers, sol-gels, carbon pastes, or carbon nanotubes [34-37].

The present work focuses on an electrospun conducting polymer PEDOT: PSS membrane based sensor electrode, which was fabricated for better binding of the bioenzyme, glucose oxidase. The electrochemical behavior of the electrode was studied for the detection of glucose and the results show the potential advantages of nanofibrous membrane based electrodes for biosensors and measurement of glucose concentration with better sensitivity, LOD, response time, durability, selectivity and repeatability.

2.3   ENFM and SCTF Glucose Sensor Fabrication

2.3.1   Materials and Apparatus Required for Fabrication of Glucose Sensor

A PEDOT:PSS with high conductivity grade from Sigma Aldrich, polyvinylidene fluoride (PVDF) with molecular weight of 534,000, and tetrahydrofuran (THF) solution was used for fabricating the electrospun-nanofibrous-membrane (ENFM). The glucose oxidase (GO_x) is a solid from Aspergillus Niger Type X-S, lyophilized powder (with no oxygen) of 100,000 - 250,000 units/g and the -D-(+)-Glucose (anhydrous) is from Sigma Aldrich used directly without purification. The potassium ferricyanide with a molecular weight of 329.26 g/mol was also from Sigma Aldrich. Deionized water was used for preparing the electrolyte and for cleaning the electrodes. The electrolyte aqueous mixture of a 1:1 ratio with solutions of 5 mM glucose and 5 mM potassium ferricyanide were prepared afresh at the time of the experiments. For measuring the response of the electrode to the glucose concentration, the concentration was increased by adding glucose to the electrolyte solution. Sputtered chromium (100 nm) and gold (100 nm) on

glass substrates of a 0.35 cm x 0.5 cm area were used for making working and counter electrodes; reference electrode as silver/silver chloride (Ag/AgCl) was used in this electrochemical experiments. Before conducting each of the experiments, the counter electrode plate was cleaned with acetone and washed with deionized water. The electrochemical measurements was conducted on VersaSTAT-4 by Princeton Applied Research (PAR), an electrochemical analyzer on a three-electrode system set up. PEDOT: PSS SCTF and ENFM based electrodes were used as working electrodes. All the electro-chemical measurements were operated in ambient conditions. Scanning electron microscope (SEM, Hitachi S800) with 25 kV acceleration voltage, 1500 magnification and 10 μm scale bar; transmission electron microscope (TEM, Tecnai TF20) with field emission gun, 200 kV acceleration voltage, 43000 magnification and 50 nm scale bar; and atomic force microscope (AFM, Veeco 3100) with tapping mode and 3 μm scale bar were used to characterize the morphology of ENFM and SCTF.

2.3.2   Fabrication Process of ENFM and SCTF Sensing Electrodes

The fabrication of an electrospun conducting polymer of PEDOT:PSS nanofiber based glucose sensor involves the following process steps, which is represented in Figure. 2.3i, As shown in Figure. 2.3i (a), first, a glass substrate was cleaned with acetone, methanol followed by plasma cleaning; then layers of Cr and Au were sputtered on the glass substrate as indicated in Figure. 2.3i (b) and Figure. 2.3i (c). The electrospinning solution was prepared by dissolving 1.18 g of PVDF and 0.22 g of PEDOT:PSS in 2 mL of THF and stirring for 1 hr at 60 $^{\circ}$C. The prepared solution was electrospun with the applied voltage of 18 kV, a flow rate of 10 μLmin^{-1} and the distance from the collector plate to the tip was 29 cm, then the fibers start spinning on to the Au coated glass substrate with the membrane thickness ~500 nm, as shown in Figure 2.3ii (g) which represents the custom designed electrospinning setup. After the fibers are spun on the gold surface,

then the ENFM electrode was dried at 60 °C for 4 hrs as shown in Figure 2.3i (d); finally, a GO_x enzyme solution of ~1.4 mg was drop casted onto the nanofibrous layer as in Figure 2.3i (e), then for immobilization of a enzyme onto the nanofibrous membrane, the ENFM electrodes were kept at 4 °C for 24 hrs. A thin film of PEDOT: PSS was fabricated by spin-coating 0.0482 g of PEDOT: PSS at the speed of 45 RPM for 2 mins on the 0.35 cm x 0.5 cm gold electrode; then dried at 60 °C for 4 hrs and then the GO_x enzyme solution of ~1.4 mg was drop casted over the spin-coated thin film, and the bare gold electrodes. For enzyme immobilization to occur, the electrodes were kept at 4 °C for 24 hrs. Figure 2.3i (f) shows the photograph of ENFM glucose sensor electrode.
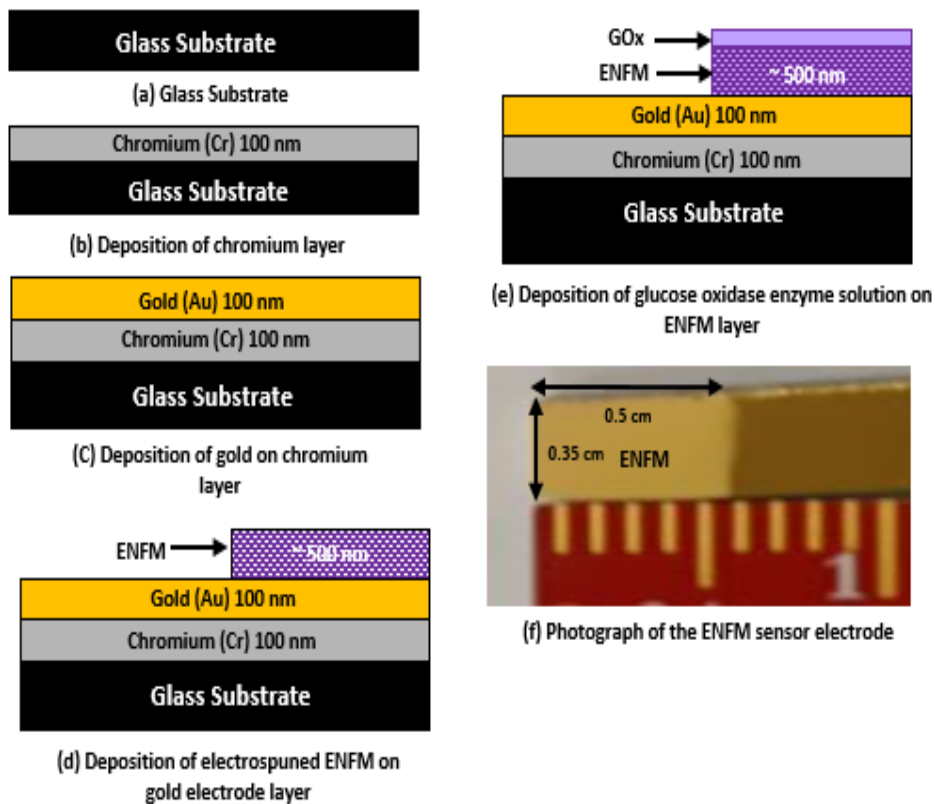
Figure 2.3i (a - e) Fabrication process of ENFM based glucose sensing electrode and (f) Photograph of the ENFM sensor electrode.
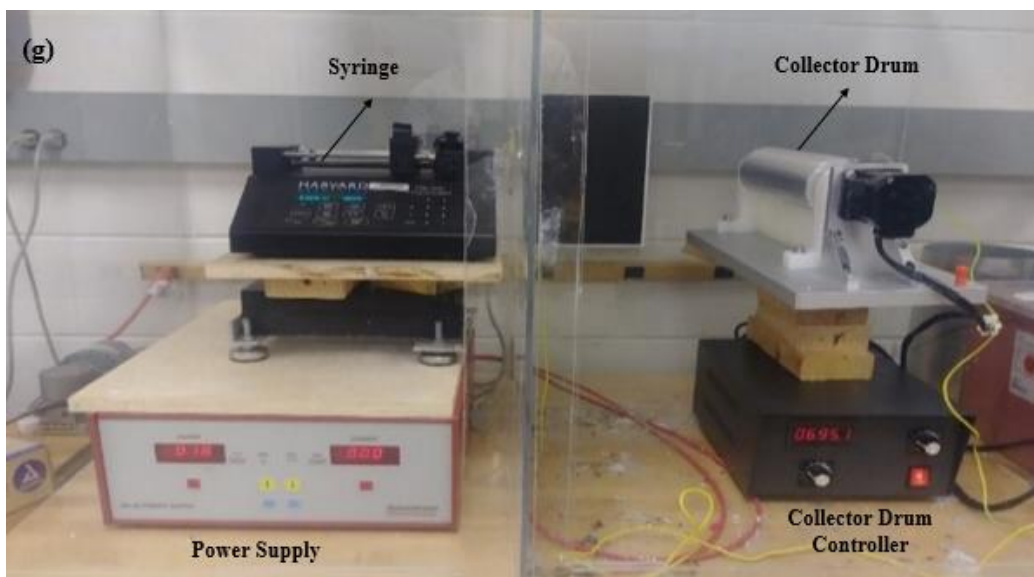
Figure 2.3ii (g) Custom designed electrospinning setup.

2.4   ENFM and SCTF Glucose Sensor Characterization

2.4.1   Morphological Characterization

The SEM of PEDOT: PSS SCTF without GO_x and with GO_x are shown in Figure 2.4 (a) and (b). The SEM, TEM, and AFM (tapping mode) pictures of the fabricated polymer based ENFM are shown in Figure 2.5 (a-c). The morphology and randomly oriented fibrous structure with a diameter in the range of 50 - 100 nm is shown in these images. Figure 2.5 (d-f) show surface coverage of closely packed mesh like structures, facilitating higher GO_x populous on the nanofibrous matrix and capitalizing on the larger surface area, which helps in binding the GO_x enzyme within the fibrous membrane of the electrode; whereas in the SCTF electrode, the non-uniform coverage of enzyme molecules leaches out very fast when placed in an electrolyte solution which affects the sensitivity, stability, repeatability and durability of the sensing electrode. Thus SEM, TEM and AFM studies reveal the discriminate surface morphology between Au/PEDOT:PSS (nanofibers) and Au/PEDOT:PSS (nanofibers)/GO_x membranes (Figure 2.5) with the spin-coated Au/PEDOT: PSS (film) and Au/PEDOT: PSS (film)/GO_x (Figure 2.4).
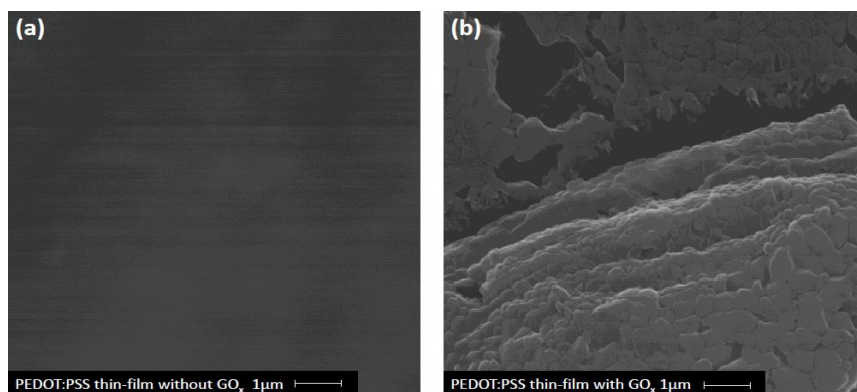
Figure 2.4 (a) SEM images of PEDOT:PSS SCTF without GO_x (b) SEM images of PEDOT:PSS SCTF with GO_x
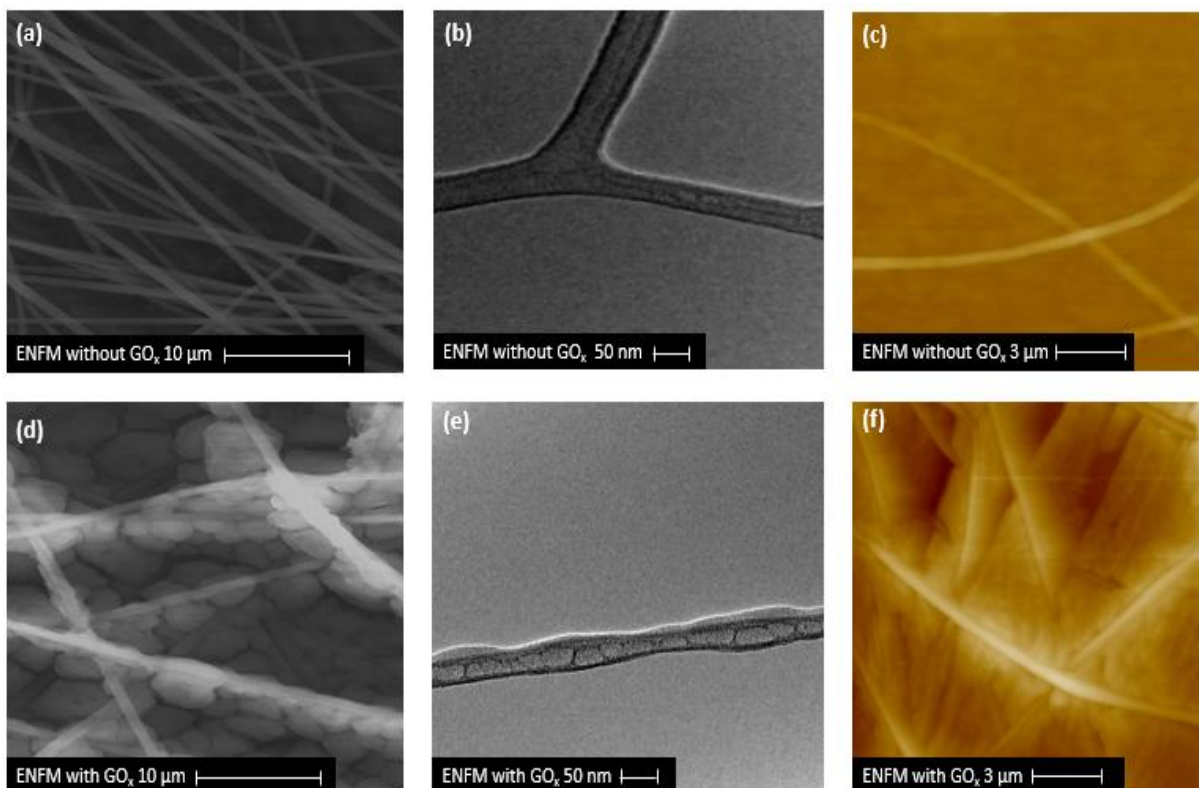
Figure 2.5 (a) SEM (b) TEM and (c) AFM images of electrospun PEDOT: PSS nanofibers without GO_x (d) SEM (e) TEM and (f) AFM images of electrospun PEDOT: PSS nanofibers with GO_x.

2.4.2   Electrochemical Characterization

The electrochemical measurements was conducted with the three-electrode test setup as shown in Figure 2.6. Au/PEDOT: PSS (nanofibers)/GO_x and Au/PEDOT: PSS (film)/GO_x electrodes were used as the working electrodes (WE). Ag/AgCl was used as a reference electrode

(RE) and a bare gold electrode was used as counter electrode (CE). The electrocatalytic activity of working electrodes was evaluated using cyclic voltammetry (CV) in 5 mM of potassium ferricyanide solution and the voltage was scanned between -0.9 V to +0.9 V (vs. Ref) at various scan rates. Chronoamperometric (CA) measurements of samples were carried out at an applied potential of +0.5 V for various glucose concentrations and the current response was recorded for 60 seconds. The electrochemical impedance spectroscopy (EIS) measurements were performed for sensing electrodes, analysed by Nyquist and Bode plots for different glucose concentrations with a frequency range of 0.1 Hz to 10 kHz and an amplitude of 10 mV. Subsequently, the current and the impedance response was recorded for each incremental addition of glucose.
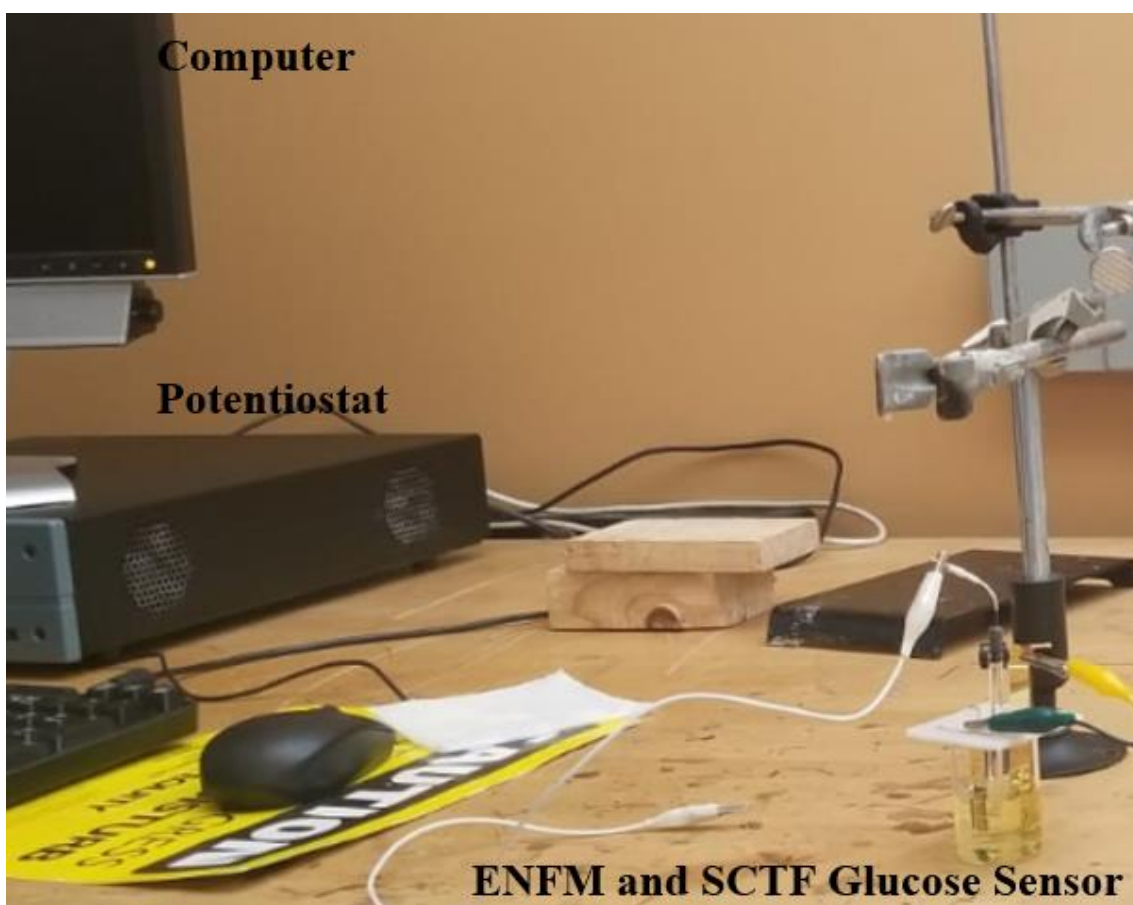
Figure 2.6   Electrochemical test setup for ENFM and SCTF based glucose sensors.

2.5 Experimental Results

2.5.1 Comparative Electrochemical Analysis of Gold, SCTF and ENFM Based Glucose Sensing Electrodes Through CV, CA and EIS

The comparative performance analysis of bare gold (Au/GO$_x$), SCTF Au/PEDOT: PSS (film)/GO$_x$ and ENFM Au/PEDOT: PSS (nanofibers)/GO$_x$ based glucose sensing electrodes were studied through various electrochemical analysis such as CV, CA and EIS. The CV of the bare gold, SCTF and ENFM electrodes at 5 mM glucose concentration with a potential range of +0.9 V to -0.9 V at a scan rate of 50 mVs^{-1} are depicted in Figure 2.7i (a). The CV of ENFM based electrode shows the oxidation peak of +0.92 mA at +0.49 V and reduction peak of -0.995 mA at -0.35 V, whereas the SCTF and the gold electrodes exhibits very less oxidation peaks of 0.589 mA and 0.029 mA at +0.46 V and +0.388 V respectively and the reduction peaks of -0.64 mA and -0.043 mA at -0.38 V and -0.29 V respectively.

Figure 2.7ii (b) shows the CA graphs of the gold, SCTF and ENFM electrodes at 5 mM glucose concentration with a potential 0.5 V and an elapsed time of 60 sec. The transient current in the ENFM electrode was found to be significantly higher than the other two electrodes. However, for sensing applications, the steady-state current value is more important. The ENFM based electrode exhibits a 43 nA at 60 sec, whereas the SCTF and bare gold based electrodes show a much lower current response of 24 nA and 9.8 nA at 60 sec respectively compared to ENFM based electrode. The EIS is performed for these bare gold (Au/GO$_x$), SCTF Au/PEDOT: PSS (film)/GO$_x$ and ENFM Au/PEDOT: PSS (nanofibers)/GO$_x$ electrodes at 5 mM glucose concentration with a frequency range of 0.1 Hz to 10 kHz and an amplitude of 10 mV is represented by bode plots which is shown in Figure 2.7ii (c). The gold and SCTF electrodes exhibit higher impedance values of 1653 Ω and 1007 Ω at 0.1 Hz. The ENFM based electrode exhibits the lower

impedance of 701 Ω at 0.1 Hz. This is particularly important because despite the nanofiber coatings, the low frequency impedance of the ENFM electrode is lower than the gold electrode. The various electrochemical results from CV, CA, and EIS indicate that the ENFM based electrode shows better performance for glucose sensing. Therefore, we focused on studying the ENFM electrode.
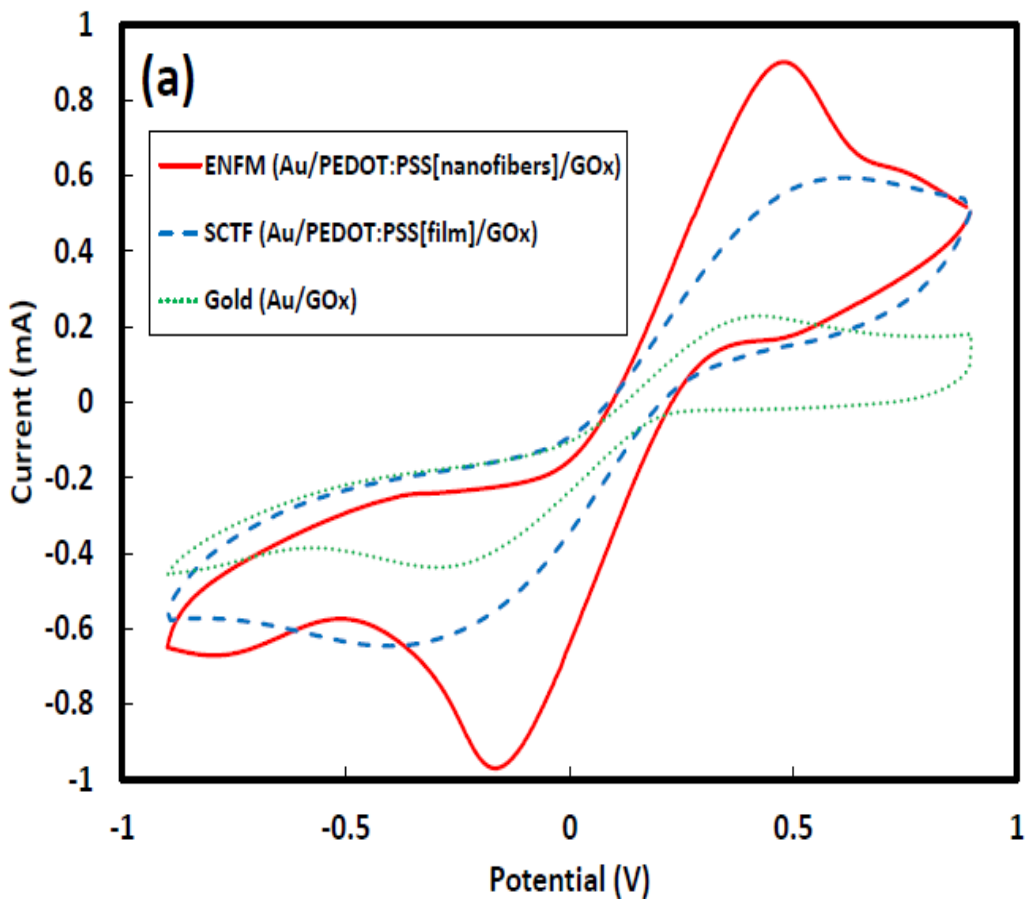
Figure. 2.7i (a) CV of gold (Au/GOx), SCTF Au/PEDOT: PSS (film)/GO_x
and ENFM Au/PEDOT:PSS(nanofibers)/GO_x electrodes.
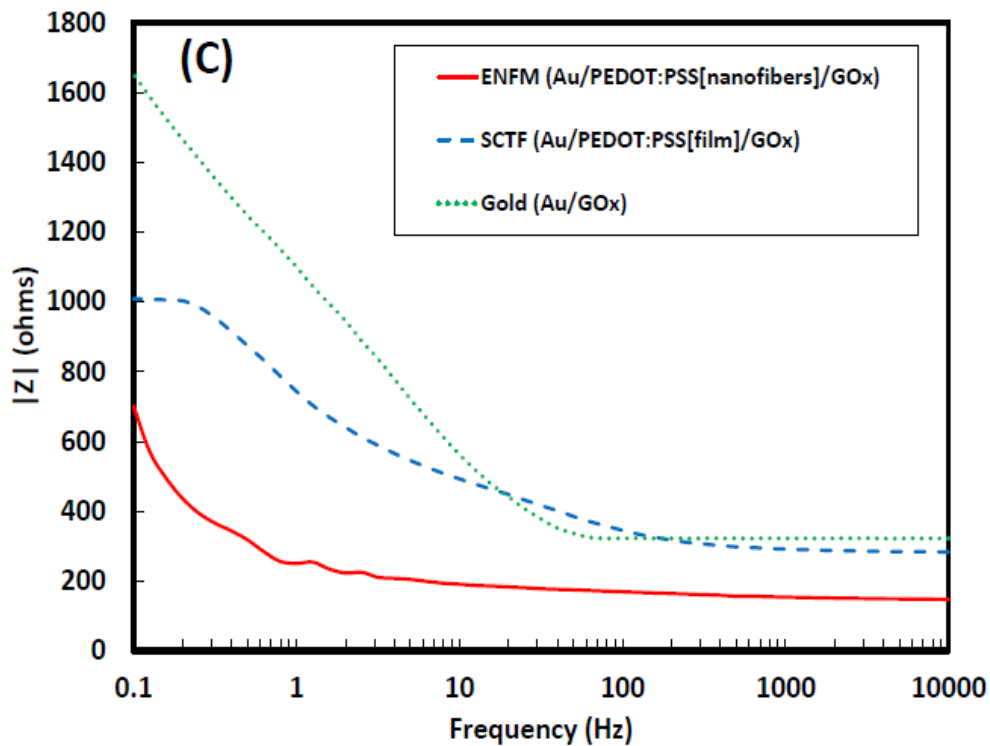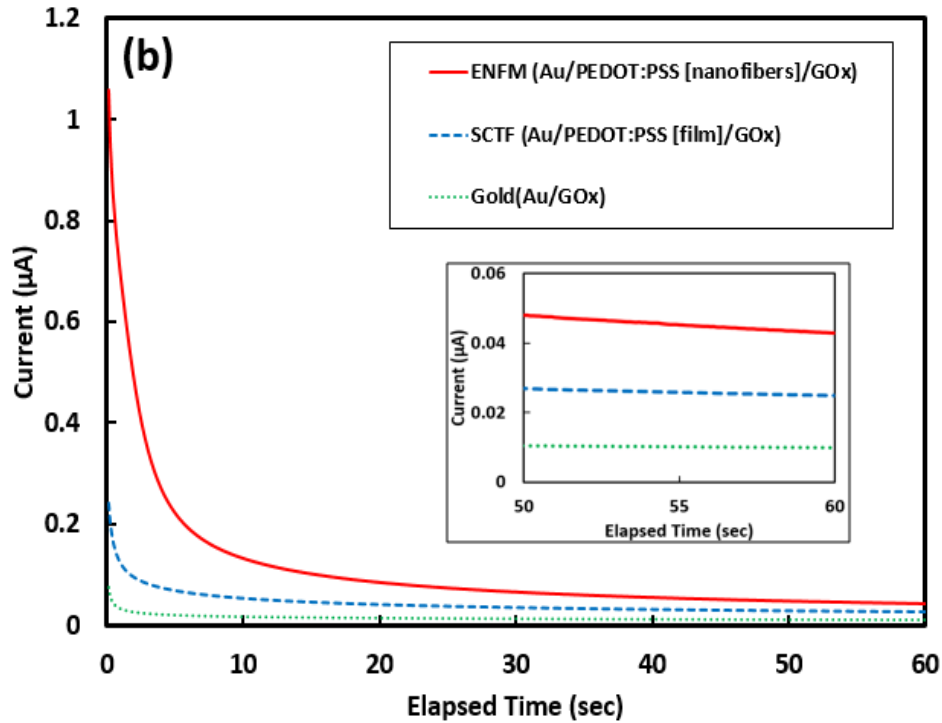
Figure. 2.7ii (b) CA graphs of gold (Au/GO$_x$), SCTF Au/PEDOT: PSS (film)/GO$_x$ and ENFM Au/PEDOT: PSS (nanofibers)/GO$_x$ electrodes. (c) Bode plots of gold (Au/GO$_x$), SCTF Au/PEDOT: PSS (film)/GO$_x$ and ENFM Au/PEDOT: PSS (nanofibers)/GO$_x$ electrodes.

2.5.2   CV of ENFM Based Glucose Sensor with Different Scan Rates

The CV was used to characterize the electrochemical behavior of Au/PEDOT:PSS (nanofibers)/GO$_x$ electrode for a solution of 5 mM of glucose in 5 mM of potassium ferricyanide at different scan rates from 25 mVs^{-1} to 200 mVs^{-1}, as the results are shown in Figure 2.8(a). As expected the results show higher redox peak currents at higher scan rates and the potential corresponding to the redox peaks were shifted away as the scan rate was changed toward 200 mVs^{-1}. The CV was deconvoluted based on two Gaussian peaks for both oxidation and reduction peaks. Figure 2.8(b) demonstrates the current variation at various scan rates where a unity ratio (I_{pa}/I_{pc}= 1.0) of cathodic peak current (I_{pc}) and anodic peak current (I_{pa}) was achieved for all scan rates (25 mV s^{-1} to 200 mVs^{-1}). With the increasing scan rates both peak currents (I_{pa} and I_{pc}) increased. The peak form of the CV is similar to the electrochemical reversible Nernst's reaction. There was direct proportionality between the peak currents and the square root of the scan rates, and an electron transfer process, occurring on the surface, was indicated by a linear trend line of the glucose redox conversion. The following linear regression equations easily express the dependency of the working electrode peak current on the square root of the scan rate:

$I_{pa} = 2.5964x + 0.363$, R² = 0.9859 .... (2.1)

$I_{pc} = -2.3078x - 0.4373$, R² = 0.9896 .... (2.2)

There was no critical shifts observed at the reduction and oxidation peaks between the range of 200 mV to 500 mV. Thus, affirming that the Au/PEDOT: PSS (nanofibers)/GO$_x$ electrode shows stability during the sensing of glucose.
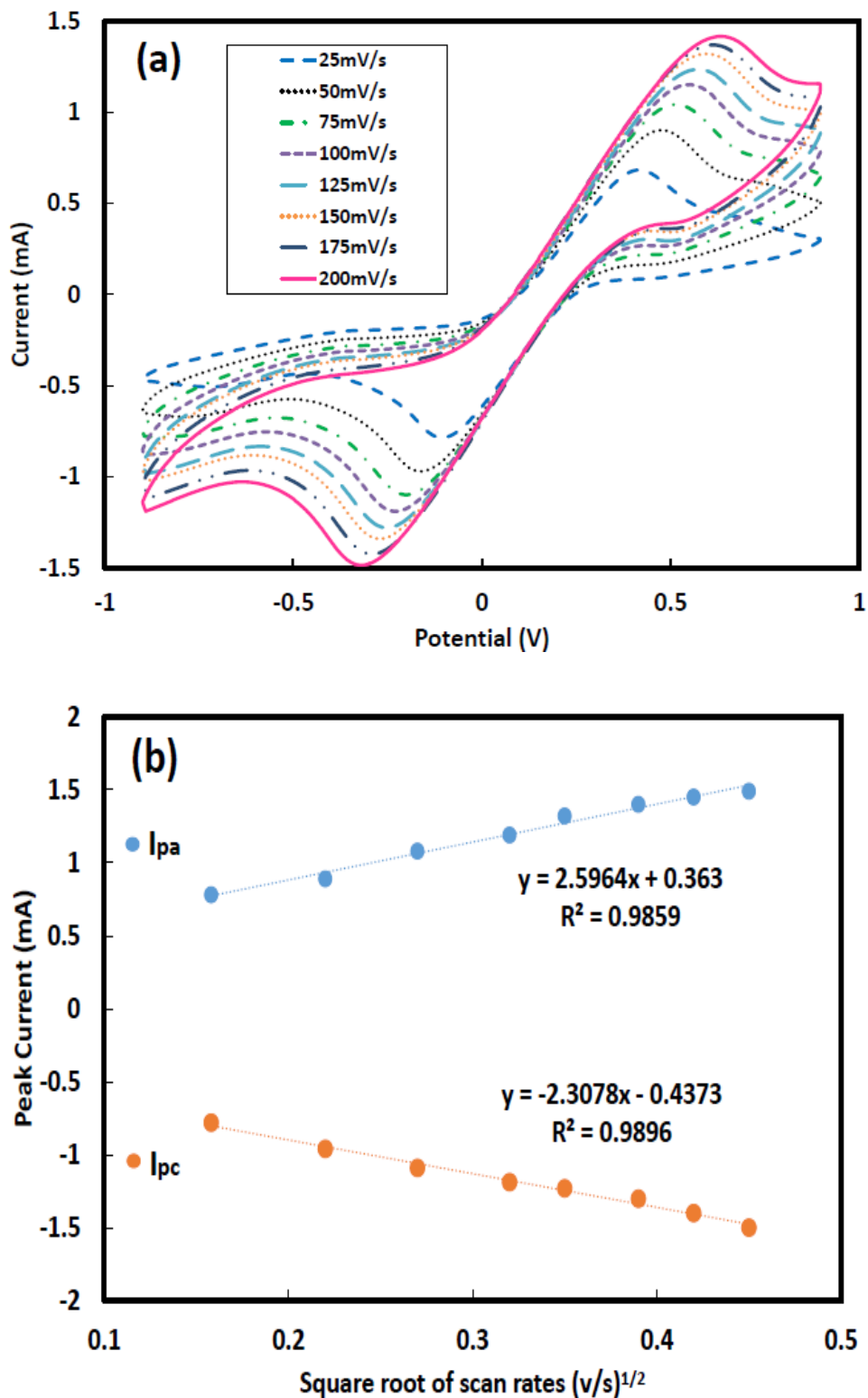
Figure. 2.8 (a) CV of Au/PEDOT:PSS (nanofibers)/GO_x electrode at different scan rates from 25 mVs^{-1} to 200 mVs^{-1}. (b) Calibrated plot of peak current versus the scan rates for Au/PEDOT:PSS (nanofibers)/GO_x electrode.

2.5.3 EIS of ENFM Based Glucose Sensor

The EIS was carried out for Au/PEDOT: PSS (nanofibers)/GO_x electrode that are depicted in Nyquist plots which is shown in Figure 2.9 (a), at an amplitude of 10 mV with the frequency range from 0.1 Hz to 10 kHz. The Nyquist plot of the imaginary part (Z_{im}) of the total impedance versus the real part of the impedance (Z_{re}) is expected to show the standard semicircle with a tail representing the Randal model. As shown, in the Figure 2.9 (a) the semicircle is relatively small, and the large variation in the slope of the tail at the low frequencies clearly imply the sensitivity of the electrode to the glucose concentration. The high frequency semicircle represents the heterogeneous electron transport (ET) kinetics between the PEDOT: PSS nanofiber and the redox reactant in solution. On the other hand, the low frequency linear response can be attributed to the diffusive transport of the redox reactant in solution phase coupled to the PEDOT: PSS nanofibrous surface. The equivalent electrical circuit model of the ENFM electrode was generated by utilizing EIS spectrum analyzer. The electrochemical setup with the ENFM electrode was modeled using a series-parallel combination of the resistor-capacitor (RC) network which includes a double-layer capacitance (C_{WE}) of 4.5 μF, solution resistance (R_s) of 200 Ω, a charge transfer or polarization resistance (R_{WE}) of 34.3 Ω, and a Warburg impedance (W_{WE}) of 367.9. Large double-layer capacitance and the Warburg impedance represents a large surface area due to the porosity of the nanofibrous membrane. The Figure 2.9 (b) indicates that bode plot of the change in glucose concentration from 0 mM to 25 mM changes the resistance. Inset Figure 2.9 (b) represents the calibration plot of Au/PEDOT: PSS (nanofibers)/GO_x electrode with addition of glucose. The analysis shows that the Au/PEDOT: PSS (nanofibers)/GO_x electrode has better response for the glucose detection. Therefore, the EIS was used to study the detailed information about the impedance response of the ENFM electrode for glucose detection.
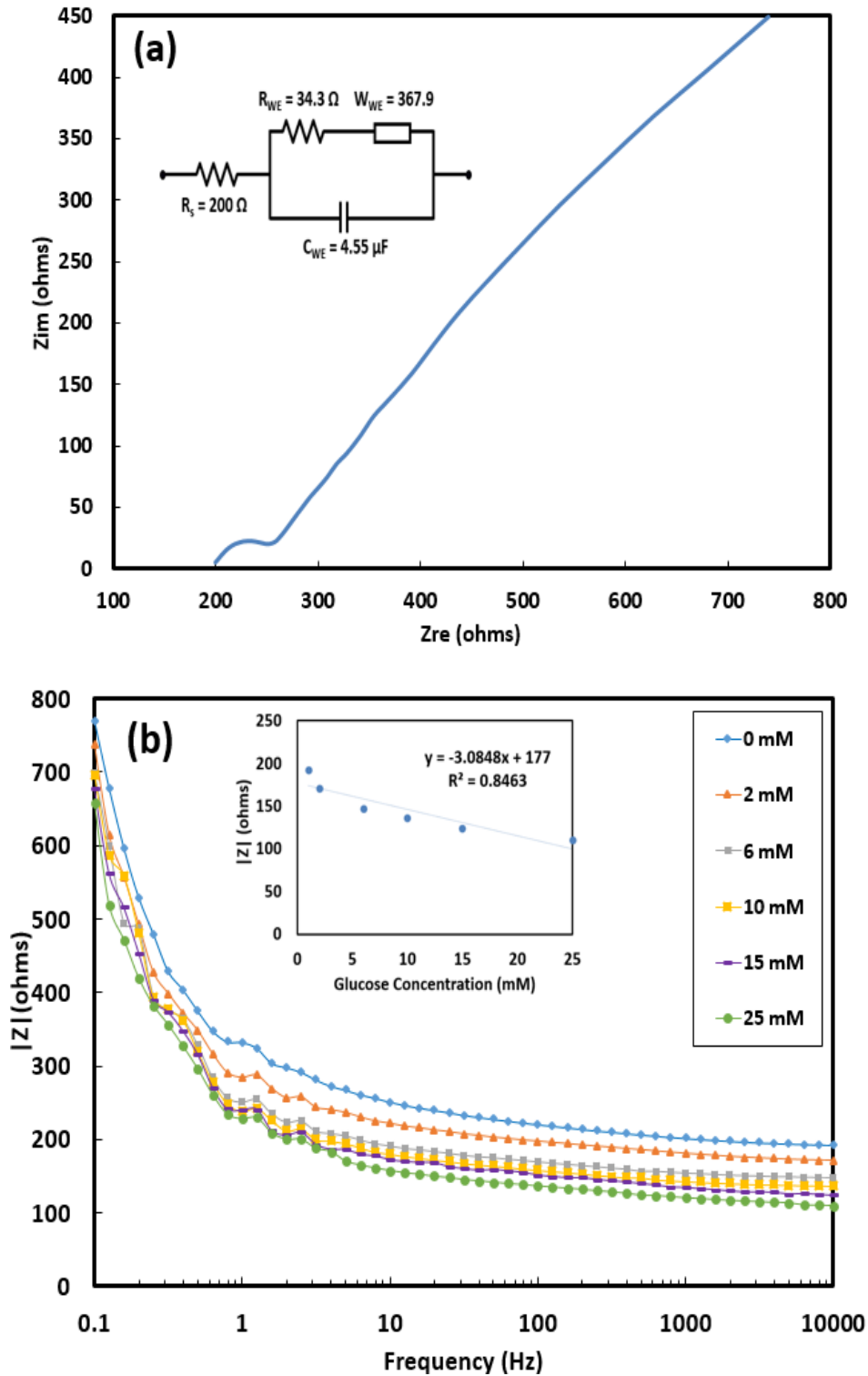
Figure 2.9 (a) Nyquist plot of Au/PEDOT:PSS (nanofibers)/GO_x electrode. (b) Bode plot of Au/PEDOT: PSS (nanofibers)/GO_x electrodes. Inset: Calibration plot at Au/PEDOT: PSS (nanofibers)/GO_x electrode at frequency 10 kHz, between |Z| versus glucose concentration.

2.5.4 CA of ENFM Based Glucose Sensor
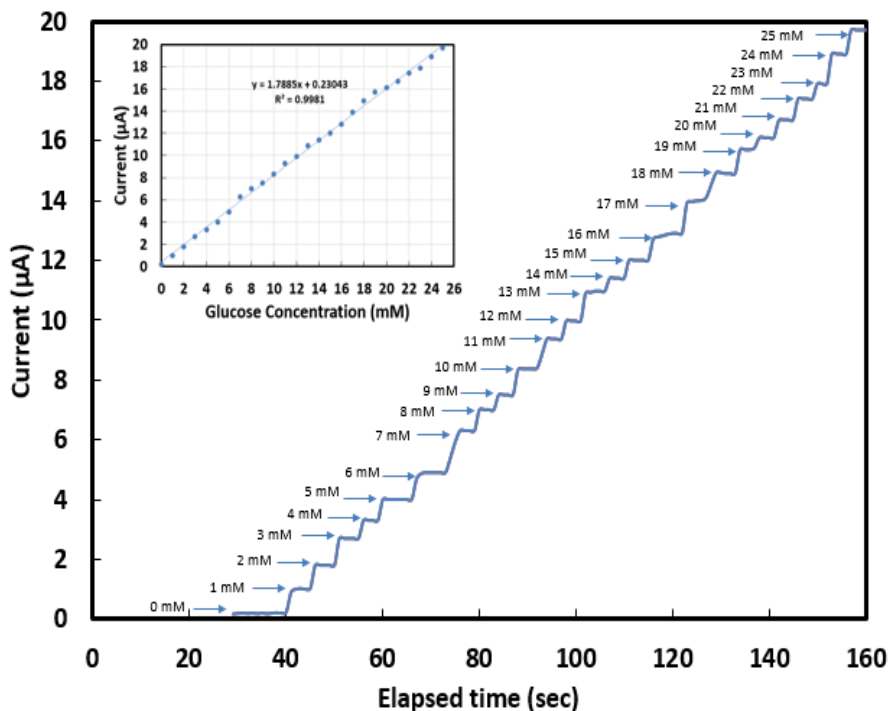
Figure 2.10 Chronoamperometric graph of Au/PEDOT:PSS(nanofibers)/GO$_x$ electrode at different glucose concentration ranges from 0 mM to 25 mM at +0.5 V potential respectively. Inset: Calibration plot of current response versus successive increase in glucose concentration for Au/PEDOT: PSS (nanofibers)/GO$_x$ electrodes.

CA is used to demonstrate the relationship between the current and the glucose concentration. Figure 2.10 represents the chronoamperometric graph for Au/PEDOT:PSS (nanofibers)/GO$_x$ electrode at constant potential +0.5 V vs. reference electrode Ag/AgCl upon successive addition of glucose into a 5 mM potassium ferricyanide electrolyte solution. A +0.5 V potential was applied to the Au/PEDOT:PSS (nanofibers)/GO$_x$ working electrode. As a function of time, the resulting current was measured. The current values were initially around 0.23 ± 0.0014 µA and it increases to 19.7 ± 0.0015 µA, where the concentration of the glucose were varied from 0 mM to 25 mM was observed within 160 sec. A linear relationship was observed between the initial current measured and an increasing concentration of the glucose. The calibration plot of Au/PEDOT: PSS (nanofibers)/GO$_x$ electrode was shown in Figure 2.10 inset, for measuring and

detecting various glucose levels. The linear regression equation is I = 1.7885x+ 0.236 with a correlation co-efficient (R^2) of 0.9905. The limit of detection was found to be 2.2 μM and the sensitivity was calculated to be 10.22 μA/mM cm^2. The Au/PEDOT:PSS (nanofibers)/GO_x working electrode demonstrates a response time of less than 4 sec for the glucose detection. The PEDOT:PSS nanofibers membrane provides larger surface area and higher loading of GO_x enzyme helps in effective electron transfer mediation that results a better response time.

2.5.5   Repeatability, Durability and Selectivity of ENFM Glucose Sensor

The repeatability of the Au/PEDOT:PSS(nanofibers)/GO_x sensing electrode was evaluated by CV measurements of oxidation and reduction current responses with a potential sweep of +0.9 V and -0.9 V at a scan rate of 50 mVs^{-1} with 4 cycles consecutively in an aqueous solution of 5 mM glucose and 5 mM potassium ferricyanide. As the results in Figure 2.11 shows repeated cycles were overlapped, confirming the repeatability of the electrode.
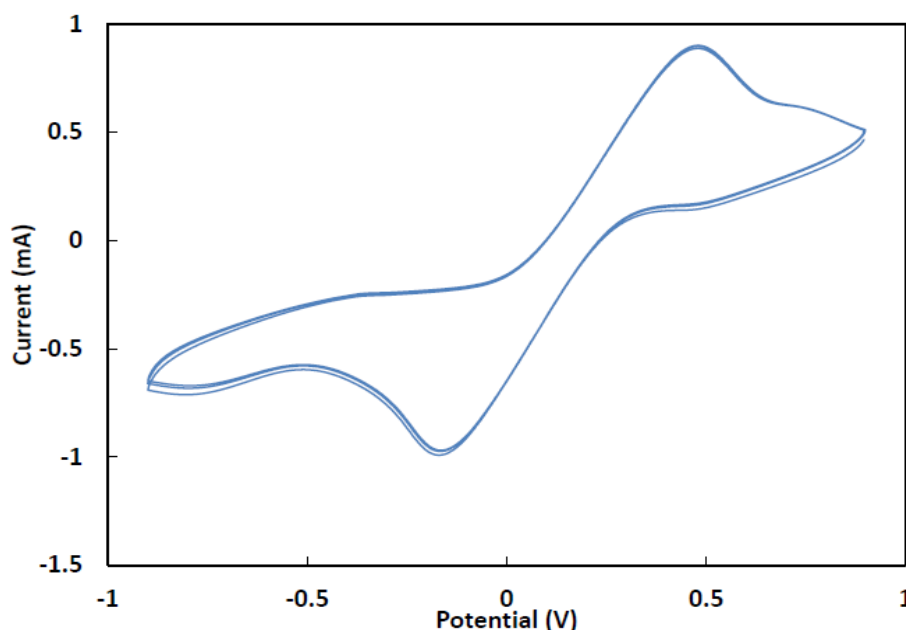
Figure 2.11 Repeatability of ENFM Au/PEDOT:PSS (nanofibers)/GO_x sensing electrode is evaluated by CV measurement graphs.

Durability of the Au/PEDOT: PSS (films)/GO$_x$ and Au/PEDOT: PSS (nanofibers)/GO$_x$ sensing electrodes were measured for 5 mM glucose concentration and 5 mM potassium ferricyanide electrolyte at +0.5 V potential and the sensing electrodes were refrigerated at less than 4 °C. Chronoamperometric measurements in Figure 2.12, shows a significant decrease in current response of 35% for SCTF based sensing electrode. However, a much lower change in current response of 11% for ENFM based sensing electrodes over 60 days was observed. The durability of the ENFM sensing electrode is considerably good because of the porous structure of the compact nanofibrous matrix, which could preserve GO$_x$ enzyme molecules on the nanofibrous membrane without loss of activity.
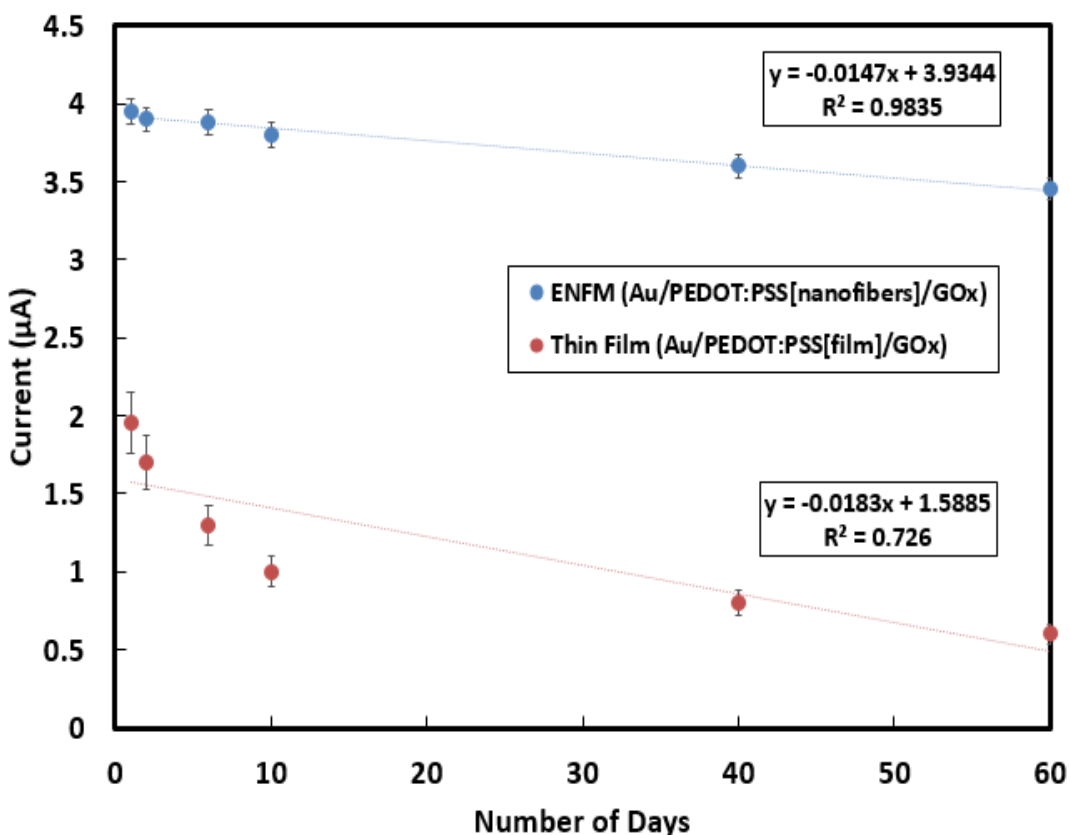
Figure 2.12 Durability of ENFM Au/PEDOT: PSS (nanofibers)/GO$_x$ and thin film Au/PEDOT: PSS (film)/ GO$_x$ sensing electrode is measured at 5 mM glucose concentration and 5 mM potassium ferricyanide electrolyte at +0.5 V. The error bars indicates the standard deviation of 6 experimental measurements.

Selectivity of the ENFM glucose sensor was validated through CA analysis at +0.5 V under the interference of various ingredient such as sodium chloride, and potassium ferricyanide with 2 mM concentration, as shown in Figure 2.13. There was a significant increase in current has been noticed when the 2 mM concentration of glucose was injected, which demonstrates that the ENFM electrode acts as a selective glucose sensor at a trace level of glucose. These electrochemical analysis results are indicative of good repeatability, durability and selectivity through strong electrochemical responses when using ENFM electrode, encouraging the application of nanofibers structures for the fabrication of potential biosensors in future.

However, we haven't tested the sensor with the real blood sample but the promising electrochemical analysis results are encouraging us to move forward to test sensor with real blood samples. The results with real blood samples are proposed for future research work.
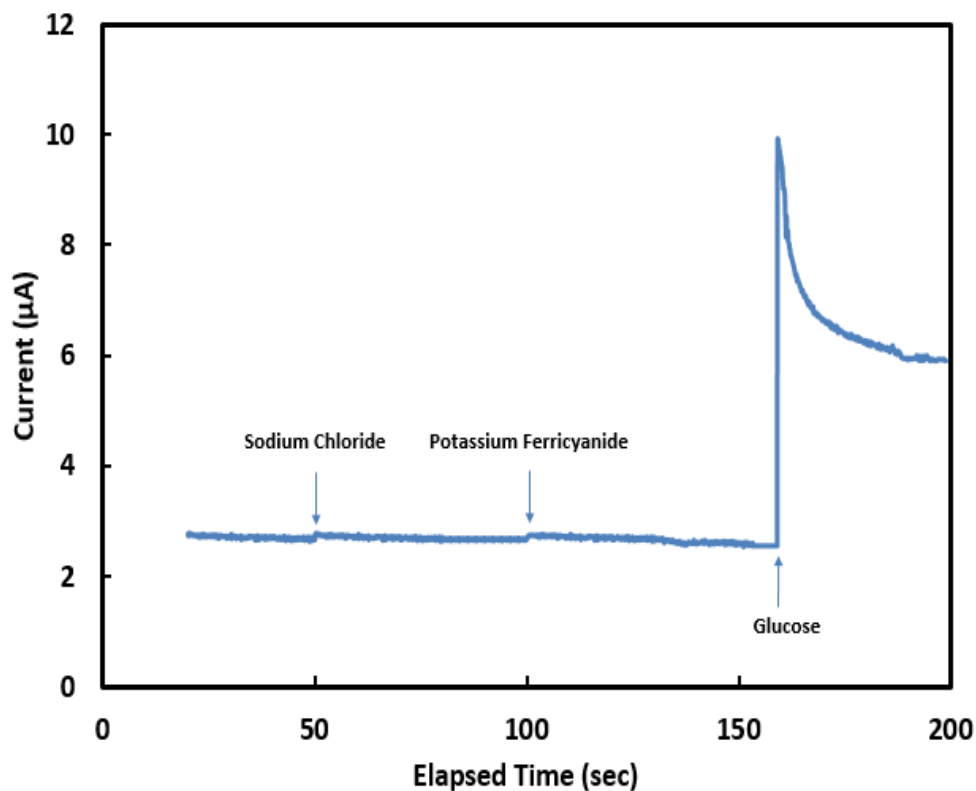
Figure 2.13 Selectivity test of ENFM Au/PEDOT: PSS (nanofibers)/GO_x glucose sensing electrode.

2.6 Performance Comparison

Table 2.1 Comparison of ENFM sensor with prior state-of-the-art glucose sensors

Reference	[34]	[37]	[52]	[54]	[55]	**This Work**
Sensing Electrode	Cu-NF/AuNPs / GO/GO_x	MWCNT /Au/GO_x	Nylon 6,6/PBI BA/GO_x	4-ATP/PVA /PEI/ GO_x	PVA-SbQ/ MWCNT-COOH/GO_x	**Au/PEDOT :PSS/PVDF / GO_x**
Sensitivity	NA	0.47 µA/ mM cm^2	NA	NA	NA	**10.22 µA/ mM cm^2**
Limit of Detection	0.018 µM	4 µM	18 µM	0.9 µM	2 µM	**2.2 µM**
Concentration Range	0.001 – 0.1 mM	0 – 30 mM	0.02 – 2 mM	10 – 200 µM	0.005 -4 mM	**0 – 25 mM**
Number of Days	20 days	14 days	32 days	21 days	5 days	**60 days**
Response Time	NA	20 sec	NA	NA	NA	**< 4 sec**

Table 2.1 depicts the comparative study of formerly reported glucose sensing electrodes [34], [37], [52], [54], and [55]. From the Table 2.1, it can be observed that the ENFM based glucose sensor has a significant improvement in performance showing fast response time, better sensitivity and limit of detection, durability, and large concentration range compared to conventional glucose sensors.

2.7   Discussion

In this chapter, we presented the development of a highly sensitive electrospun nanofibrous membrane based electrochemical glucose sensor which can potentially be used for monitoring diabetic patients. A fibrous morphology of PEDOT: PSS indicated high distribution of GO_x onto the electrospun nanofibrous matrix as compared to a PEDOT: PSS thin film. The electrospun nanofibers used as a unique sensing electrode matrix helped to facilitate GO_x immobilization. The conductive polymer PEDOT: PSS based nanofibers presented as a membrane greatly facilitated the electron transfer between GO_x and the sensor electrode. The improved durability, repeatability

30

and stability of the ENFM based sensing electrode compared to the thin film based electrode suggests application of nanofiber structures for practical biosensing applications.

Chapter 3: Silicon Carbide Nanoparticles Based Glucose Sensors

3.1 Introduction

In latest years, considerable progress has been made in the development of highly sensitive, highly durable, low-cost, point-of-care and accurate biosensors that can continuously monitor different health care issues such as glucose levels of a diabetic patient. Glucose sensors are used to measure the glucose concentration of a blood in a patient and are an important part of managing diabetes mellitus [1-6]. However, to be truly beneficial, the glucose sensor must be able to function properly for a long period of time. The critical issues of a glucose sensor limits the device longevity, sensitivity and biocompatibility. Silicon carbide (SiC) is one of the biocompatible material and, has been used for many biomedical devices [56-59]. A SiC has also been used for clinical studies in bone prosthetics, heart stents and glucose sensors, which confirmed the biocompatibility of these forms of SiC [60-64].

Among various conductive polymers (CP), poly(3,4-ethylenedioxythiophene) : poly(styrene sulfonate) (PEDOT:PSS) thin-films have been studied widely, due to higher enzyme immobilization capability, good electrical conductivity, better processability, excellent electrochemical stability, reliability, and biocompatibility [65-66]. In addition to the use of a conductive polymer material, the surface structure also contributes to the effective immobilization of the enzyme. Of particular interest for this work is the utilization of electrospun nanofibrous structures, which offer large surface area, high porosity, biocompatibility, and dimensionality

advantages, leading to better binding of the enzyme with the electrode for efficient electron-transfer and higher sensitivity [67-69].

In the present work, fabrication, morphological and electrochemical characterization of glucose oxides (GO_x) enzyme entrapped in PEDOT:PSS CP with SiCNPs spin-coated-thin-film (SCTF) as well as in PEDOT:PSS CP with SiCNPs electrospun-nanofibrous-membrane (ENFM) based glucose sensing electrodes were measured. The SiCNPs-ENFM exhibits higher sensitivity, quick response time, better limit of detection and durability compared to SiCNPs-SCTP electrodes. It has been shown that conducting polymers could be utilized as mediator for detection of glucose. This is presumably due to direct electron transfer between glucose oxidase and the CP, which is an oxygen-independent detection. This work is intended to study the feasibility of using SiCNPs-ENFM electrode as an alternative approach to the SiCNPs-SCTF electrode for fabricating glucose sensors.

The remainder of this chapter 3 is arranged as follows; The electrochemical enzymatic SiCNPs-ENFM and SiCNPs-SCTF based glucose sensors are provided in Section 3.2; the experimental results were explained in Section 3.3; the performance comparison was discussed in Section 3.4; and the conclusions are discussed in Section 3.5.

3.2   SiCNPs-ENFM and SiCNPs-SCTF Based Glucose Sensors

3.2.1   Materials and Apparatus

The PEDOT:PSS with 3.0-4.0% in H_2O, high-conductivity grade, D-Glucose with molecular weight 180.16 g/mol and potassium ferricyanide with molecular weight of 329.26 g/mol from Sigma Aldrich. The SiCNPs with molecular weight of 40.1 g/mol from Sigma Aldrich with the particle size of ~45-65 nm. The glucose oxidase (without added oxygen) from Aspergillus niger, tetrahydrofuran (THF), polyvinylidene fluoride (PVDF) with the molecular weight of

~534,000 also from Sigma Aldrich were used for the fabrication of SCTF and SiCNPs-ENFM electrodes.

Electrolyte solution was prepared using deionized water with 1:1 ratio of 5 mM potassium ferricyanide and 5 mM glucose. Sputtered chromium (100 nm) and gold (100 nm) on glass substrates were used for working and counter electrodes; reference electrode as Silver/silver chloride (Ag/ AgCl) was used in this electrochemical experiments.

3.2.2   Experimental Methods

The fabrication of an electrospun conducting polymer of PEDOT:PSS with addition of SiCNPs nanofiber based glucose sensor involves the following process steps; the solution for electrospinning was prepared by dissolving 1.18 g of polyvinylidene fluoride (PVDF) in 2 mL of tetrahydrofuran (THF), add 0.05 g of SiCNPs and add 0.22 g of PEDOT: PSS followed by vigorous stirring for 1 hr at 60 °C. The resulting mixture was electrospun using the following parameters: single 18 gauge syringe nozzle; applied voltage of 20 kV; flow rate of 15 μL min^{-1}. The distance from the tip to the collector plate was fixed at 32 cm. A rotating mandrel was used to collect a bead free fibrous matrix, which helps the uniform distribution of fibers on the electrode surface. The gold coated glass substrate was affixed on to the mandrel surface and the mandrel was rotating at 54 RPM. After the fibers are spun on the gold surface of area 0.35 cm x 0.5 cm, then the SiCNPs-ENFM electrode was dried at 70 °C for 4 hrs. A thin film of SiCNPs-PEDOT: PSS was fabricated by spin-coating the mixture of 0.05g of SiCNPs and 0.0482 g of PEDOT: PSS at the speed of 49 RPM for 1.5 mins on the 0.35 cm x 0.5 cm gold electrode with the thickness of ~110 nm; then dried at 70 °C for 4.5 hrs. The GO$_x$ enzyme solution of 1.5 mg was drop casted over the nanofibrous membrane and the spin-coated electrodes. For enzyme immobilization to occur, the electrodes were kept at less than 4 °C for 24 hrs.

3.3 Experimental Results

3.3.1 Morphological Characterization
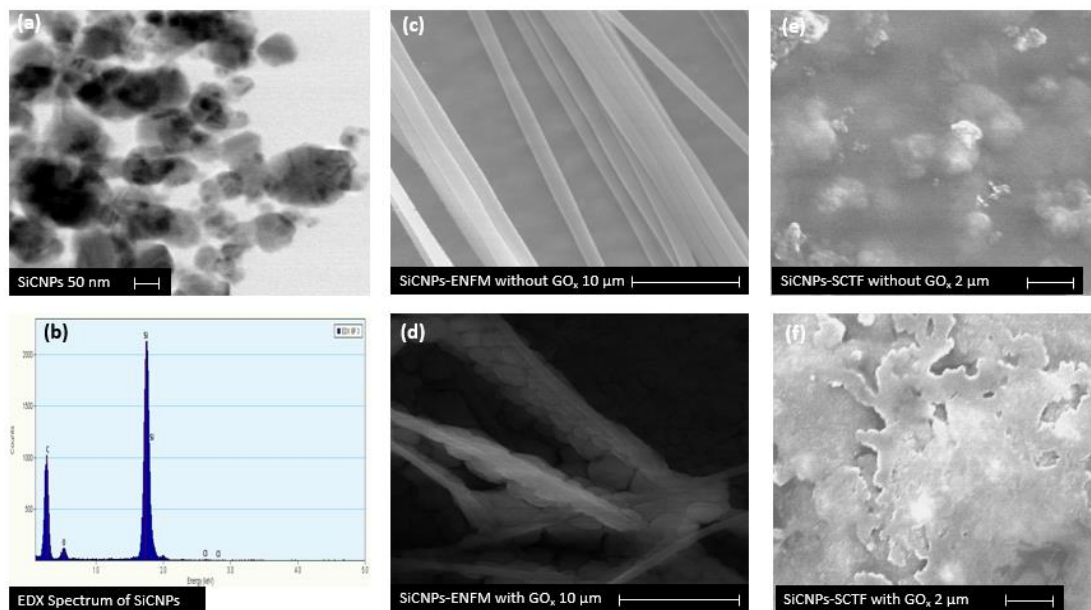
Figure 3.1 (a) TEM image of SiCNPs. (b) EDX spectrum of SiCNPs. (c) SEM image of electrospun PEDOT: PSS + SiCNPs nanofibers without GO_x. (d) SEM image of electrospun PEDOT: PSS + SiCNPs nanofibers with GO_x. (e) SEM image of PEDOT: PSS+SiCNPs SCTF without GO_x. (f) SEM image of PEDOT:PSS+SiCNPs SCTF with GO_x.

The Transmission electron microscopy (TEM, Tecnai TF20) were used to characterize the morphology of SiCNPs with 50 nm scale bar and it's EDX spectrum graph is shown in Figure 3.1 (a) and (b). Scanning electron microscope (SEM, Hitachi SU800) were used to characterize the morphology of SiCNPs-ENFM and SiCNPs-SCTF. The Figure 3.1 (c) shows SEM micrographs with 25 kV acceleration voltage, 1100 magnification and 10 μm scale bar, of the fabricated conductive polymer based SiCNPs-ENFM without GO_x. These images depict a fibrous morphology structure having an average diameter range of 110 - 140 nm. Figure 3.1 (d) shows SEM micrographs with 25 kV acceleration voltage, 1100 magnification and 10 μm scale bar, of closely packed matrix like structures which facilitated higher GO_x surface coverage of the nanofibrous matrix. The larger surface area helped to promote the binding of the GO_x enzyme

35

within the fibrous membrane of the electrode. The SEM images with 25 kV acceleration voltage, 15000 magnification and 2 μm scale bar of SiCNPs-PEDOT: PSS SCTF without GO_x and with GO_x are shown in Figure 3.1 (e) and (f). As for the SCTF electrode, when the sensor is placed in an electrolyte solution, the non-uniform coverage of enzyme molecules leaches out very fast, which affects the sensitivity, stability, repeatability and durability of the sensing electrode. Thus SEM studies reveal the discriminate surface morphology between Au/SiCNPs-PEDOT:PSS (nanofibers) and Au/SiCNPs-PEDOT:PSS (nanofibers)/GO_x membranes with the spin-coated Au/SiCNPs-PEDOT: PSS (film) and Au/SiCNPs-PEDOT: PSS (film)/GO_x.

3.3.2   Electrochemical Characterization

The electrochemical measurements was conducted on VersaSTAT-4 by Princeton Applied Research (PAR) analyzer on a three-electrode system set up. The comparative performance analysis of SiCNPs-ENFM Au/SiCNPs-PEDOT: PSS (nanofibers)/GO_x and SCTF Au/SiCNPs-PEDOT: PSS (film)/GO_x based glucose sensing electrodes were studied through electrochemical measurements such as CV, CA and EIS. The CV of SiCNPs-ENFM and SiCNPs-SCTF electrodes with a range of potential from +0.9 V to -0.9 V at scan rate of 50 mVs^{-1} with 5 mM glucose concentration were depicted in Figure 3.2i (a). The CV of SiCNPs-ENFM based electrode shows the oxidation peak of +1.42 mA at +0.5 V and reduction peak of -1.46 mA at -0.24 V, whereas the SiCNPs-SCTF electrode exhibits very less oxidation peaks of +0.589 mA at +0.46 V and the reduction peaks of -0.64 mA at -0.38 V. Figure 3.2ii (b) shows the CA graphs of the SiCNPs-ENFM and SiCNPs-SCTF electrodes at 0.5 V potential with 5 mM potassium ferricyanide for glucose concentration ranges from 0 mM to 11 mM. The current response varies from 2.5 ± 0.0015 to 29.38 ± 0.0019 for SiCNPs-ENFM and 0.28 ± 0.0025 to 6.98 ± 0.003 for SiCNPs-SCTF electrodes with the elapsed time of 100 sec. From the calibration plots of Figure 3.2ii (c), the

sensitivity is calculated by slope divided by the surface area of the sensing electrode and the LOD (3*standard deviation by the slope of calibration curve) of the SiCNPs-ENFM electrode was found to be 14.27 µA/mM cm^2 and 1.8 µM which is significantly better than 3.54 µA/mM cm^2 and 12.09 µM of the SiCNPs-SCTF electrode. The EIS was performed for the SiCNPs-ENFM and SiCNPs-SCTF electrodes with equivalent circuit models at 5 mM glucose concentration with a range of frequency from 0.1 Hz to 10 kHz and an amplitude of 10 mV is represented by Nyquist plots which is shown in Figure 3.2iii (d). The SiCNPs-ENFM based electrode exhibits the lower solution and charge-transfer resistance (R_s) and (R_{WE}) of 185.2 Ω and 31.9 Ω, double-layer capacitance (C_{WE}) of 4.32 µF and Warburg impedance of 343.4 compared to the SCTF electrode. The various electrochemical results from CV, CA, and EIS indicate that the SiCNPs-ENFM based electrode shows better performance for glucose sensing.
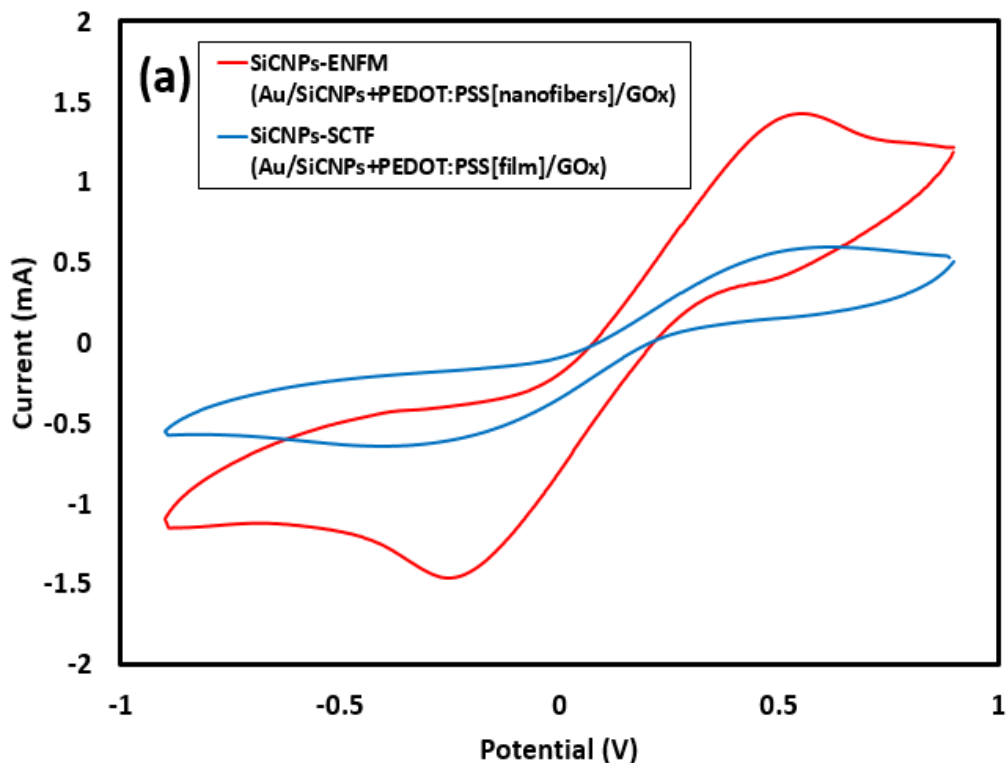
Figure 3.2i (a) CV of SiCNPs-SCTF Au/SiCNPs+PEDOT:PSS (film)/GO$_x$ and SiCNPs-ENFM Au/SiCNPs+PEDOT:PSS (nanofibers)/GO$_x$ electrodes.
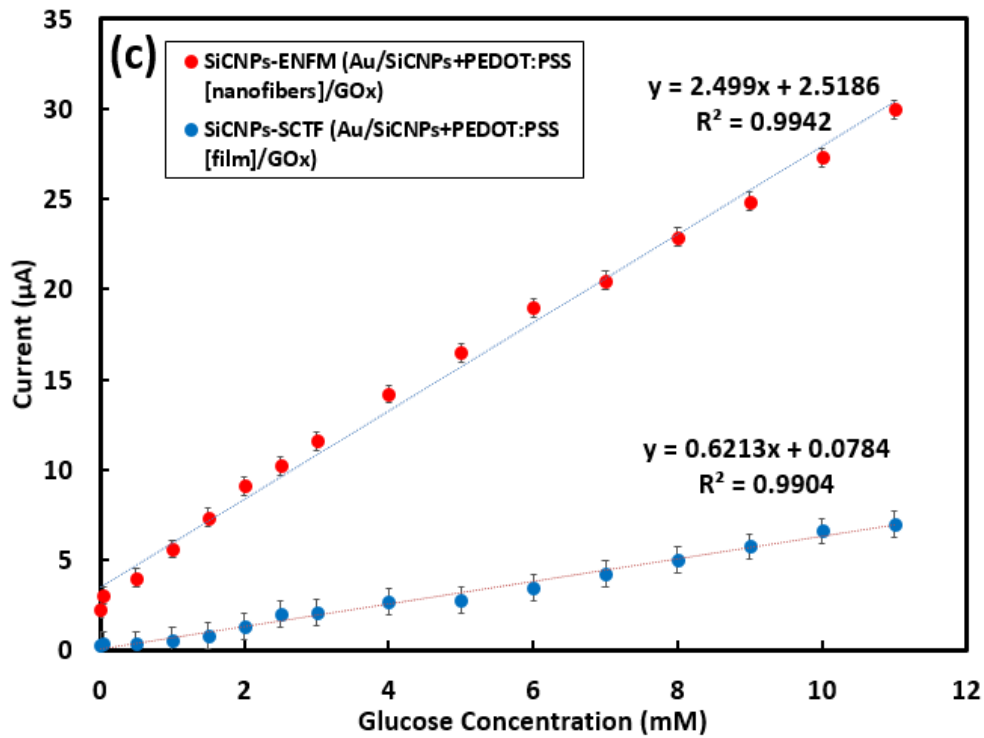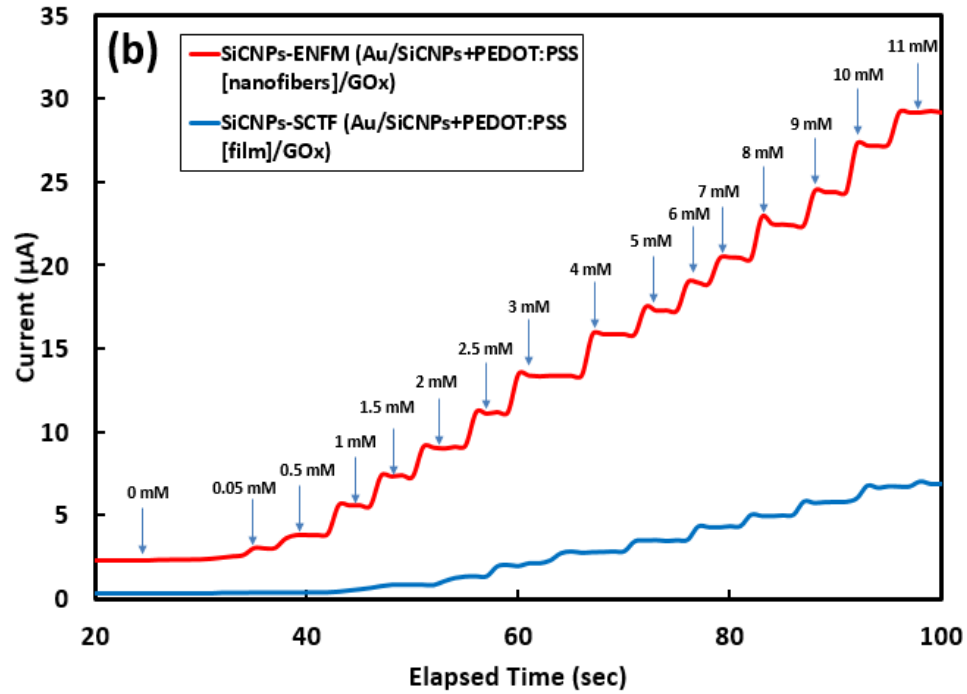
Figure. 3.2ii (b) CA graphs of SiCNPs-SCTF Au/SiCNPs+PEDOT:PSS (film)/GO$_x$ and SiCNPs-ENFM Au/SiCNPs+PEDOT:PSS (nanofibers)/GO$_x$ electrodes. (c) Calibration plots of current response verses varied glucose concentrations (0 mM to 11 mM) for SiCNPs-SCTF Au/SiCNPs+PEDOT:PSS (film)/GO$_x$ and SiCNPs-ENFM Au/SiCNPs+PEDOT:PSS (nanofibers)/GO$_x$ electrodes.
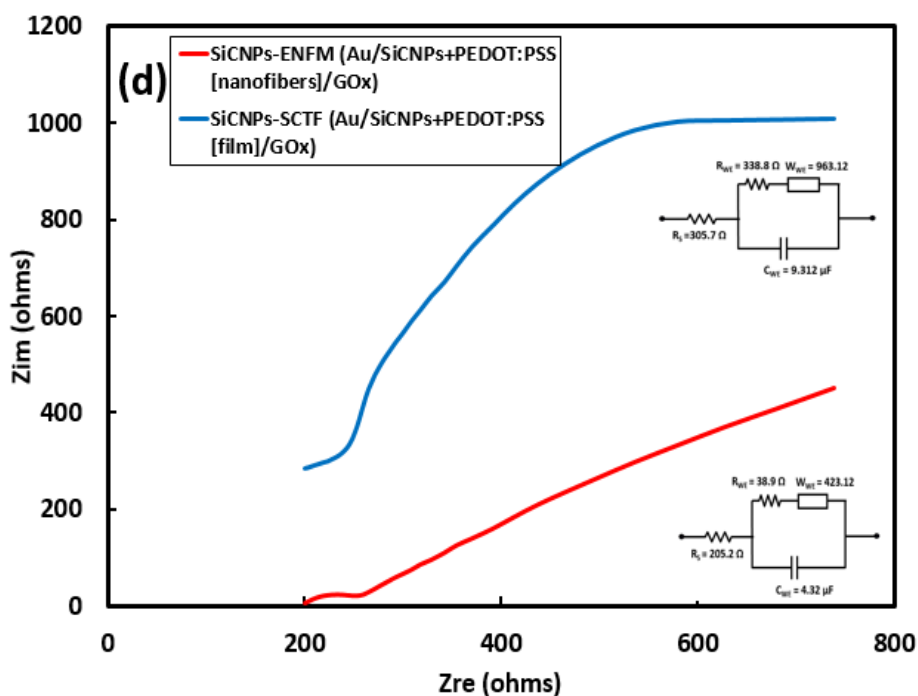
Figure 3.2iii (d) Nyquist plots of SiCNPs-SCTF Au/SiCNPs+PEDOT:PSS (film)/GO$_x$ and SiCNPs-ENFM Au/SiCNPs+PEDOT:PSS(nanofibers)/GO$_x$ electrodes.

Durability of SiCNPs-ENFM and SiCNPs-SCTF electrodes were measured for 5 mM glucose concentration at +0.5 V potential and the electrodes were refrigerated at 4 ^{o}C. The CA measurements in Figure 3.2iv (e), shows a lower change in current response of ≈14 % for SiCNPs-ENFM electrode and significant decrease in current response of ≈79 % for SiCNPs-SCTF based electrode was observed over 50 days period. Due to the porous structure of the compact nanofibrous matrix, GO$_x$ enzyme molecules were entrapped on the nanofibrous membrane surface. The selectivity of SiCNPs-ENFM glucose sensor was validated through CA analysis at +0.5 V under the interference of various ingredient such as sodium chloride, potassium ferricyanide, and ascorbic acid as shown in Figure 3.2iv (f). It can be noticed that the current was significantly increased only when the glucose was injected, which demonstrates that the SiCNPs-ENFM acts as a selective glucose sensor at a trace level of glucose. These results are indicative of good durability

39

and selectivity through strong electrochemical responses when using SiCNPs-ENFM electrode, encouraging the application of nanofibers for the fabrication of potential biosensors in future.
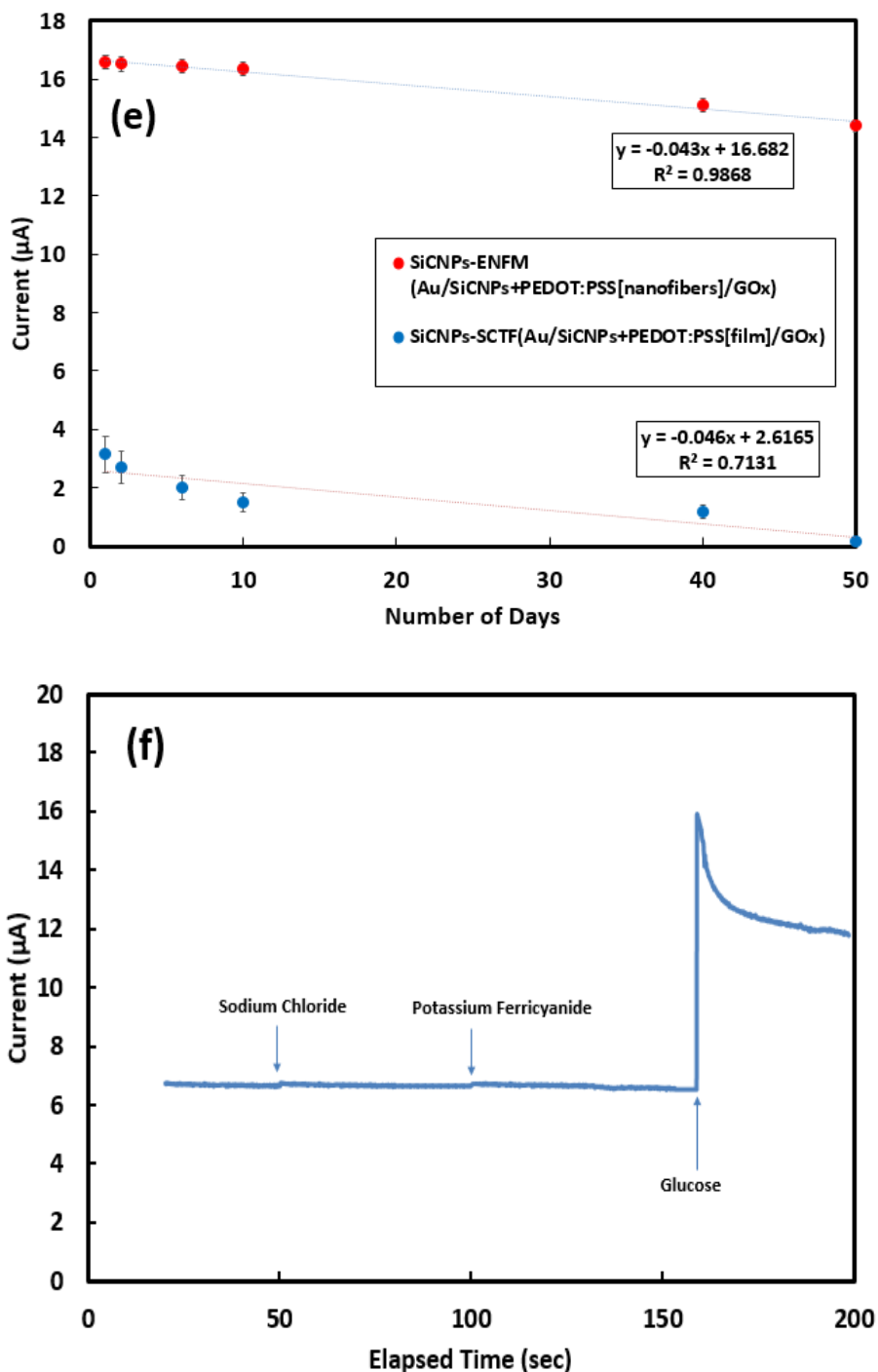
Figure 3.2iv (e) Durability of SiCNPs-ENFM and SiCNPs-SCTF electrodes and the error bars indicates the standard deviation of 6 experimental measurements. (f) Selectivity test for the SiCNPs-ENFM based sensing electrode.

3.4   Performance Comparison

Table 3.1 Comparison of SiCNPs-ENFM sensor with PEDOT glucose sensors

Reference	[66]	[68]	**This Work**
Sensing Electrode	Pt/PEDOT-NFs/GO$_x$	NPG/PEDOT/ GO$_x$	**Au/SiCNPs-PEDOT:PSS/ PVDF/GO$_x$**
Sensitivity	9.2 µA/mM cm^2	7.3 µA/mM cm^2	**14.27 µA/ mM cm^2**
Limit of Detection	0.26 mM	10 mM	**1.8 µM**
Concentration Range	0.1 – 25 mM	0.1 – 15 mM	**0 – 11 mM**
Number of Days	30 days	7 days	**50 days**
Response Time	~ 30 sec	15 sec	**< 4 sec**

From the Table 3.1, it can be observed that the SiCNPs-ENFM glucose sensor has a significant improvement in performance showing better sensitivity, LOD, stability and durability, compared to the previously published state-of-the-art PEDOT conductive polymer based glucose sensors [66], [68].

3.5   Discussion

This chapter demonstrated the comparative analysis of a SiCNPs-ENFM and SiCNPs-SCTF based enzymatic electrochemical glucose sensor which can be potentially used for monitoring the blood glucose level in diabetic patients. Electrochemical analyses indicate a SiCNPs-PEDOT:PSS ENFM will promote higher distribution and entrapment of GO$_x$, as compared to a SiCNPs-PEDOT:PSS SCTF electrode. Electrospun SiCNPs-CP nanofibers, used as a unique sensing electrode matrix, help to accelerate the GO$_x$ immobilization. The charge transfer between sensor electrode and GO$_x$ enzyme was greatly enhanced when using the CP PEDOT: PSS with SiCNPs nanofibrous membrane electrode. The SiCNPs-ENFM based sensing electrode

shows the improved sensitivity of 14.27 µA/mM cm^2, minimum LOD of 1.8 µM, fast response time of < 4 sec, and better durability for upto 50 days compared to the SiCNPs-SCTF electrode, suggests application of nanofibrous membranes for practical biosensing applications.

Chapter 4: Low-Power Low-Noise Transimpedance Amplifier

4.1 Introduction

Per the International Technology Roadmap for Semiconductors (ITRS) [70], there continues to be a movement toward "energy efficient sensing and computing, real-time communications, and multi-level and scalable security". These advancements will address the global need to "create computer chips that are 100 times faster yet consume less power" as we embark upon the Internet of Things (IoT) [70-71].

With the rapid growth of these ultra-low power devices needed for biomedical, hardware security, RADAR, and space applications, the challenge for the semiconductor industry and researchers continues to be the identification of different designs and structures to overcome the limitations of conventional MOSFET technology [72-78]. The usage of MOSFETs can be limited by the short channel effect, drift velocity, accumulation of mi0pnority carriers and exponential increase of leakage current. These limitations are grand challenges for the semiconductor industry as technology features are being miniaturized to the nano scale, particularly for the bioelectronics arena [79-80].[2]

K. Puttananjegowda, S. Thomas, "A Low-Power Low-Noise Multi-Stage Transimpedance Amplifier for Ampherometric based Blood Glucose Monitoring Systems", *Analog Integrated Circuits and Signal Processing Journal*, vol. 102, no. 4, pp. 659–666, 2020.
K. Puttananjegowda, S. Thomas, "Cascode common source transimpedance amplifiers for analyte monitoring systems", US Patent App. 16/008,864, 2019.
K. Puttananjegowda, S. Thomas, "A CNTFET based Multi-Stage Transimpedance Amplifier for Blood Glucose Monitoring System", *IEEE IEMCON*, 2018.
K. Puttananjegowda, S. Thomas, "The Design of Ultra Low Noise CMOS Transimpedance Amplifier for Biosensing Applications", *IEEE UEMCON*, 2017.

Despite recent advancements in the bioelectronics field, there is still a critical need for low cost, low power, miniaturized electronic circuitry to support biosensors for sensing applications, such as monitoring blood glucose levels in diabetic patients. These biosensors can require very high sensitive readout circuitry, small size and low power [81-86].

To begin understanding how circuit architecture for glucose sensing can be optimized, it is important to evaluate the various electronic components needed to measure the glucose levels. In general, carbohydrates in food get digested by the stomach and are converted to glucose. This glucose is then released in the blood stream and distributed to various parts of the body, organs and cells. Cells need insulin to use glucose for energy and insulin is a hormone secreted by the pancreas. If the body fails to generate enough insulin or cannot not respond to the insulin the glucose levels in the blood rises giving rise, presenting conditions for the disorder called Diabetes. A large number of people around the world suffer from this disorder, which can result in damages to eyes, kidneys, nerves and even death. Approximately 285 million people suffer from diabetes and this number is expected to increase to 430 million by 2030 [1-8].

Continuous monitoring of glucose levels in the blood is very important for diabetic people. Several commercially available glucose meters are available for this purpose [87-88]. The architecture of a blood glucose monitoring system shown in Figure 3.1. When the blood on the test strip (sensor) is detected, an electrochemical reaction occurs and the current from the sensor is converted to the proportional voltage. This is accomplished with the help of a current to voltage converter, generally known as a transimpedance amplifier. This voltage is fed to an analog to digital converter (ADC) and the resulting digital signal is passed to the signal processing unit. The output analysis of the glucose concentration is displayed on the liquid crystal display (LCD) [89].

There are two popular topologies of a TIA that is open loop based TIA and closed loop based TIA. The open loop TIAs are designed based on common gate amplifier configuration. The main drawbacks of this configuration are the high input referred current noise due to low input impedance and the noise current directly coupled to the input. Hence, a common gate configuration is not very well suited for achieving improved transimpedance gain and low-noise, when using low supply voltages [90-92]. The closed loop TIAs are designed based on feedback amplifier configuration. This configuration is commonly used for biosensing because it provides better performance compared to open loop in terms of gain, higher input impedance, and drive capability, by maintaining a large feedback resistor to improve noise behavior [93-97].

In the proposed system, the MSCCS-TIA has a resistor-capacitor feedback configuration which assist in amplifying the input signal, improves stability, minimizes noise, and power consumption. In addition, the complexity of the circuit is reduced by eliminating the filter circuit between the TIA and ADC, which was used in blood glucose sensing systems [98-99]. For a system-on-chip (SOC) design, this architecture provides an advantage in terms of integration, reduction in footprint and power.
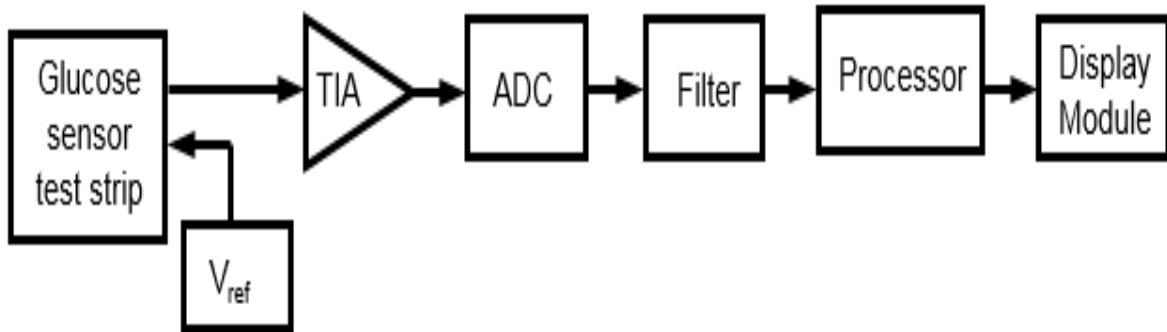
Figure 4.1 Architecture of blood glucose monitoring system.

The remainder of this chapter 4 is arranged as follows. The literature review of the basic transimpedance amplifier and its topologies is discussed in Section 4.2, proposed transimpedance

amplifier is discussed in Section 4.3, simulation results were explained in Section 4.4 and the performance comparison was discussed in Section 4.5.

4.2 Literature Review

4.2.1 Basics of Transimpedance Amplifier

The blood glucose sensor produces a current output due to an electrochemical reaction of blood glucose on a test strip. When the sensor current is very small then the sensor output becomes very weak. Therefore, this produced current from the sensor needs to be amplified. In signal processing, analog to digital converters (ADC) are used to convert from analog signals to digital signals. Most of the ADCs convert voltage signals [100], therefore the current signal from the sensor is converted to voltage. A transimpedance amplifier (TIA) is required for this conversion and to amplify the signal.

The main parameters of the transimpedance amplifier are the gain, input referred noise current and power. The TIA gain is a ratio of the output voltage to the input current which is given in equation (4.1). Hence, it defines the output voltage produced from the given current.

$$Z_T = \frac{\partial V_{out}}{\partial I_{in}} \quad \text{..}(4.1)$$

Noise of TIA is defined by the input referred noise. Input referred noise is the current noise that would be added to an equivalent noiseless TIA. The input-referred current noise is calculated by the ratio of output voltage noise to the transimpedance gain and with a unit is A/√Hz which is given in equation (4.2). The minimum detectable TIA current is determined by the input referred current noise [101]. To explore the benefits of various approaches, there are several TIA topologies analyzed.

$$\overline{i_{n,in}^2} = \frac{\overline{v_{n,out}^2}}{Z_T^2} \quad \text{..}(4.2)$$

4.2.2   Various Topologies of TIA

There are two popular topologies of a TIA, that is open loop based TIA and closed loop based TIA, where the open loop TIAs are designed based on common gate amplifier configuration and the closed loop TIAs are designed based on feedback amplifier configuration.

(1) Open loop TIA, based on common gate (CG) amplifiers

- Regulated common gate TIA [102]

- Capacitive coupled common gate TIA [103]

- Differential common gate TIA [104]

(2) Closed loop TIA, based on feedback amplifiers

- Common source with resistive feedback TIA [105]

- Current reuse feedback TIA [106]

- Capacitive feedback TIA [107]

4.2.3   The Open Loop TIA Topology

The open loop TIA is designed based on common gate configuration as shown in Figure 4.2, which is a designed with two NMOS transistors and a resistor R_D to achieve low input resistance and better gain.
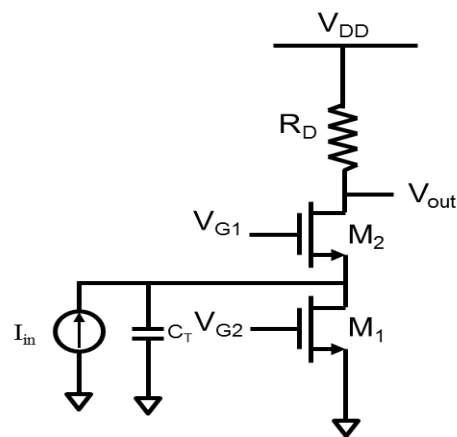
Figure 4.2 Open loop TIA based on common gate configuration [108]

The transimpedance gain (Z_T) is given in equation (4.3) and the input resistance (R_{in}) is in equation (4.4) as follows.

$$Z_T = \frac{R_D}{1 + s\dfrac{C_T}{R_{in}}} \quad\dotfill\quad (4.3)$$

$$R_{in} = \frac{1}{g_m} \quad\dotfill\quad (4.4)$$

The output voltage noise is given below.

$$\overline{V_{n,OUT}^2} = \left(\overline{I_{n,M_2}^2} + \overline{I_{n,RD}^2}\right)Z_T^2 \quad\dotfill\quad (4.5)$$

The input referred current noise is given by,

$$\overline{i_{n,in}^2} = \left(\overline{i_{n,M_2}^2} + \overline{i_{n,RD}^2}\right) \quad\dotfill\quad (4.6)$$

$$\overline{i_{n,in}^2} = 4kT\left(\gamma g_{m2} + \frac{1}{R_D}\right) \quad\dotfill\quad (4.7)$$

where g_m is the transconductance, γ is the transistor noise coefficient.

The main drawback to this configuration is the input referred current noise of the circuit, where the noise currents of M_2 and R_D are directly referred to the input, which makes a common gate configuration not suitable for achieving improved transimpedance gain and low noise when using low supply voltages. Hence this configuration is often used in conjunction with a resistive feedback which is discussed in the following section.

4.2.4   The Closed Loop TIA Topology

The closed loop TIA is designed based on feedback amplifier configuration as shown in Figure 4.3. This configuration is commonly used because it provides a large bandwidth by

synthesizing a small input resistance by maintaining a large feedback resistor to improve noise behavior [109].
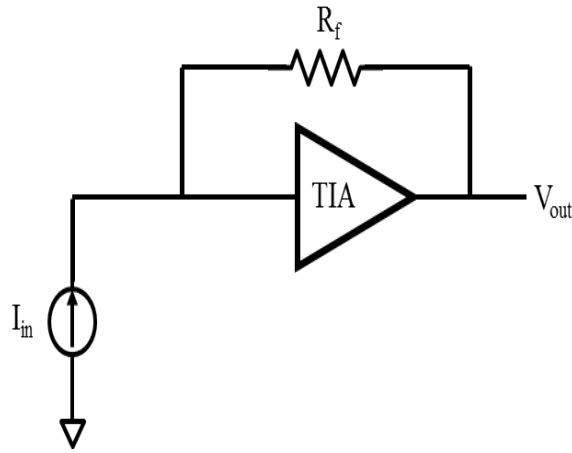
Figure 4.3 Closed loop TIA based on feedback amplifier [109]

The transimpedance gain is dependent on the feedback resistor (R_f) which is shown below in equation (4.8).

$$Z_T = \frac{R_f}{A_0}$$ .... (4.8)

where the open loop gain $A_0 \approx 1$, then $Z_T \approx R_f$.

Noise of the feedback resistor (R_f) directly couples into input. For a low noise TIA, very high (R_f) is required to minimize the input referred current noise which is explained in equation (4.9).

$$\overline{i_{n,in}^2} = \frac{\overline{v_{n,out}^2}}{Z_T^2}$$ .... (4.9)

From the equation (4.8) and (4.9), to improve the transimpedance gain, feedback resistance (R_f) needs to be increased. However increasing R_F increases the input resistance which results in reduction of the input pole frequency. This type of feedback is chosen because it offers better performance in terms of noise, input and output resistance, and drive capability. At low voltage

supplies, the headroom required by load resistance reduces the achievable transimpedance gain of each stage [109].

Table 4.1 Performance comparisons of various conventional TIA designs

Parameter	Open-loop TIA Topologies			Closed-loop TIA Topologies		
Topology	Regulated Common gate TIA[102]	Capacitive Coupled Common Gate TIA [103]	Differential Common Gate TIA [104]	Common Source Resistive Feedback [105]	Current Reuse Feedback TIA [106]	Capacitive Feedback TIA [107]
Technology	130 nm	180 nm	180 nm	0.7 μm	180 nm	180 nm
Input Current	2.25 μA	1 μA	50 nA	5 μA	11.54 μA	73 μA
Transimpedance	198 kΩ	150 kΩ	215 MΩ	1 kΩ	687 Ω	56 MΩ
Bandwidth	10 MHz	100 Hz	615 kHz	1.5 GHz	2 GHz	1.8 MHz
Power Consumption	0.34 mW	90 mW	139 μW	26.5 mW	2.85 mW	436 μW
Supply Voltage	1.2 V	1.8 V	1.8 V	3.3 V	1.5 V	1.8 V
Input referred noise current	0.62 mA/√Hz	1.6 pA/√Hz	910 fA/√Hz	7 pA/√Hz	767.3 nA/√Hz	65 fA/√Hz

Based on the comparison with literature reviews shown in Table 4.1, a closed loop TIA based feedback amplifier exhibits better gain, low-noise and lower-power, hence will be used to build the novel TIA design for this work.

4.3   Proposed Transimpedance Amplifier

A transimpedance amplifier (TIA) is a vital block which is used as a current to voltage converter and it is also used to amplify current output from the sensor to the usable voltage. The implementation of a multi-stage cascode common source TIA (MSCCS-TIA) is a combination of different classes of amplifiers which includes biasing stage, cascode stage and source-follower stage, where cascoding is a combination of both common-source and common-gate configuration, which significantly improves gain and bandwidth performance compared to common-source topology [90]. This work demonstrates a CMOS based MSCCS-TIA, which has lower-noise, higher gain and dissipates low-power. The proposed MSCCS-TIA consists of NMOS and PMOS

transistors as shown in Figure 4.4. The transistors are made to operate in saturation region to get the maximum gain. The current mirror technique was used to design the biasing stage [90, 110-112]. The sizes of transistors in current mirror and cascode amplifier circuit is same to minimize the effect of channel length modulation. The gain of core amplifier depends on the M_1 and M_2 NMOSFETs which are cascode connected. M_3 and M_4 PMOSFETs are also cascoded to boost the output impedance of the cascode stage amplifier, acts as a constant current source. A source follower stage composed of M_5 NMOSFET and M_6 NMOSFET which is connected to the output of the cascode amplifier. R_f is the feedback resistor implemented using poly resistors and C_f is the compensation capacitor, mitigates the oscillations and also improves the stability of the circuit which is implemented in the design using metal-insulator-metal capacitor (MIMCAP) device by 180 nm CMOS library.
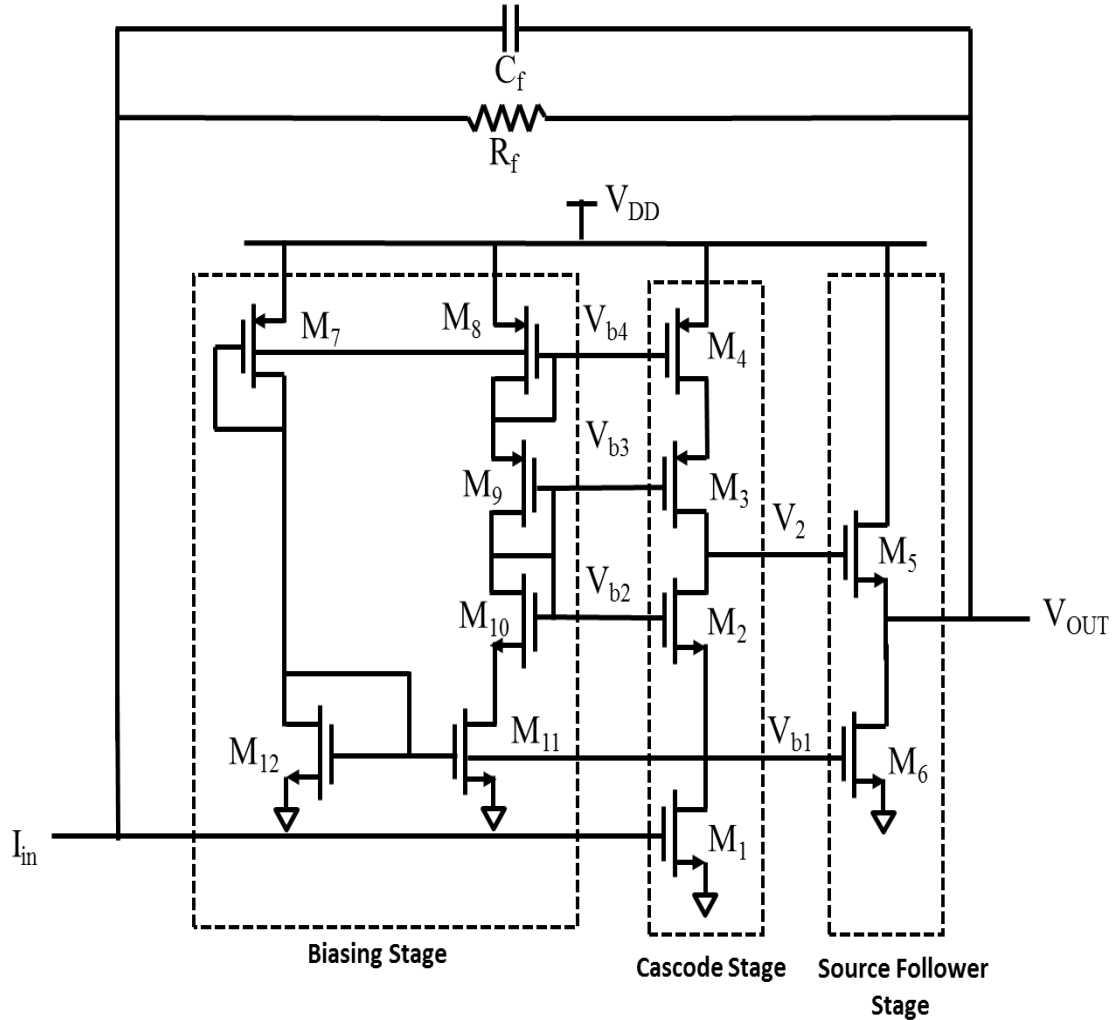
Figure.4.4 Proposed multi-stage cascode common source TIA with biasing circuit.

4.3.1   AC Small Signal Analysis

The small signal equivalent circuit model of a proposed MSCCS-TIA is shown in Figure 4.5. The cascode amplifier gain (A_{v2}) is the product of $G_m = g_{m1}$ and R_{out} , the output resistance (R_{out}) of the cascode amplifier can be found using equation (4.10) and the gain (A_{v2}) can be found from V_{in} to V_2 which is shown in equation (4.11) and (4.12).
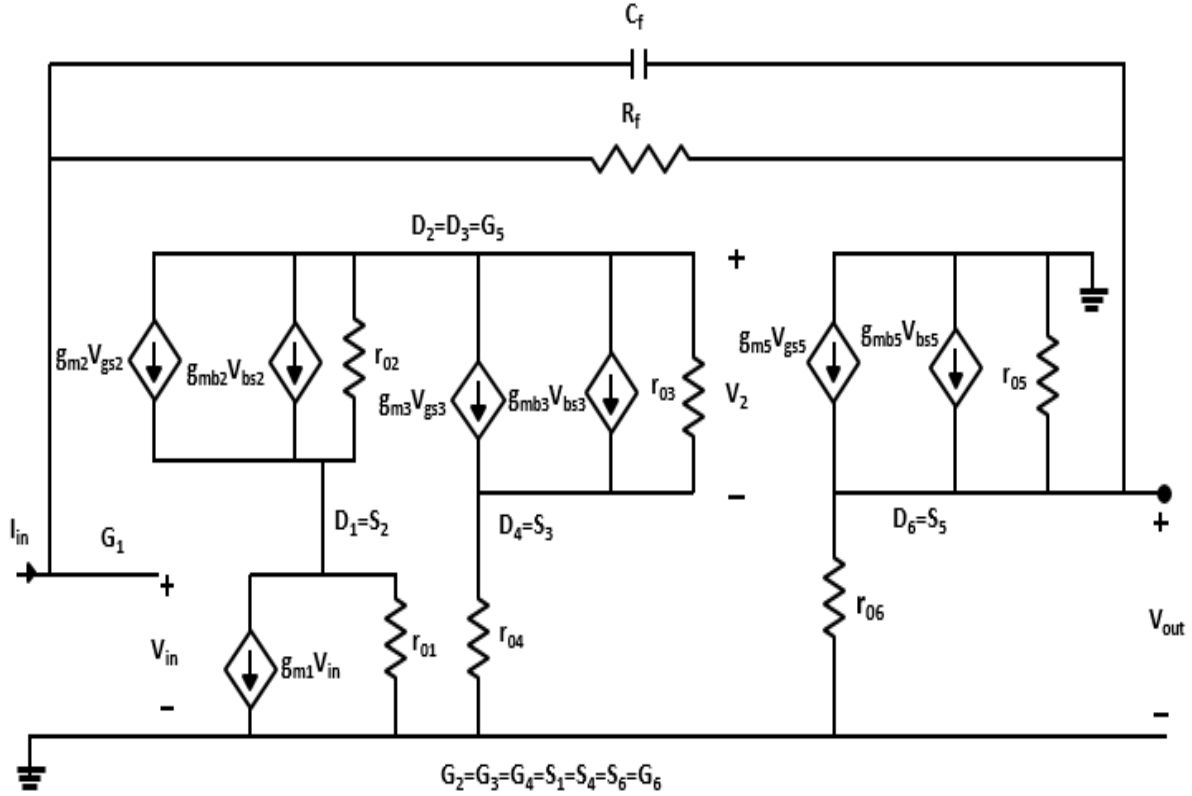
Figure 4.5 Small signal equivalent circuit model of the proposed MSCCS-TIA.

$$R_{out2} = \{[(g_{m2} + g_{mb2})r_{02}r_{01}] \| [(g_{m3} + g_{mb3})r_{03}r_{04}]\}$$ ....(4.10)

$$A_{V2} = \frac{V_2}{V_{in}} = g_{m1}\{[(g_{m2} + g_{mb2})r_{02}r_{01}] \| [(g_{m3} + g_{mb3})r_{03}r_{04}]\}$$ ....(4.11)

$$A_{V2} = \frac{V_2}{V_{in}} = \left(-g_{m1} \frac{(g_{m2} + g_{mb2})(g_{m3} + g_{mb3})r_{o1}r_{o2}r_{o3}r_{o4}}{(g_{m2} + g_{mb2})r_{o2}r_{o1} + (g_{m3} + g_{mb3})r_{o3}r_{o4}} \right)$$ ....(4.12)

The source-follower gain (A_{v3}) is given in equation (4.13):

$$A_{V3} = \frac{V_{out}}{V_2} = \left(\frac{g_{m5}}{g_{m5} + g_{mb5}} \right) \leq 1$$ ....(4.13)

The last step to calculate the overall open-loop gain (A_{VOL}) of the MSCCS amplifier, which

is from V_{in} to V_{out}, is shown in equation (4.14).

$$A_{V_{OL}} = A_{V2} \cdot A_{V3} = \frac{V_{out}}{V_{in}} = \left(-g_{m1} \frac{(g_{m2} + g_{mb2})(g_{m3} + g_{mb3})r_{01}r_{02}r_{03}r_{04}}{(g_{m2} + g_{mb2})r_{02}r_{01} + (g_{m3} + g_{mb3})r_{03}r_{04}} \right) \dots\dots\dots(4.14)$$

Input impedance (Z_{inOL}) of the open-loop MSCCS amplifier is given by equation (4.15).

$$Z_{in_{OL}} = \frac{V_{in}}{I_{in}} = \infty \dots\dots\dots\dots\dots\dots\dots\dots\dots\dots\dots\dots\dots\dots\dots\dots\dots\dots\dots\dots\dots\dots\dots\dots\dots(4.15)$$

Output impedance (Z_{outOL}) of the open-loop MSCCS amplifier is given by equation (4.16).

$$Z_{out_{OL}} = \frac{V_{out}}{I_{out}} = r_{05} \parallel r_{06} \dots\dots\dots\dots\dots\dots\dots\dots\dots\dots\dots\dots\dots\dots\dots\dots\dots\dots\dots\dots\dots(4.16)$$

The closed-loop gain (A_{VCL}) of the MSCCS-TIA circuit is shown in equation (4.17).

$$A_{V_{CL}} = \frac{V_{out}}{I_{in}} = A_{V_{OL}} \frac{Z_f}{1 - A_{V_{OL}}} \dots\dots\dots\dots\dots\dots\dots\dots\dots\dots\dots\dots\dots\dots\dots\dots\dots(4.17)$$

$$Z_f = \frac{R_f}{1 + R_f C_f s} \dots\dots\dots\dots\dots\dots\dots\dots\dots\dots\dots\dots\dots\dots\dots\dots\dots\dots\dots\dots\dots(4.18)$$

where A_{VOL} is the open-loop gain, A_{VCL} is the closed-loop gain, $S = j\omega$, Z_f is the feedback impedance, R_f and C_f are the feedback resistor and capacitor.

The input impedance (Z_{inCL}) of the closed-loop MSCCS-TIA is shown in equation (4.19).

$$Z_{in_{CL}} = \frac{V_{in}}{I_{in}} = \frac{Z_f}{\left(1 - A_{V_{OL}}\right)} = \frac{R_f}{\left(1 + R_f C_f s\right)\left(1 - A_{V_{OL}}\right)} \dots\dots\dots\dots\dots\dots\dots(4.19)$$

The output impedance (Z_{outCL}) of the closed-loop MSCCS-TIA is shown in the below equation (4.20).

$$Z_{out_{CL}} = \frac{V_{out}}{I_{out}} = \frac{Z_f}{\left(1 - \dfrac{1}{A_{V_{OL}}}\right)} = \frac{R_f}{\left(1 + R_f C_f s\right)\left(1 - \dfrac{1}{A_{V_{OL}}}\right)} \dots\dots\dots\dots\dots\dots(4.20)$$

4.3.2   Noise Analysis
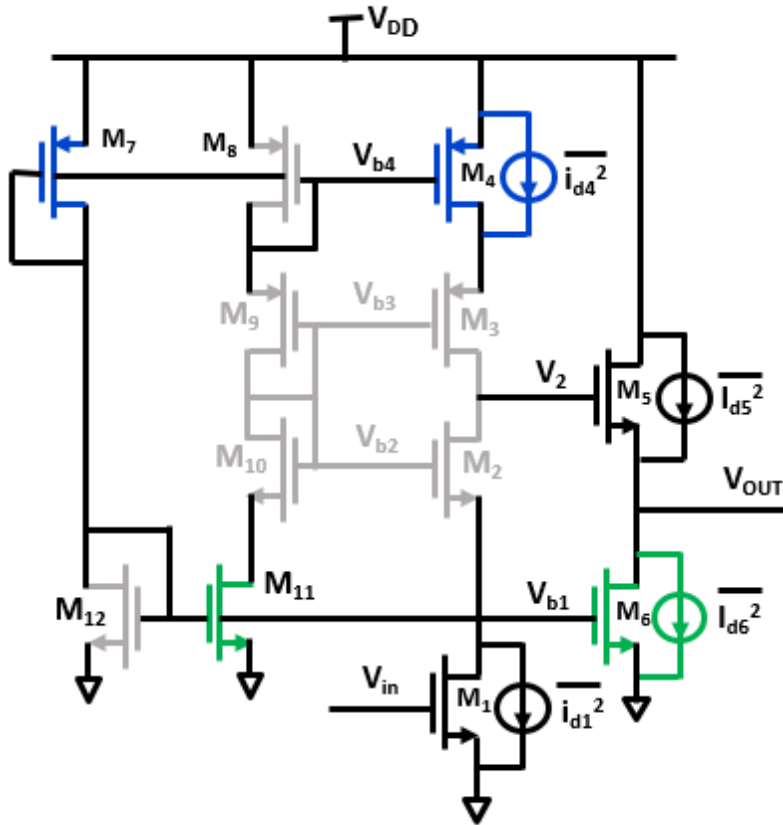
Figure 4.6 Noise model of MSCCS amplifier.

The voltage noise of the amplifier is one of the most significant components in achieving lower noise. The source follower noise contribution can be neglected to simplify the analysis. The Figure 4.6 shows the noise model of MSCCS amplifier. The noise current in a MOS transistor is given by both thermal noise and flicker noise are modeled by a current source connected between drain and source terminals [113-114] which is given by following expression (4.21).

$$\overline{i_d^2} = \underbrace{4kT\gamma g_m}_{Thermal\,noise} + \underbrace{\frac{K_f}{C_{ox}W.L} \cdot \frac{1}{f} \cdot g_m^2}_{Flic\,ker\,noise} \quad \text{...(4.21)}$$

where $k = 1.3807 \times 10^{-23} J/K$ is the Boltzmann constant, T is temperature, g_m is the transconductance, K_f is a constant related to the interface state density of the MOS structure, C_{ox} is the gate capacitance, W is the channel width, L is the channel length, and f is frequency.

The primary noise sources of the MSCCS amplifier with biasing circuit are M_1, M_4-M_7, M_6-M_{11} and M_5. The total noise current sources of the MSCCS amplifier with the biasing circuit is shown in below equation (4.22) and (4.23).

$$\overline{i_{d,tot}^2} = \overline{i_{d1}^2} + \overline{i_{d4,7}^2} + \overline{i_{d6,11}^2} + \overline{i_{d5}^2} \dots\dots\dots\dots\dots\dots\dots\dots\dots\dots\dots\dots\dots\dots\dots(4.22)$$

$$\overline{i_{d,tot}^2} = 4kT\gamma(g_{m1} + g_{m4,7} + g_{m6,11} + g_{m5}) + \frac{K_f}{C_{ox}f.L}\left(\frac{g_{m1}^2}{W_1} + \frac{g_{m4,7}^2}{W_{4,7}} + \frac{g_{m6,11}^2}{W_{6,11}} + \frac{g_{m5}^2}{W_5}\right)(4.23)$$

The output voltage noise of the MSCCS amplifier is given by equation (4.24) and (4.25).

$$V_{n,out}^2 = \left[\frac{4kT\gamma}{g_{m1}} + \frac{4kT\gamma g_{m4,7}}{g_{m1}^2} + \frac{4kT\gamma}{g_{m5}} + \frac{4kT\gamma g_{m6,11}}{g_{m5}^2}\right]\dots\dots\dots\dots\dots\dots\dots\dots(4.24)$$

$$V_{n,out}^2 = \frac{I_{n1}^2}{g_{m1}^2} + \frac{I_{n4,7}^2}{g_{m1}^2} + \frac{I_{n5}^2}{g_{m5}^2} + \frac{I_{n6,11}^2}{g_{m5}^2} + \left[\frac{K_f}{C_{ox}f.W_1.L_1} + \frac{K_f}{C_{ox}f.L_{4,7}}\frac{g_{m4,7}^2}{W_{4,7}g_{m1}^2} + \frac{K_f}{C_{ox}f.W_5.L_5} + \frac{K_f}{C_{ox}f.L_{6,11}}\frac{g_{m6,11}^2}{W_{6,11}g_{m5}^2}\right]\dots(4.25)$$

From the equation (4.25), the MSCCS amplifier voltage noise can be minimized by increasing the transconductance g_{m1}. When the transistor operates in saturation region, the equation of g_{m1} is given in (4.26).

$$g_{m1} = \sqrt{2\mu_0 C_{ox} I_{D1}\frac{W_1}{L_1}}\dots\dots\dots\dots\dots\dots\dots\dots\dots\dots\dots\dots\dots\dots\dots\dots\dots(4.26)$$

where μ_0 is the mobility, C_{ox} is the gate oxide capacitance, I_{D1} is the brain current, W_1 is the width and L_1 is the length of the transistor.

To minimize the voltage noise, g_{m1} should be higher by making M_1 transistor wider which results in smallest noise.

56

4.3.3   Simulation Results

The proposed MSCCS-TIA is simulated at post-layout level by CADENCE virtuoso custom IC design in 180 nm CMOS technology. The Figure 4.7 shows the layout design of the circuit used for post-layout simulations, which occupies a chip area of 110 μm x 140 μm. The proposed MSCCS-TIA topology shows better performance compared to previous work [99, 91, 116-117]. Figure 4.8 shows a DC curve of the proposed MSCCS-TIA. Figure 4.8 shows the transimpedance gain of 1.72 GΩ with a bandwidth of 180 kHz being achieved and Figure 4.9 shows the input referred current noise of 18 fA/√Hz for the proposed MSCCS-TIA. The TIA consumes 52 μW of power from a single supply voltage of 1.4 V. Practically, performance of the circuit suffers from transistor mismatch due to difference in threshold voltage, body effect, and process fluctuations are due to chip to chip dissimilarity in mobility, temperature, and velocity saturation, were evaluated through Monte Carlo simulation.

A Monte-Carlo analysis was performed on the proposed MSCCS-TIA for over 100 random samples to evaluate the circuit performance. From Figure 4.10 it is evident that if both process variation and device mismatch are considered mean gain would be 1.7 GΩ with the standard deviation of 115.6 MΩ. The lower tail of the Monte-Carlo gain plot caused by transistor mismatch. The proposed MSCCS-TIA is a closed loop configuration where the transimpedance amplifier is less susceptible to variations.
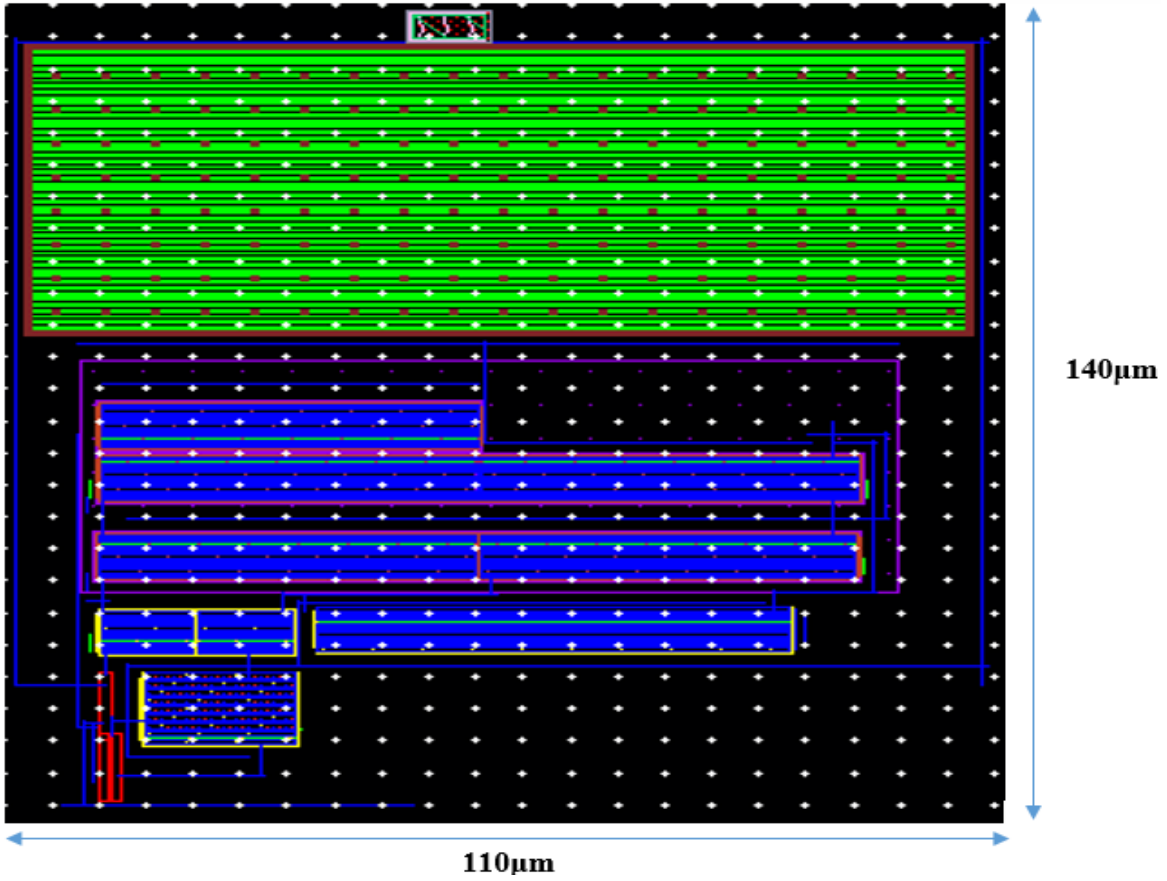
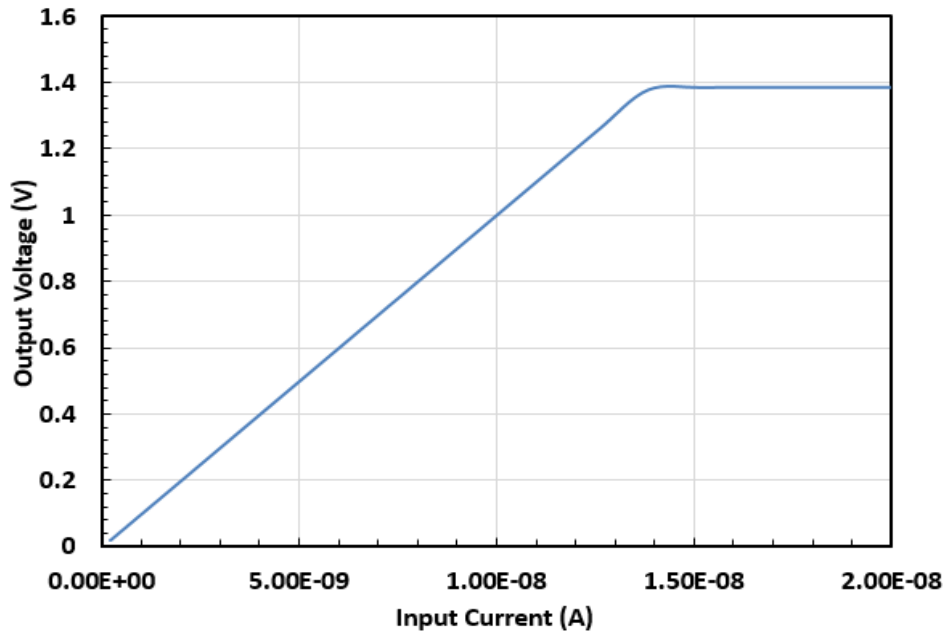Figure 4.7 Layout design of proposed MSCCS-TIA.

Figure 4.8 DC curve of the proposed MSCCS-TIA.
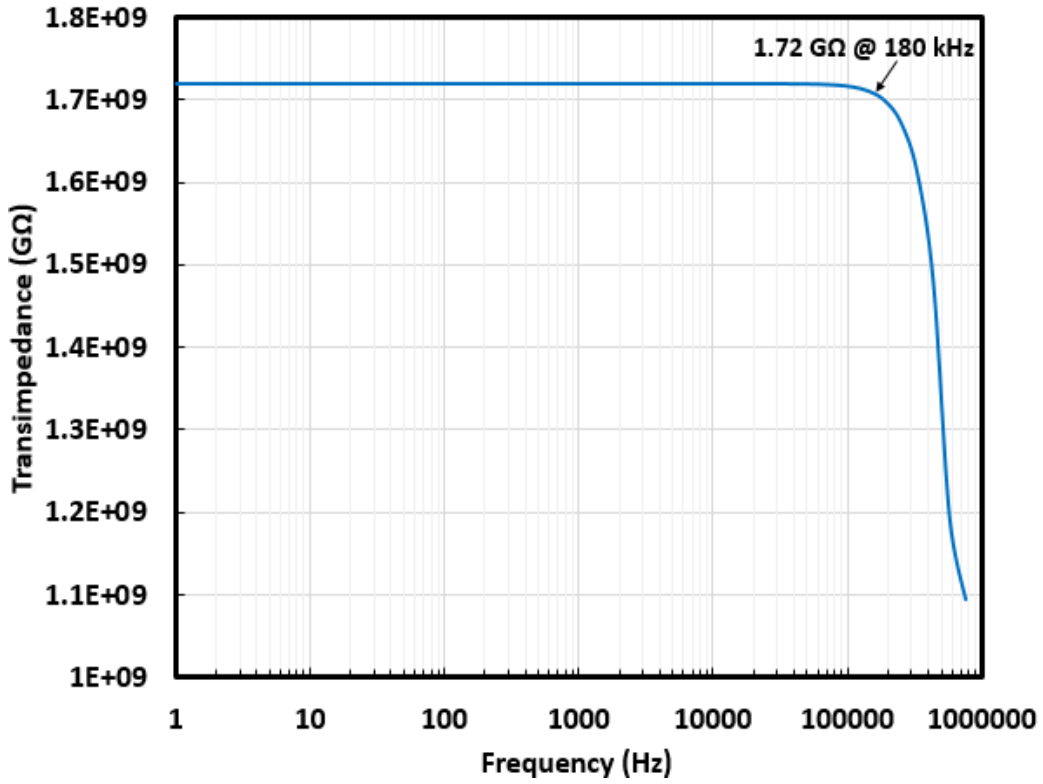
Figure 4.9 Transimpedance gain of proposed MSCCS-TIA.
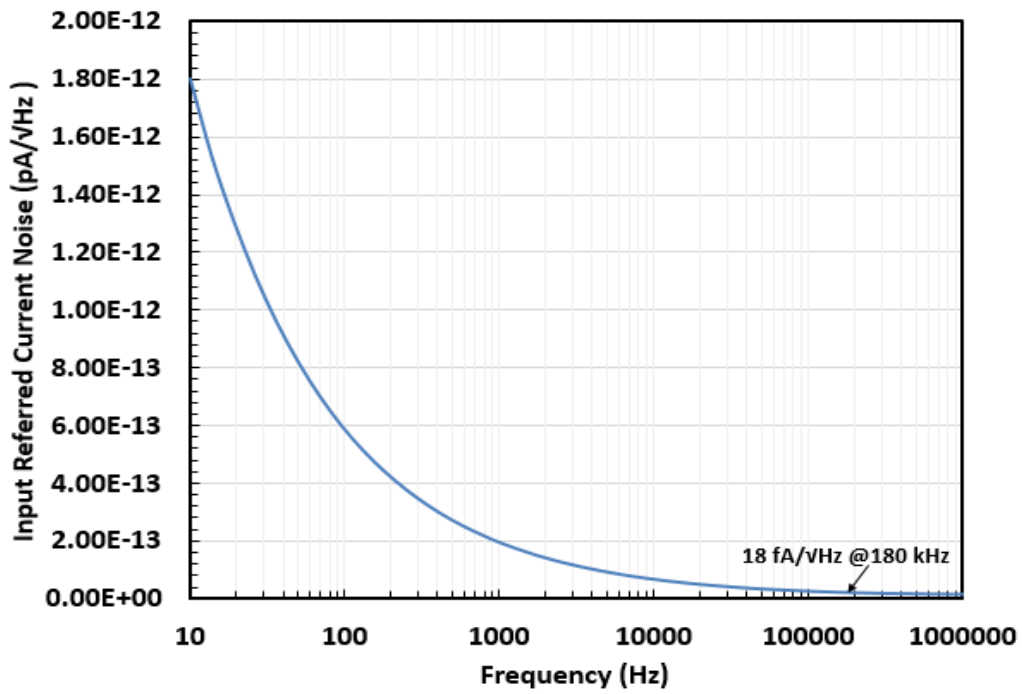
Figure 4.10 Input referred current noise of proposed MSCCS-TIA.
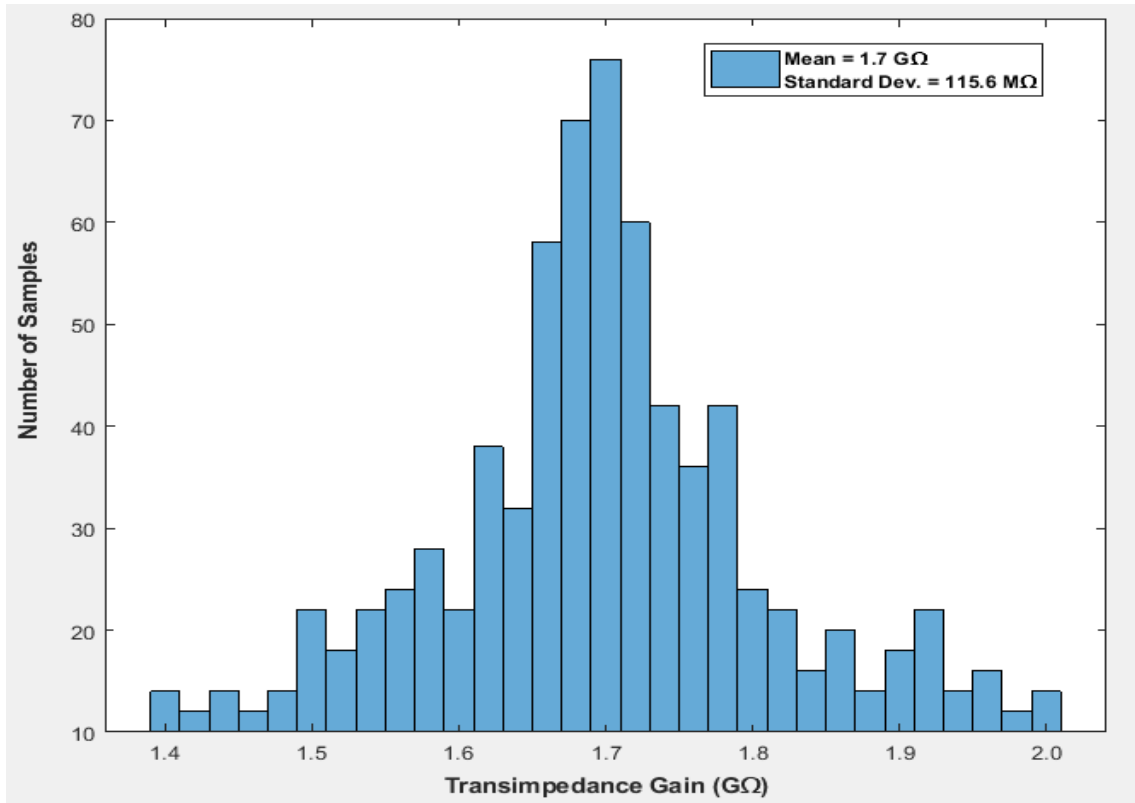
Figure 4.11 Monte Carlo analysis for transimpedance gain of proposed MSCCS-TIA.

4.4 Performance Comparison

Table 4.2 compares proposed MSCCS-TIA design with several previously reported CMOS TIAs for biosensors [99], [91], [116], and [117]. From Table 4.2, it can be seen that the proposed MSCCS-TIA circuit has a significant improvement in performance showing low-noise, better gain, less power dissipation, better figure of merit (FOM) and reduced footprint compared to conventional CMOS based TIAs.

A widely accepted figure of merit (FOM) for the TIA performance is

$$FOM = \frac{G.BW}{P_{diss}.IRCN} \dots\dots\dots\dots\dots\dots\dots\dots\dots\dots\dots\dots\dots\dots\dots\dots\dots\dots\dots\dots\dots\dots\dots\dots\dots\dots\dots(4.29)$$

where G is the gain, BW is the bandwidth, P_{diss} is the average power dissipation and IRCN is the input referred current noise.

Table 4.2 Comparison of MSCCS-TIA performance with prior state-of-the art TIAs.

Reference	[99]	[91]	[116]	[117]	Proposed MSCCS-TIA
Applications	Biosensor	Biosensor	Biosensor	Biosensor	**Biosensor**
Technology	CMOS 130 nm	CMOS 180 nm	CMOS 350 nm	CMOS 180 nm	**CMOS 180 nm**
Input Current	30 μA	500 nA	20 μA	~150 nA	**200 pA**
Transimpedance Gain	3.5 MΩ	40 kΩ	0.042 MΩ	1 MΩ	**1.72 GΩ**
Bandwidth	500 Hz	12.72 kHz	800 kHz	100 Hz	**180 kHz**
Power Consumption	26.4 μW	71.7 μW	9.3 mW	62.8 μW	**52 μW**
Supply Voltage	1.2 V	1.8 V	3.3 V	1.2 V	**1.4 V**
Input referred current noise	260 pA/√Hz	8.1 nA/√Hz	0.47 pA/√Hz	3.34 pA/√Hz	**18 fA/√Hz**
Figure of Merit	2.53×10^{26}	8.76×10^{20}	7.68×10^{24}	4.76×10^{23}	**3.3×10^{32}**

4.5   Discussion

In this chapter, a multi-stage cascode common source TIA (MSCCS-TIA) topology has been developed for amperometric based continuous blood glucose monitoring systems for wearable devices. A fully integrated CMOS based MSCCS-TIA exhibits improved performance in terms of low-noise, low-power consumption and high transimpedance gain has been demonstrated in this work. The proposed MSCCS-TIA is a highly reliable and robust design, which consumes 52 μW of power from 1.4 V voltage supply. The TIA shows a high transimpedance gain of 1.72 GΩ with a bandwidth of 180 kHz and input referred current noise of 18 fA/√Hz. The transimpedance amplifier were implemented in a 180 nm CMOS technology and the chip area of 110 μm x 140 μm. These results provide the bases for utilizing this MSCCS-TIA for integrated biosensing applications requiring very high sensitive readout circuitry for low-noise and low-power front end amplification. To further optimize the integrated circuit for the glucose sensing system, this works will also evaluate a design for the potentiostat circuit configuration.

Chapter 5: Chronoamperometric Potentiostat for ENFM Based Glucose Sensor

5.1   Introduction

This chapter presents a low-voltage, low-noise, low-power and highly integrated 180 nm CMOS potentiostat for miniaturized electrospun-nanofibrous-membrane (ENFM) based amperometric glucose sensor. The electrochemical current from the glucose sensor ranges from 200 nA to 20 µA, has been detected by the sensing unit with a high degree of linearity, and the current depends on glucose concentration in the blood. The proposed potentiostat circuit includes both voltage control unit (VCU) and transimpedance amplifier (TIA), where both VCU and TIA were implemented using difference-differential telescopic cascode configuration. The simulation results confirm the circuit operation with a low supply voltage of 1.4 V and demonstrate a power consumption of 250 µW.

Potentiostats are generally used for electrochemical analysis such as chronoamperometry, cyclic voltammetry, and impedance spectroscopy [118-121] and are a popular choice of measurement in amperometric biosensors [122-124]. A general design for applying constant voltages and measuring the current in an electrochemical cell requires both positive and negative power supplies for the circuits [125]. Some designs have sacrificed the exact potential that has to be applied between working and reference electrodes for the operation of the circuit with a single supply [126].

Potentiostat circuit required for three electrode electrochemical sensors consists of two parts, a voltage control unit (VCU) and transimpedance amplifier (TIA). Different configurations

are used to design the TIA, one of which is an instrumentation amplifier. This instrumentation amplifier uses a large number of components generating high noise making it difficult to measure low current level [127-128]. A switched capacitor configuration in a more complex TIA helps to overcome the thermal noise in the feedback resistance, but the substrate noise due to digital switching remains an issue for output linearity [129-130].

Furthermore, when using a current mirror configuration in a TIA design for biosensing, to control the cell potential a single-ended output was used [131-132], which limits the current measurement in only one direction and causes nonlinearity at high current levels [133]. With the recent advancement in the bioelectronics arena, increasing demand for power reduction in potentiostats has presented a challenge to the industry. In a robust integrated circuitry, very low-power consumption, high current accuracy and low-noise performance is essential [134,136].
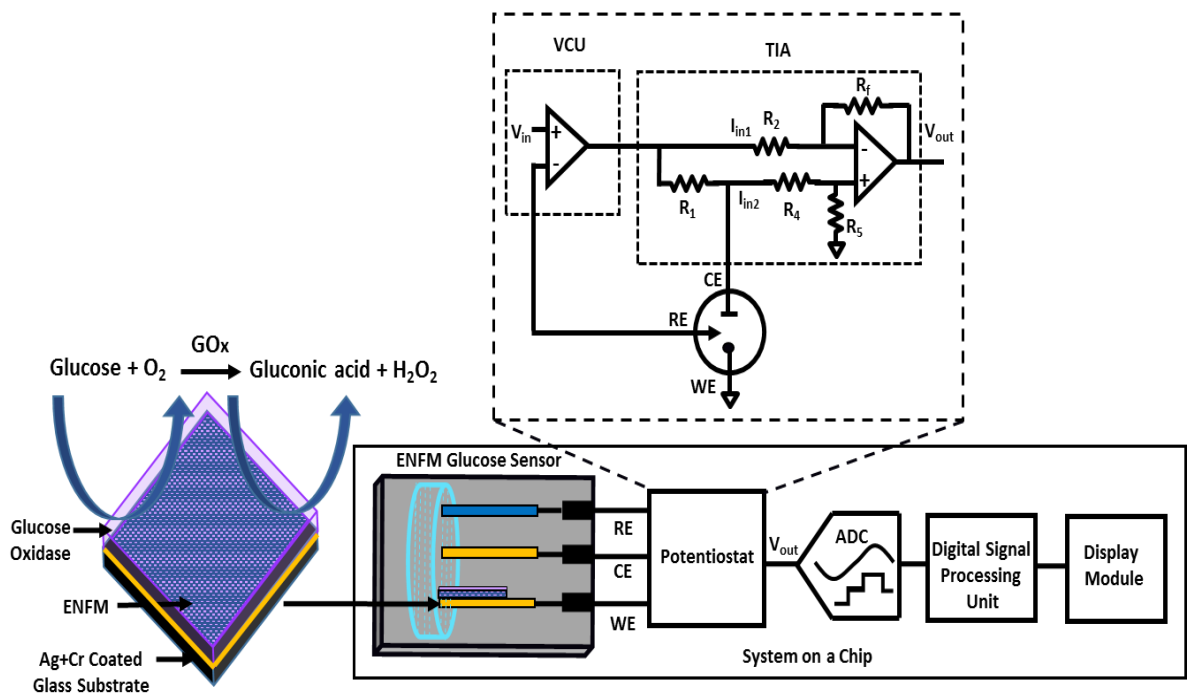

Figure 5.1   Pictorial representation of the electrochemical test setup of ENFM based chronoamperometric blood glucose sensing system.

The proposed potentiostat sensing system achieves competitive performance in terms of low-noise, high gain, increased linearity and stability with a significantly lower-power and less area compared to the prior state-of-the-art potentiostats [135, 137-140]. As shown in Figure 4.1, the proposed CMOS based potentiostat circuit (VCU and TIA) has the potential to be equipped with the ENFM glucose sensor and be integrated with an analog to digital converter (ADC) and a digital signal processing circuit for development of a compact and portable device in the form of a system on a chip.

In Section 5.2, the literature review of various potentiostats were discussed. The proposed potentiostat circuit design were presented in Section 5.3. The performance comparison was discussed in Section 5.4 and the chapter is concluded in Section 5.5.

5.2   Literature Review

The CMOS based potentiostat introduced in 1987 [141], which helped to integrate microelectronics into electrochemical instrumentation for sensing applications. This first original circuit was purposed for a sensing system with two electrodes, where the operational amplifier (OpAmp) acted as a potentiostat. As technology progressed, so did the design for most CMOS based potentiostats, which have more recently been designed using three electrodes in contrast to a two electrode sensing system setup. In the three-electrode sensing structure, the potentiostat maintains constant potential between working electrode (WE) and reference electrode (RE). The counter electrode (CE) provides path for reaction current [142-144].

In its simplest form shown in Figure 5.2 (a), the set up for potentiostat with WE connected to ground can be characterized by an OpAmp component. The non-inverting terminal of the OpAmp is connected to the input voltage (V_{in}), and the inverting terminal is connected to the RE. Hence the constant potential is maintained between WE and RE. In this configuration, the

electrochemical cell potential (V_{cell}) and the input voltage are equal. The output of the OpAmp connects to the CE, and a connective path for the sensing current is provided by the electrochemical cell to the WE which is connected to the ground.
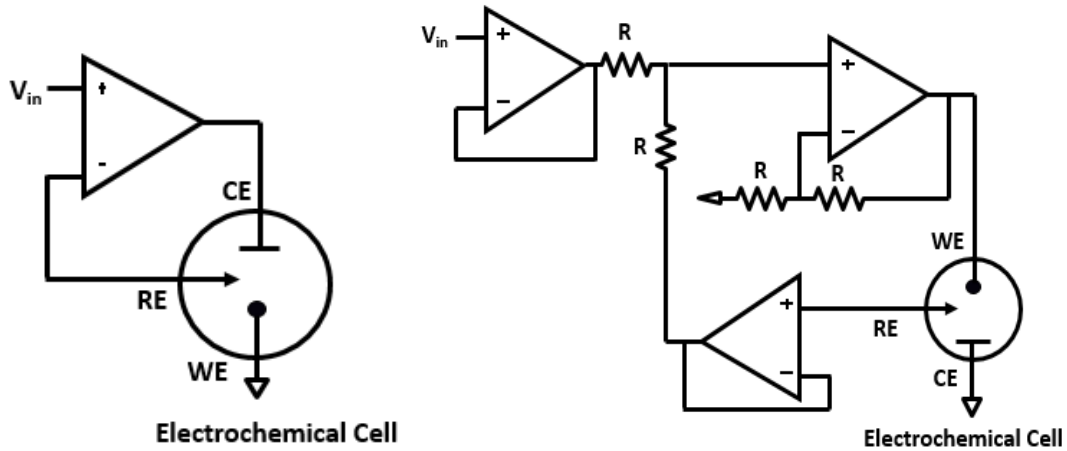

Figure 5.2 Potentiostat with three electrode test set-up (a) WE grounded (b) CE grounded [144].

For the grounded-CE potentiostat configuration (Figure 5.2 (b)), the current response from the sensor is collected by the grounded-CE. Since the WE and RE potentials can both vary over time, for circuit stability it is necessary to maintain V_{cell} is equal to V_{in}. The three OpAmp grounded-CE potentiostat configuration is shown in Figure 5.2 (b). The grounded-CE potentiostat configuration is not used often, and when used, it is generally paired with a uniquely designed electrochemical transducer [145]. Due to intricacy of the grounded-CE configuration most reported potentiostats are based on grounded-WE configuration [146-148].

Figure 5.3 represents the fully-differential potentiostat configuration. The single-ended potentiostat structures have limited advantage because of the power consumption and supply voltage. To overcome this challenge a low-voltage fully-differential CMOS potentiostat circuit can be implemented by dynamically maintaining the constant potential between WE and RE. This potentiostat configuration has double output cell potential compared to a single-ended potentiostat.

Hence fully-differential OpAmp based potentiostat is a very useful configuration in terms of high-speed and low-power consumption.
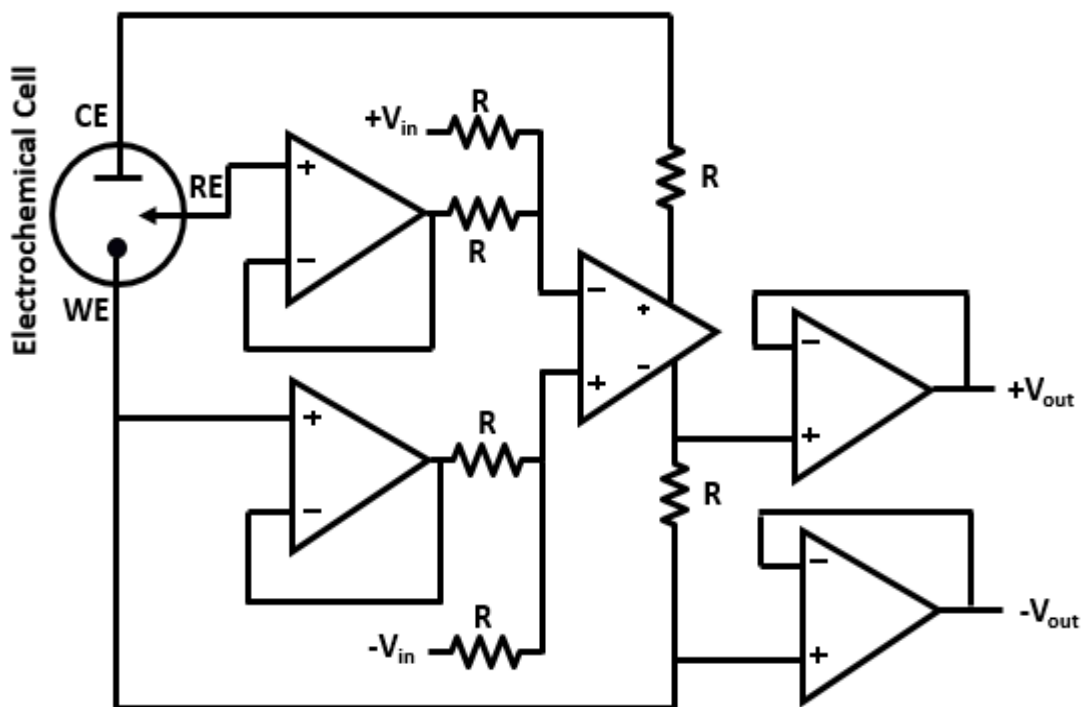

Figure 5.3 Fully-differential OpAmp based potentiostat circuit [142]

5.3 Proposed Low-Power Low-Noise Chronoamperometric Potentiostat Circuit

The potentiostat circuit connected to the electrochemical cell utilizes a three electrode system which includes RE, CE and WE for chronoamperometric measurements. A consistent potential needs to be maintained between the working and the reference electrodes then the electrochemical reaction happens at the WE which is functionalized with the enzyme. The CE provides a path for the sensing current to the grounded WE, and the current through the cell is controlled by the VCU so that the reference electrode always at the fixed potential throughout the reaction.
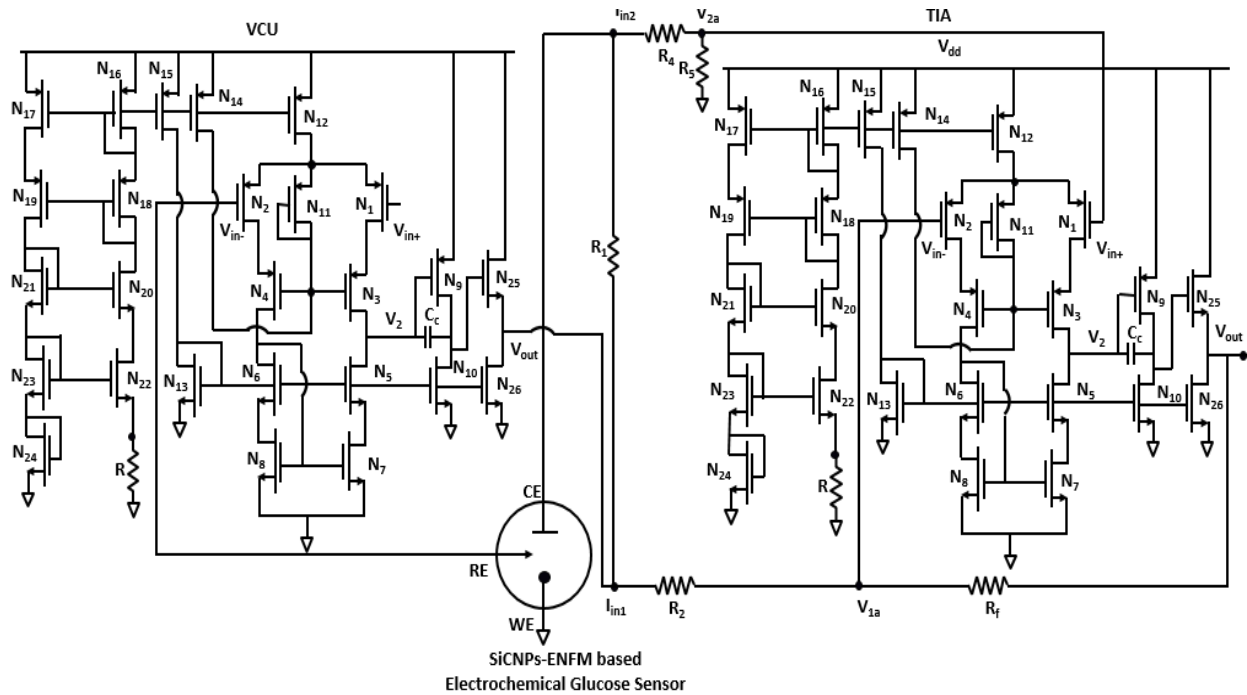
Figure 5.4 Pictorial representation of ENFM based electrochemical glucose sensor with proposed chronoamperometric potentiostat circuit design

Figure 5.4 shows the pictorial representation of proposed potentiostat circuit design with ENFM electrochemical-based glucose sensor, the WE as a ENFM sensing electrode, RE was used as an Ag/AgCl electrode and CE as a gold-coated electrode. The potentiostat circuit consists of both VCU and the electrochemical current measuring / current to voltage converter unit called as TIA. The CMOS based potentiostat circuit was implemented using the proposed multi-stage difference-differential telescopic cascode operational amplifier (OpAmp) configuration.

5.3.1 Multi-Stage Difference-Differential Telescopic Cascode TIA

The proposed multi-stage difference-differential telescopic cascode TIA circuit is represented in Figure 5.5 with a biasing circuit. Transistors are made to operate in a saturation region to get the maximum gain. The bias circuit was designed using the current mirror technique, to minimize the effect of channel length modulation the sizes of current mirrors and cascode amplifier is the same. The resistors R_1, R_2, R_4, R_5, and R_f was implemented using poly resistors

and C_c is the coupling capacitor implemented in the design using a metal-insulator-metal capacitor (MIMCAP) device by gpdk180 nm CMOS library.
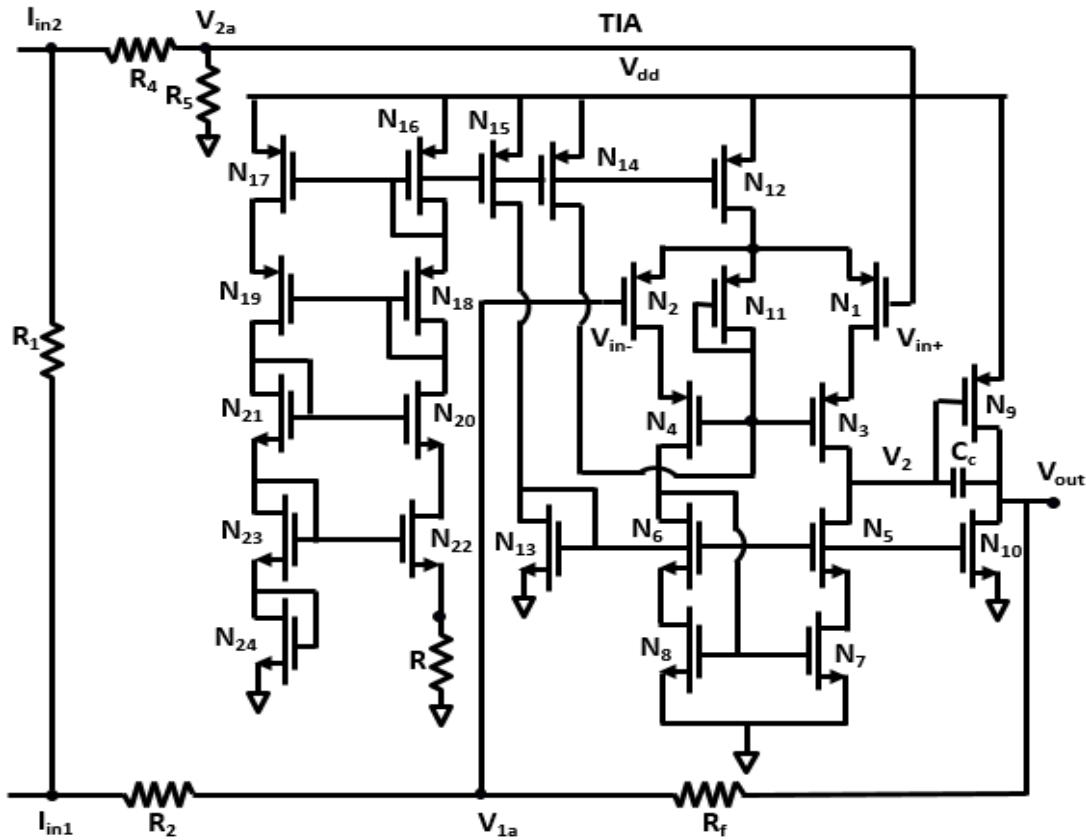

Figure 5.5 Multi-stage difference-differential telescopic cascode TIA

The multi-stage difference-differential telescopic cascode TIA amplifies the difference between two signals, it rejects any common signals to the two input terminals (I_{in1} and I_{in2}).

The circuit is shown in Figure. 5.5, with inputs I_{in1} and I_{in2}. To analyze the circuit, we will use superposition and virtual short concept. If the input $I_{in2} = 0$, then there is no current in R_4 and R_5; therefore $V_{2a} = 0$. The resulting circuit acts as an inverting amplifier.

$$V_{o1} = -\frac{R_f}{R_2}I_{in1}$$ .... (5.1)

If the input $I_{in1}=0$, since the current into the amplifier is zero, R_4 and R_5 form a voltage divider. Therefore,

$$V_{2a} = \frac{R_5}{R_4 + R_5} I_{in2} \quad\text{..} \quad (5.2)$$

from the virtual short concept, $V_{1a}=V_{2a}$ and the circuit becomes a non-inverting amplifier, for which

$$V_{o2} = \left(1+\frac{R_f}{R_2}\right)V_{1a} = \left(1+\frac{R_f}{R_2}\right)V_{2a} \quad\text{..} \quad (5.3)$$

substituting (5.2) into (5.3), we obtain (5.4)

$$V_{o2} = \left(1+\frac{R_f}{R_2}\right)\left(\frac{R_5}{R_4 + R_5}\right)I_{in2} \quad\text{..} \quad (5.4)$$

since the net output voltage is the sum of individual terms,

$$V_o = V_{o1} + V_{o2} \quad\text{..} \quad (5.5)$$

$$V_o = \left(1+\frac{R_f}{R_2}\right)\left(\frac{R_5}{R_4 + R_5}\right)I_{in2} - \left(\frac{R_f}{R_2}\right)I_{in1} \quad\text{..} \quad (5.6)$$

if $\frac{R_5}{R_4} = \frac{R_f}{R_2}$ .... (5.7)

where I_{in1} & $I_{in2} \approx I_{cell}$ is the current across the resistor R_1 and the $R_1 << R_f$ and R_2 therefore,

$$V_o = \frac{R_f}{R_2} R_1 I_{cell} \quad\text{...} \quad (5.8)$$

5.3.2   Small Signal Analysis of Multi-Stage Differential Telescopic Cascode OpAmp

The multi-stage difference-differential telescopic cascode OpAmp configuration consisting of N_1 and N_3 transistors has a high output resistance and the cascode load was replaced by a cascode current source load as shown in Figure 5.6. The coupling capacitor C_c was used to improve the stability of the amplifier. It was most efficient to consider the output resistance of this circuit. Figure 5.6 shows the small signal analysis of a multi-stage difference-differential telescopic cascode OpAmp and small-signal output resistance R_{out} for the first stage OpAmp can be found using (5.9) and the overall open-loop output impedance is shown in equation (5.10).

$$R_{out} = [(g_{m3,4}r_{ds3,4} + 1)r_{ds1,2} + r_{ds3,4}] \| [(g_{m5,6}r_{ds5,6} + 1)r_{ds7,8} + r_{ds5,6})]$$

$$R_{out} = (g_{m3,4}r_{ds3,4}r_{ds1,2}) \| (g_{m5,6}r_{ds5,6}r_{ds7,8}) \quad \text{...................................} (5.9)$$

$$Z_{out_{OL}} = \frac{V_{out}}{I_{out}} = (r_{ds25} \| r_{ds26}) \text{..} (5.10)$$
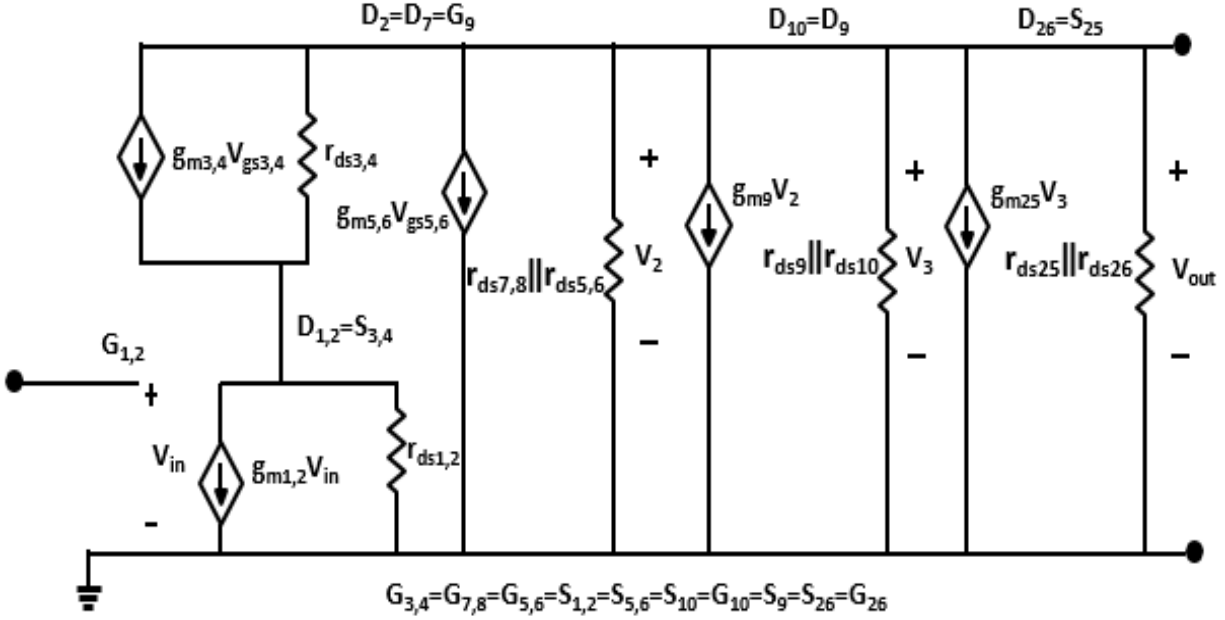

Figure 5.6 Small signal analysis of a multi-stage differential telescopic cascode OpAmp

The open loop gain was calculated from differential inputs (V_{in1} -V_{in2}) to the single-ended output V_2, which was shown in (5.11).

$$A_{V2} = \frac{V_2}{V_{in1} - V_{in2}} = \left(-g_{m1,2} \frac{g_{m3,4}g_{m7,8}r_{ds1,2}r_{ds3,4}r_{ds7,8}r_{ds5,6}}{g_{m3,4}r_{ds3,4}r_{ds1,2} + g_{m7,8}r_{ds7,8}r_{ds5,6}} \right) \text{.................................} (5.11)$$

To find the total gain of the amplifier from V_{in} to V_{out}, we need to consider a common source amplifier gain. The common source amplifier gain is given as.

$$A_{V3} = -g_{m9} (r_{ds9} \| r_{ds10}) \text{...} (5.12)$$

$$A_{V3} = \frac{V_{out}}{V_2} = \left(-g_{m9} \frac{r_{ds9} \cdot r_{ds10}}{r_{ds9} + r_{ds10}} \right) \text{...} (5.13)$$

$$A_{V4} = \frac{V_{out}}{V_3} \leq 1 \ \dots\dots\dots\dots\dots\dots\dots\dots\dots\dots\dots\dots\dots\dots\dots\dots\dots\dots\dots\dots\dots\dots\dots\dots\dots \ (5.14)$$

substitute (5.11), (5.13) and (5.14) in the (5.15), then the total open-loop gain of the multi-stage differential telescopic cascode amplifier becomes:

$$A_V = A_{V2}.A_{V3}.A_{V4} = \frac{V_{out}}{V_{in}} = \left(-g_{m1,2} \frac{g_{m3,4} g_{m7,8} r_{ds1,2} r_{ds3,4} r_{ds7,8} r_{ds5,6}}{g_{m3,4} r_{ds3,4} r_{ds1,2} + g_{m7,8} r_{ds7,8} r_{ds5,6}} \right) \left(-g_{m9} \frac{r_{ds9}.r_{ds10}}{r_{ds9} + r_{ds10}} \right) \ \dots\dots\dots\dots\dots\dots\dots\dots\dots \ (5.15)$$

5.3.3   Noise Analysis of Multi-Stage Differential Telescopic Cascode OpAmp

Let's consider the noise analysis of a multi-stage differential telescopic cascode OpAmp as shown in Figure. 5.7 .The primary noise sources of the amplifier are N_1-N_2, N_5-N_6 and N_9. The input-referred noise voltage per unit bandwidth is given by both the thermal noise and flicker noise are expressed in (5.16):

$$\overline{V_{n,in}^2} = 4kT \underbrace{\left(2\frac{2}{3g_{m1,2}} + 2\frac{2g_{m7,8}}{3g_{m1,2}^2} + \frac{2}{3g_{m9}} + \frac{2g_{m10}}{3g_{m9}^2} + \frac{2}{3g_{m25}} + \frac{2g_{m26}}{3g_{m25}^2} \right)}_{Thermal\,noise} + \underbrace{2\frac{K_N}{C_{ox}(W.L)_{1,2}}.\frac{1}{f} + 2\frac{K_P}{C_{ox}(W.L)_{7,8}}.\frac{1}{f}.\frac{g_{m7,8}^2}{g_{m1,2}^2}}_{Flicker\,noise}$$

$$+ \underbrace{\frac{K_P}{C_{ox}(W.L)_9}.\frac{1}{f} + \frac{K_N}{C_{ox}(W.L)_{10}}.\frac{1}{f}.\frac{g_{m10}^2}{g_{m9}^2} + \frac{K_P}{C_{ox}(W.L)_{25}}.\frac{1}{f} + \frac{K_N}{C_{ox}(W.L)_{26}}.\frac{1}{f}.\frac{g_{m26}^2}{g_{m25}^2}}_{Flicker\,noise} \quad \dots\dots \ (5.16)$$

where K_N and K_P are the flicker noise coefficients of NMOS and PMOS transistors, f is the frequency, g_m is the transconductance, C_{ox} is the oxide gate capacitance, W is the channel width and L is length of transistors.
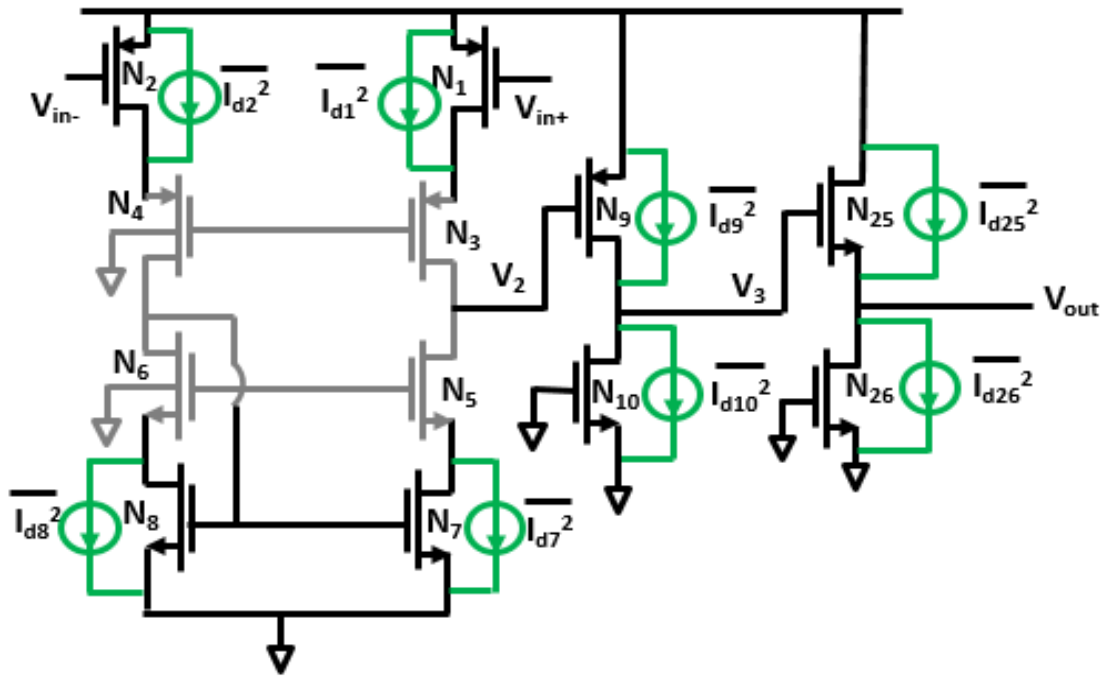
Figure 5.7 Noise analysis of a multi-stage differential telescopic cascode OpAmp

The output voltage of the noisy circuit when its input is open:

$$\overline{V_{n,out}^2} = \overline{V_{n,in}^2}.A_V^2 \quad \text{.. (5.17)}$$

In this OpAmp configuration the input transistors are PMOS which has holes are the majority charge carriers which offers less noise compared to NMOS transistors. Hence by making the PMOS transistor width larger, then the input-referred noise voltage can be further minimized

5.3.4   Simulation Results

The proposed chronoamperometric potentiostat circuit topology shows better performance compared to previous work [135,137-139]. The VCU requires a high gain amplifier to maintain a constant voltage difference by regulating the current. The TIA needs to have a low-noise and high gain to satisfy the output voltage swing for the maximum electrochemical current from ENFM sensing electrode of 20 µA. The VCU and TIA in the potentiostat was designed using multi-stage differential telescopic cascode OpAmp topology, which has a 98 dB open loop gain and 72° phase

margin with a 10 kHz bandwidth. Figure 5.8 shows the input-referred noise current response of the proposed multi-stage differential telescopic cascode OpAmp was 11 fA/√Hz at 10 kHz. Figure 5.9 shows the simulated open loop gain and phase responses of the multi- stage difference-differential telescopic cascode OpAmp. The total power consumption of the proposed chronoamperometric potentiostat was 250 μW from a single supply voltage of 1.4 V.
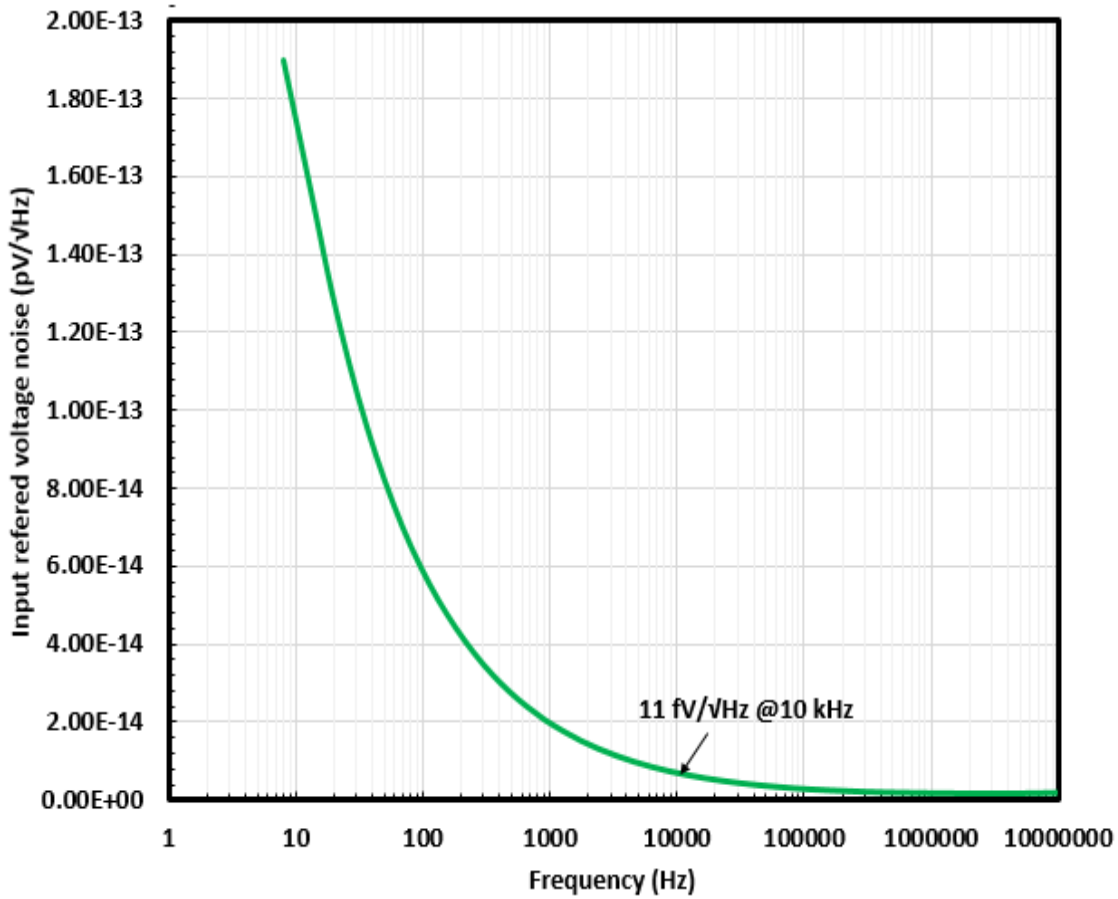

Figure 5.8 The input-referred noise current response of the proposed multi-stage differential telescopic cascode OpAmp.
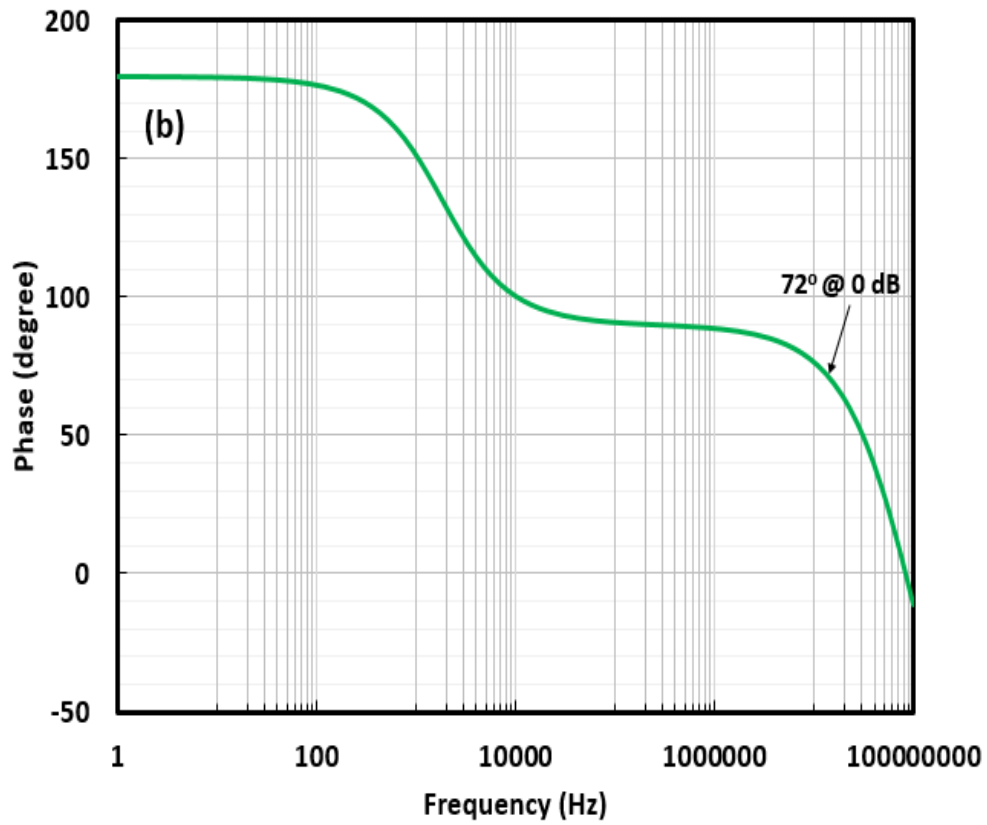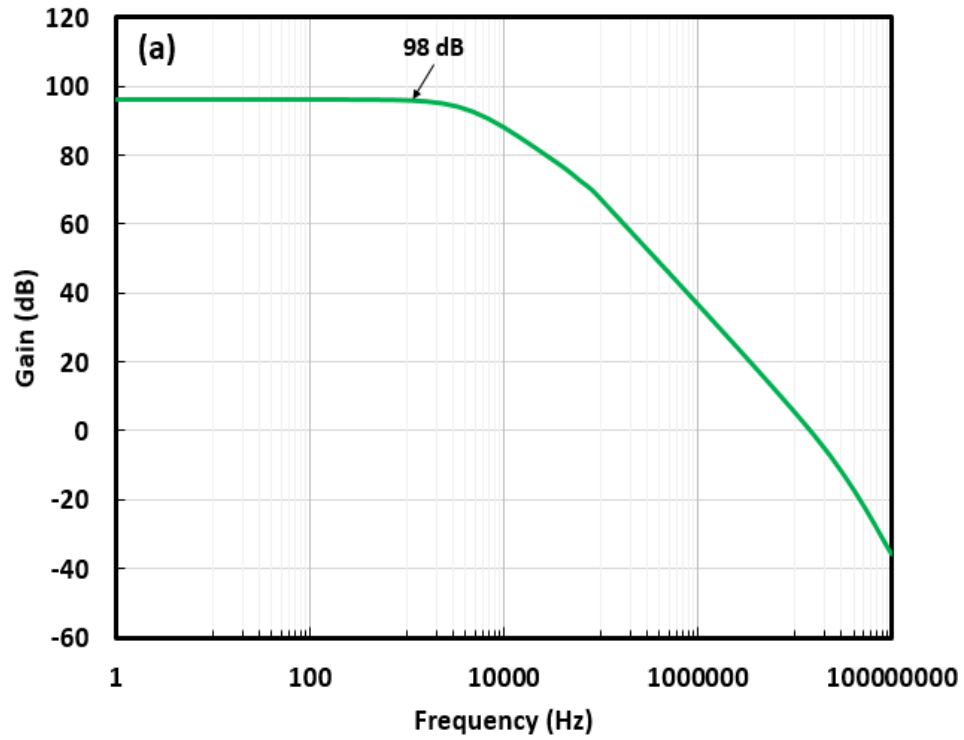
Figure 5.9 The (a) open-loop gain and (b) the phase response of a proposed multi-stage
difference differential telescopic cascode OpAmp.

5.4   Performance Comparison

Table 5.1 Comparison of proposed potentiostat with prior state-of-the-art potentiostats.

Reference	[135]	[137]	[138]	[139]	**This Work**
Applications	Bio sensor	Bio sensor	Bio sensor	Gas sensor	**Bio sensor**
Technology	CMOS 350 nm	CMOS 0.5 μm	CMOS 180 nm	CMOS 0.5 μm	**CMOS 180 nm**
Sensing Electrode	Micro needle	Nanopore	MEA	RTIL arrays	**ENFM**
Input Current Range	5 μA- 30 μA	-10 pA- 10 pA	200 pA – 50 nA	127 nA – 16 μA	**200 nA – 20 μA**
Power Consumption	5.1 mW	380 μW	3.21 mW	241 μW	**250 μW**
Supply Voltage	1. 65 V	3.3V	1.8 V	5 V	**1.4 V**
Input Referred Noise Current	0.14 μA/ √Hz	3 pA/ √Hz	0.48 pA/ √Hz	3.1 pA/ √Hz	**11 fA/ √Hz**

Table 5.1 depicts the comparative study of formerly reported CMOS based chronoamperometric potentiostats [135], [137], [138], and [139]. From the Table 5.1, it can be observed that the proposed potentiostat circuit has a significant improvement in performance showing low noise, better gain, less-power dissipation, and lower footprint compared to conventional CMOS based potentiostats.

5.5   Discussion

In this chapter, a chronoamperometric potentiostat circuit has been developed for ENFM based amperometric glucose sensor. A fully integrated CMOS based potentiostat demonstrates improved performance in terms of low-voltage, low-noise, low-power consumption, high-gain, and miniaturized design. The proposed potentiostat includes both VCU and TIA which was designed using differential telescopic cascode OpAmp configuration, which consumes 250 μW of power from 1.4 V voltage supply and a detection range of 200 nA to 20 μA. The potentiostat shows a high gain of 98 dB, better phase margin 72° with a bandwidth of 10 kHz and the input-referred

noise current of 11 fA/√Hz. The chronoamperometric potentiostat was implemented in 180 nm CMOS technology. The fabricated enzyme immobilized ENFM based sensing electrode demonstrates the sensitivity of 10.22 µA/mM cm^2 in a glucose solution and it can be used for up to 60 days. These results provide the basis for utilizing this proposed low-noise and low-power potentiostat circuit design for integrated biosensing applications.

Chapter 6: Conclusions and Future Work

6.1 Conclusions

Although the wearable and portable devices are the pillar of modern and smart societies, a large portion of its infrastructure stills under development, operates with poor monitoring and automation, and lacks sufficient communication among its components. Moreover, demand for wearable devices is expected to increase in the coming years. This situation presents a unique opportunity in history for electrical engineers to design novel strategies that allow the point-of-care diagnostics to satisfy the increasing demand of wearable devices. Current sensor technology requires large area and the use of several device components, making the devices bulky and more cumbersome to wear during continuous monitoring. The proposed innovation will provide a device technology design that reduces the number of device components, uses less power, is light weight, and makes the technology smaller and easier to handle and carry, while enhancing the sensitivity of the measurement – primarily changing the face of wearable and flexible devices.

This dissertation work presents, a comparative analysis of conductive polymer SCTF and ENFM; SiCNPs-SCTF and SiCNPs-ENFM based electrochemical enzymatic glucose sensing electrodes. The chronoamperometric analysis results demonstrated that the SiCNPs-ENFM based glucose sensor provides enhanced sensitivity, better limit of detection (LOD), good stability, and fast response time compared to ENFM, SCTF and SiCNPs-SCTF based sensing electrodes however ENFM electrode shows the better durability compared to SiCNPs-ENFM electrode. Hence ENFM based glucose sensing electrode is suitable for long term implantable glucose

sensors with the integration of proposed potentiostat for continuous blood glucose monitoring systems.

The novel TIA was designed in multi-stage cascode common source TIA configuration and simulated in 180 nm CMOS process which demonstrates improved performance in terms of low-noise, low-power consumption, high gain and miniaturized design. The novel potentiostat were implemented using multi-stage difference-differential telescopic cascode operational amplifier configuration and simulated with 180 nm CMOS technology library. The simulation results confirm that the circuit operation with a supply voltage of 1.4 V and demonstrates a power consumption of 250 µW. The integration of ENFM glucose sensor with proposed potentiostat for continuous monitoring of blood glucose level, provides the basis for future wearable and portable biosensors.

6.2   Future Work

There are several future paths of innovative work that can be anticipated following these transformative results. An integrated system with a CMOS based low-power, low-noise potentiostat circuit and silicon carbide nanoparticles (SiCNPs) based ENFM glucose sensor on a single chip for wearable continuous blood glucose monitoring systems. The integration of sensor and the IC in a single chip will compliment circuit miniaturization, and process implementation which is strategic for scaling implantable, wearable and portable biosensing devices. For integrated systems on a chip, this also reduces the parasitics, resulting in an increase in the overall speed of the device.

As a proof of concept we did simulation on Si-MOSFET based potentiostat circuit because the GPDK library was reliable for Si-MOSFET based simulation. All ready SiC-MOSFETs (silicon-carbide-metal-oxide-field-effect-transistors) are in the market hence our simulation on Si-

MOSFET based potentiostat circuit shows that it is feasible for the response that we want, so there is no reason that it wouldn't work for the SiC-MOSFETs based potentiostat. Hence the SiC-MOSFETs based potentiostat circuit could be a feasible and a potential configuration with the integration of glucose sensors for future biosensing applications.

References

[1] "Biosensors Market Size, Share & Trends Analysis Report By Application (Medical, Agriculture, Bioreactor) By Technology (Thermal, Electrochemical, Optical), By End Use, By Region, And Segment Forecasts, 2020 - 2027" [Online] Available: https://www.grandviewresearch.com/industry-analysis/biosensors-market-2020. [Accessed: Jan 2020].

[2] "Smartphone Users Worldwide Will Total 1.75 Billion in 2014," [Online]. Available: http://www.emarketer.com/Article/Smartphone-Users-Worldwide-Will-Total-175Billion 2014/1010536. [Accessed: 30-May-2014].

[3] C. Idlebrook, "39 Potential New Continuous Glucose Monitors for Diabetes," *Diabetes Mine*, 2020.

[4] T. Battelino, K. Dovc, and B. W. Bode, "Continuous and Intermittent Glucose Monitoring in 2019," *Diabetes Tech. & Therap.*, vol. 22, no. 1, pp. 3-16, 2020.

[5] American Diabetes Association, "Diabetes Technology: Standards of Medical Care in Diabetes," *Diabetes Care*, vol. 43, pp. 5-8, 2020.

[6] G.S. Wilson, Y. Zhang, G. Reach, "Progress toward the development of an implantable sensor for glucose," *Clin. Chem.*, vol. 38, no. 9, pp. 1613-7, 1992.

[7] H. E. Koschwanez, and W. M. Reichert, "In vitro, in vivo and post explanation testing of glucose-detecting biosensors: current methods and recommendations," *Biomat.*, vol. 28, no.25, pp. 3687-703, 2007.

[8] P. Saeedi, et. al., "Global and regional diabetes prevalence estimates for 2019 and projections for 2030 and 2045: Results from the International Diabetes Federation Diabetes Atlas, 9th edition," *Diabetes Res. Clini. Prac.*, vol. 157, pp. 1-10, 2019.

[9] E. Renard, "Implantable glucose sensors for diabetes monitoring," *Mini. Inv. Thera. & Alli. Techn.*, vol. 13, pp. 78-86, 2004.

[10] M. R. Burge, et. al., "Continuous Glucose Monitoring: The Future of Diabetes Management," *Diabetes Spect.*, vol. 21, no.2, pp. 112-119, 2008.

[11] Y. Hyeonseok, "Current trends in sensors based on conducting polymer nanomaterials," Nanomaterials, vol. 3, pp. 524–549, 2013

[12]   Y. Yanyan, C. Zuanguang, H. Sijing, Z. Beibei, L. Xinchun, and Y. Meicun, "Direct electrontransfer of glucose oxidase and biosensing for glucose based on PDDA-capped gold nanoparticle modified graphene/multi-walled carbon nanotubes electrode," *Biosens. Bioelectron.,* vol. 52, pp. 147–152, 2014.

[13]   K. Yuna et al., "A glucose sensor based on an organic electrochemical transistor structure using a vapor polymerized poly (3, 4-ethylenedioxythiophene) layer," *Jpn. J. Appl. Phys.*, vol. 49, pp. 1–6, 2010.

[14]   A. B. Engel, M. Bechelany, O. Fontaine, A. Cherifi, D. Cornu, and S. Tingry, "One pot route to gold nanoparticles embedded in electrospun carbon fibers as an efficient catalyst material for hybrid alkaline glucose biofuel cells," *Chem. Electro. Chem.*, vol. 3, pp. 629–637, 2016.

[15]   M. A. Rahman, P. Kumar, D. S. Park, and Y. B. Shim, "Electrochemical sensors based on organic conjugated polymers," *Sensors*, vol. 8, pp. 118–141, 2008.

[16]   Y. Yu, Z. Chen, S. He, B. Zhang, X. Li, and M. Yao, "Direct electron transfer of glucose oxidase and biosensing for glucose based on PDDA-capped gold nanoparticle modified graphene/multi-walled carbon nanotubes electrode," *Biosens. Bioelectron.*, vol. 52, pp. 147–152, 2014.

[17]   S. Y. Yang et al., "Electrochemical transistors with ionic liquids for enzymatic sensing," *Chem. Commun*., vol. 46, pp. 7972–7974, 2010.

[18]   K. Puttananjegowda, A. Takshi, and S. Thomas, "Electrospun nanofibrous structures for electrochemical enzymatic glucose biosensing: A perspective," *J. Electrochem. Soc*., vol. 167, pp. 1–7, 2020.

[19]   J. Liu, M. Agarwal, and K. Varahramyan, "Glucose sensor based on organic thin film transistor using glucose oxidase and conducting polymer," *Sens. Actuators B*, vol. 135, pp. 195–199, 2008.

[20]   K. Puttananjegowda, A. Takshi, and S. Thomas, "An Electrospun Nanofibrous Membrane Based Electrochemical Glucose Sensor," *IEEE Sensors*, vol. 4, no. 2, pp. 1–7, 2020.

[21]   B. A. Young, E. Lin, M. V. Korff, G. Simon, P. Ciechanowski, and E. J. Ludman, "Diabetes complications severity index and risk of mortality, hospitalization, and healthcare utilization," *Am. J. Manag. Care.*, vol. 14, no. 23, pp. ,2008.

[22]   E. S. Huang et al., "Projecting the future diabetes population size and related costs for the US," *Diabetes Care*, vol. 32, pp. 22-29, 2009.

[23]   A. T. Syed, "Is diabetes becoming the biggest epidemic of the twenty-first century?" *Int. J. Health Sci.*, vol 1, no. 8, pp. 24-26, 2007.

[24]   M. R. Burge, "Continuous glucose monitoring: the future of diabetes management," *Diabetes Spectr.*, vol. 21, no. 119, 12-18, 2008.

[25]   O. Schnell, H. Alawi, T. Battelino, et al., "Self-monitoring of blood glucose in type 2 diabetes: recent studies," J. Diabetes Sci Technol., vol. 7, no. 2, pp. 478-488, 2013.

[26]   C. Yang, Y. Huang, B. L. Hassler, R. M. Worden, and A. J. Mason, "Amperometric electrochemical microsystem for a miniaturized protein biosensor array," IEEE *Trans. Biomed. Cir. Syst.,* vol. 3, no. 168, pp. 12-14, 2009.

[27]   A. Heller and B. Feldman, "Electrochemical glucose sensors and their applications in diabetes management," *Chem. Rev.*, vol. 108, no.3, pp. 2502-2511, 2008.

[28]   D. R. Thevenot, K. Toth, R. A. Durst, and G. S. Wilson, "Electrochemical biosensors: recommended definitions and classification," *Biosens. Bioelectron.*, vol. 16, no.5, pp.131-139, 2001.

[29]   N. J. Ronkainen, H. B. Halsall, and W. R. Heineman, "Electro-chemical biosensors," *Chem. Soc. Rev.*, vol. 39, no.3, pp.1763-1769, 2010.

[30]   G. G. Guilbault and G. J. Lubrano, "An enzyme electrode for the amperometric determination of glucose," *Anal. Chim. Acta.*, vol. 64, no. 5, pp. 455-459, 1973.

[31]   E. Sapountzi, M. Braiek, C. Jean-François, N. Jaffrezic-Renault, and F. Lagarde, "Recent advances in electrospun nanofiber interfaces for biosensing devices," *Sensors*, vol. 1, no.5, pp.1887-1889, 2017.

[32]   S. Thomas, R. Khan, K. Puttananjegowda, W. Serrano-Garcia, "Conductive polymers and metal oxide polymeric composites for nanostructures and nanodevices", *Advances in Nanostructured Materials and Nanopatterning Technologies*, pp. 243-271, 2020.

[33]   W. Song, B. Zhao, C. Wang, and X. Lu, "Electrospun nanofibrous materials: a versatile platform for enzyme mimicking and their sensing applications," *Composite Comm.*, vol. 12, no. 1, pp. 23-26, 2019.

[34]   H. B. Seung, R. Jihyeok, Y. P. Chan, W. K. Min, S. Rongjia, K. K. Suresh, and P. T. Jung, "Cu-nanoflower decorated gold nanoparticles-graphene oxide nanofiber as electrochemical biosensor for glucose detection," *Mater. Sci. Eng. C*, vol. 107, no. 5, pp. 110273-110279, 2020.

[35]   A. B. Engel, M. Bechelany, O. Fontaine, A. Cherifi, D. Cornu, and S. Tingry, "One pot route to gold nanoparticles embedded in electrospun carbon fibers as an efficient catalyst material for hybrid alkaline glucose biofuel cells," *Chem Electro Chem.*, vol. 3, no.6, pp. 629-639, 2016.

[36] M. Qianwen, F. Rong, D. Yaping, L. Li, W. Anqing, D. Duan, and Y. Daixin, "Electrospinning of highly dispersed Ni/CoO carbon nanofiber and its application in glucose electrochemical sensor," *J. Electroana. Chem.*, vol. 847, no. 4, pp. 113075-113079, 2019.

[37] M. V. Jose, S. Marx, H. Murata, R. R. Koepsel, and A. J. Russell, "Direct electron transfer in a mediator-free glucose oxidase-based carbon nanotube-coated biosensor," *Carbon*, vol. 50, no. 5, pp. 4010-4019, 2012.

[38] S. J. Updike and G. P. Hicks, "The enzyme electrode," *Nature*, vol. 214, no.9, pp. 986-989, 1967.

[39] K. Chen, W. Chou, L. Liu, Y. Cui, P. Xue, and M. Jia, "Electrochemical sensors fabricated by electrospinning technology: an overview," *Sensors*, vol. 1, no.9, pp. 3676-3683, 2019.

[40] Y. Li, M. A. Abedalwafa, L. Tang, D. Li, and W. Lu, "Electrospun nanofibers for sensors," *Electrospinning: Nanofabrication and Applications*, vol. 30, no. 8, pp. 571-579, 2019.

[41] H. Jianshe and Y. Tianyan, "Electrospun nanofibers: from rational design, fabrication to electrochemical sensing applications," *Adv. Nanofibers*, vol. 35, no. 9, pp. 571-591, 2013.

[42] L. Matlock-Colangelo and A. J. Baeumner, "Biologically inspired nanofibers for use in translational bioanalytical systems," *Annu. Rev. Anal. Chem.*, vol. 7, no. 8, pp. 23-24, 2014.

[43] F. Arduini, C. Zanardi, S. Cinti, F. Terzi, D. Moscone, G. Palleschi, and R. Seeber, "Effective electrochemical sensor based on screen-printed electrodes modified with a carbon black-Au nanoparticles composite," *Sens. Actuators B Chem.*, vol.212, no.9, pp. 536-542, 2015.

[44] Z. G. Wang, Y. Wang, H. Xu, G. Li, and Z. K. Xu, "Carbon nanotube-filled nanofibrous membranes electrospun from poly (acrylonitrile-co-acrylic acid) for glucose biosensor," *J. Phys. Chem. C*, vol. 113, no. 14, pp. 2955-2965, 2009.

[45] M. Zhang, G. Y. Zhou, Y. Feng, T. R. Xiong, H. Q. Hou, and Q. H. Guo, "Flexible 3D nitrogen-doped carbon nanotubes nanostructure: a good matrix for enzyme immobilization and biosensing," *Sens. Actuators B Chem.*, vol. 22, no. 3, pp. 829-839, 2016.

[46] A. Benoudjit, M. M. Bader, W. Wardatul, and A. W. Salim, "Study of electropolymerized PEDOT:PSS transducers for application as electrochemical sensors in aqueous media," *Sensing Bio-sensing Res. J.*, vol. 17, no.18, pp. 13-16, 2018.

[47] D. Liu, X. Zhang, and T. You, "Electrochemical performance of electrospun freestanding nitrogen-doped carbon nanofibers and their application for glucose biosensing," *ACS Appl. Mater. Inter.*, vol. 6, no. 9, pp. 6275-6281, 2014.

[48] X. Jia, G. Hu, F. Nitze, H. R. Barzegar, T. Sharifi, C. W. Tai, and T. Wagberg, "Synthesis of palladium/helical carbon nanofiber hybrid nanostructures and their application for hydrogen peroxide and glucose detection," *ACS Appl. Mater. Inter.*, vol. 5, no. 6, pp.12017-12021, 2013.

[49] W. Li, Y. Yinjian, Z. Haozhi, S. Yonghai, H. Shuijian, X. Fugang, and H. Haoqing "Controllable growth of Prussian blue nanostructures on carboxylic group functionalized carbon nanofibers and its application for glucose biosensing," *Nanotechnology*, vol. 23, no. 3, pp. 455502- 455515, 2012.

[50] P. Wang, M. Zhang, Y. Cai, S. Cai, M. Du, H. Zhu, S. Bao, and Q. Xie, "Facile fabrication of palladium nanoparticles immobilized on the water-stable polyvinyl alcohol/polyethylenimine nanofibers via In-Situ reduction and their high electrochemical activity." *Soft Mater.*, vol. 12, no. 2, pp. 387-391, 2014.

[51] D. Crespy, K. Friedemann, and A. M. Popa, "Colloid-electrospinning: fabrication of multicompartment nanofibers by the electrospinning of organic or/and inorganic dispersions and emulsions," *Macromol. Rapid Commun.*, vol. 33, no. 2, pp. 1995-1921, 2012.

[52] S. D. Uzun, F. Kayaci, T. Uyar, S. Timur, and L. Toppare, "Bioactive surface design based on functional composite electrospun nanofibers for biomolecule immobilization and biosensor applications," *ACS Appl. Mater. Interfaces*, vol. 6, pp. 5243-5243, 2014.

[53] H. Zhu, M. L. Du, M. Zhang, P. Wang, S. Y. Bao, L. N. Wang, Y. Q. Fu, J. M. Yao, H. Zhu, and M. L. Du, "Facile fabrication of AgNPs/(PVA/PEI) nanofibers: high electrochemical efficiency and durability for biosensors." *Biosens. Bioelectron.*, vol. 49, no. 2, pp. 210-221, 2013.

[54] E. Sapountzi, M. Braiek, F. Vocanson, J. F. Chateaux, N. Jaffrezic-Renault, and F. Lagarde, "Gold nanoparticles assembly on electrospun poly(vinyl alcohol)/poly (ethylenimine)/glucose oxidase nanofibers for ultrasensitive electrochemical glucose biosensing," *Sens. Actuators B Chem.*, vol. 238, no. 7, pp. 392-399, 2017.

[55] E. Sapountzi, M. Braiek, F. Vocanson, J. Chateaux, N. Jaffrezic-Renault, and F. Lagarde, "One-step fabrication of electrospun photo-cross-linkable polymer nanofibers incorporating multiwall carbon nanotubes and enzyme for biosensing," *J. Electrochem. Soc.*, vol. 162, no. 10, pp. 275–281, 2015.

[56] Fabiola Araujo Cespedes, Sylvia Thomas, Shamima Afroz, and Stephen E. Saddow, "SiC RF Antennas for In Vivo Glucose Monitoring and WiFi Applications," 2016, no. 6, Silicon Carbide Biotechnology, Elsevier, pp. 179-205.

[57] C. L. Frewin, C. Coletti, J. J. Register, M. Nezafati, S. Thomas, and S. E. Saddow, "Silicon Carbide Materials for Biomedical Applications," 2015, no. 7, Carbon for Sensing Devices, Springer, pp. 29-45.

[58] Y. Xu, et.al., "Silicon-Based Sensors for Biomedical Applications: A Review," Sensors, vol. 19, pp. 1-22, 2019.

[59] M. M. Ababneh, K. Puttananjegowda, et al., "Design of a SiC implantable rectenna for wireless in-vivo biomedical devices," *in IEEE 8th Annual Ubiquitous Computing, Electronics and Mobile Communication Conference (UEMCON)*, 2017, pp. 254-257.

[60] S.E. Saddow, et.al., "Single-crystal silicon Carbide: A Biocompatible and Hemocompatible Semiconductor for Advanced Biomedical Applications," Mater. Rs. Soc. Symp. Proc., vol. 12, no.46, pp. 193-198, 2010..

[61] X. Li, X. Wang, R. Bondokov, J. Morris, Y. H. An, and T. S. Sudarshan, "Micro/nanoscale mechanical and tribological characterization of SiC for orthopedic applications," J. Biomed. Mater. Res. B Appl. Biomater., vol. 72, no. 2, pp. 353 − 361, 2005.

[62] U. Kalnins, A. Erglis, I. Dinne, I. Kumsars, and S. Jegere, "Clinical outcomes of silicon carbide coated stents in patient with coronary disease", Med. Sci. Monit., vol.2, pp. 16 − 20, 2002.

[63] S. Santavirta, M. Takagi, L. Nordsletten, A. Anttila, R. Lappalainen, and Y. T. Konttinen, "Biocompatibility of silicon carbide in colony formation test in vitro: A promising new ceramic THR implant coating material," Arch. Orthop. Trauma Surg., vol. 118, no. 1 − 2, pp. 89 − 91, 1998.

[64] A. C. Fabiola, G. Mumcu, S. E. Saddow, "SiC RF Sensor for Continuous Glucose Monitoring," MRS Advances, vol. 1, no. 55, pp. 3691-3696, 2016.

[65] G. Yang , K. L. Kampstra , and M. R. Abidian, "High-Performance Conducting Polymer Nanofiber Biosensors for Detection of Biomolecules," *Adv. Mater.*, vol. 26, pp. 4954–4960, 2014.

[66] Yana Aleeva, et. al, "Amperometric Biosensor and Front-End Electronics for Remote Glucose Monitoring by Crosslinked PEDOT-Glucose Oxidase," IEEE Sensors J., vol. 18, no. 12, 2018.

[67] R. K. Pal, A. A. Farghaly, C. Wang, M. M. Collinson, S. C. Kundu, and V. K. Yadavalli, "Conducting polymer-silk biocomposites for flexible and biodegradable electrochemical sensors," Biosensors Bioelectron., vol. 81, pp. 294–302, Jul. 2016.

[68]   X. Xiao, M. Wang, H. Li, and P. Si, "One-step fabrication of bio-functionalized nanoporous gold/poly(3,4-ethylenedioxythiophene) hybrid electrodes for amperometric glucose sensing," Talanta, vol. 116, pp. 1054–1059, 2013.

[69]   D. Runsewe, et al., "Biomedical Application of Electroactive Polymers in Electrochemical Sensors: A Review," Materials, vol. 12, no. 16, pp. 26-29, 2019.

[70]   "International technology roadmap for semiconductors," 2012. [Online] Available:http://www.itrs.net/Links/2012ITRS/Home2012.html.

[71]   A. Chen, J. Hutchby, G. Bourianoff, and V. Zhirnov, "Emerging Nanoelectronic Devices," *Wiley*, pp.6-450, 2015.

[72]   P. Kavyashree, and S. S. Yellampalli, "The design of ultra low power differential CGLNA for IEEE 802.15.4 applications," *in Proc. IEEE RFM*, 2015, pp. 54-56.

[73]   R. Govindaraj, S. Ghosh, and S. Katkoori, "Design, Analysis and Application of Embedded Resistive RAM based Strong Arbiter PUF," *IEEE Trans. Dependable and Secure Comp.*, pp. 1-1, 2018.

[74]   K. Puttananjegowda and S. Thomas, "A Detailed Review on Physical Unclonable Function Circuits for Hardware Security," *in IEEE 9th Annual Information Technology, Electronics and Mobile Communication Conference (IEMCON)*, 2018, pp. 609-612.

[75]   P. Kavyashree and S. S. Yellampalli, "The design of ultra low power CMOS CGLNA in nanometer technology," *in IEEE Symposium on Electronic System Design*, 2014, pp. 15-19.

[76]   P. Kavyashree, and S. S. Yellampalli, "The Design of Low Noise Amplifiers in Nanometer Technology for WiMAX Applications," International J. Scientific and Research Pub., vol.3, no.10, pp. 1 – 6, 2013.

[77]   M. M. Ababneh, K. P. A. Qaroot, S. Perez, S. Thomas and Y. K. Tan, "Optimized power management circuit for implantable rectenna for in-body medical devices," in IEEE International Conference on Power Electronics and Drive Systems (PEDS), 2017, pp. 30-34.

[78]   P. Kavyashree, and S. S. Yellampalli, "The Design of Ultra Low Power RF CMOS LNA in Nanometer Technology," *Design and Modeling of Low Power VLSI Systems, IGI Global*, 2016, pp. 229-251.

[79]   C. Marschilok, and J. Hitchcock, "Understanding insulin pumps and continuous glucose sensors," *School Nurse News*, vol. 29, no. 2, pp. 32-34, 2009.

[80] Z. Lei, Z. Yu, and X. He, "Design and verification of ultra low current mode amplifier aiming at biosensor applications," *IEEE Conference on Electronics, Circuits and Systems, 2007*, pp. 1304–1307.

[81] Y. Liu, B. Huang, and Y. Yao, "Micromachined biosensor system for interstitial fluid sampling and glucose monitoring," *IEEE Conference on Mechatronics and Automation, 2012*, pp. 647–652.

[82] C. Yang, Y. Huang, B. L. Hassler, R. M. Worden, and A. J. Mason, "Amperometric electrochemical microsystem for a miniaturized protein biosensor array," *IEEE Trans. on Biomed. Circ. and Syst.*, vol. 3, no. 3, pp. 160–168, 2009.

[83] C. M. Girardin, C. Huot, and M. Gonthier, "Continuous glucose monitoring: A review of biochemical perspectives and clinical use in type-1 diabetes," *J. of Clinical Biochem.*," vol. 42, pp. 4136–4142, 2009.

[84] K. Puttananjegowda, and S. Thomas, "The Design of Ultra Low Noise CMOS Transimpedance Amplifier for Biosensing Applications," in *IEEE Ubiquitous Computing, Electronics and Mobile Communication Conference, 2017,* pp. 16-19.

[85] K. Puttananjegowda, and S. Thomas, "A CNTFET based Multi-Stage Transimpedance Amplifier for Blood Glucose Monitoring Systems," in *IEEE Information Technology, Electronics and Mobile Communication Conference,* 2018, pp. 383–388.

[86] K. Puttananjegowda, and S. Thomas, "A Low-Power Low-Noise Multi-Stage Transimpedance Amplifier for Ampherometric based Blood Glucose Monitoring Systems", Analog Integrated Circuits and Signal Processing Journal, vol. 102, no. 4, pp. 659–666, 2020.

[87] K. Puttananjegowda, and S. Thomas, "Cascode common source transimpedance amplifiers for analyte monitoring systems", US Patent App. 16/008,864, Apr 2019.

[88] https://www.accu-chek.com/meters/guide-meter.

[89] N. Dalvi, "Glucose meter reference design", AN1560, Microchip Technology Inc., 2013.

[90] B. Razavi, "Design of analog CMOS integrated circuits," New York: McGraw-Hill Education, 2016.

[91] A. M. Khandaker, S. K. Islam, D. K. Hensley, and M. Nicole, "A glucose biosensor using CMOS potentiostat and vertically aligned carbon nanofibers," *IEEE Trans. Biomed. Circuits and Systems*, vol. 10, no. 4, pp. 807–816, 2016.

[92]   S. M. Park, and H. J. Yoo, "A 1.25Gb/s regulated cascode CMOS transimpedance amplifier for gigabit Ethernet applications," *IEEE J. Solid-State Circuits*, vol.39, no.1, 2004, pp.112-120, 2004.

[93]   H. K. Jiaping, Yong-Bin, and J. Ayers, "A low-power 100 MX CMOS front-end transimpedance amplifier for biosensing applications," *in IEEE Midwest symposium circuits and systems*, 2010, pp. 541–544.

[94]   D. Kim, B. Goldstein, W. Tang, F. J. Sigworth, and E. Culurciello, "Noise analysis and performance comparison of low current measurement systems for biomedical applications," *IEEE Trans. Biome. Circuits and Systems*, vol. 7, pp. 52–62, 2013.

[95]   M. Crescentini, M. Bennati, M. Carminati, and M. Tartagni, "Noise limits of CMOS current interfaces for biosensors: A review," *IEEE Trans. Biomed. Circuits and Systems*, vol. 8, pp. 278–292, 2014.

[96]   M. R. I. Mark, and M. L. Peter, "CMOS transimpedance amplifier for biosensor signal acquisition," *in IEEE international symposium on circuits and systems*, 2014, pp. 25–28.

[97]   M.N.Khiarak, E. Martianova, C. Bories, S. Martel, C. D. Proulx, Y. D. Koninck, and B. Gosselin, "A Wireless Fiber Photometry System Based on a High-Precision CMOS Biosensor With Embedded Continuous-Time ΣΔ Modulation," *IEEE Trans. Biomed. Circuits and Systems*, vol.12, no.3, pp. 495 – 509, 2018.

[98]   K. Jongpal, and H. Ko, "Reconfigurable Multiparameter biosignal acquisition SoC for low power wearable platform," *Sensors J.*, vol. 2002, no. 16, pp. 1–13, 2016.

[99]   K. Jongpal, K. Jihoon, and K. Hyoungho, "Low-power photoplethysmogram acquisition integrated circuit with robust light interference compensation," *Sensors J.*, vol. 16, no. 46, pp. 1–11, 2016.

[100]   G. Ferrari, F. Gozzini, and M. Sampietro, "A current-sensitive front-end amplifier for nano-biosensors with a 2MHz BW," *ISSCC Dig. Tech. Papers*, pp. 164-165. 2007.

[101]   A. Sharma, M. Zaman, and F. Ayazi, "A 104-dB dynamic range transimpedance-based CMOS ASIC for tuning fork microgyroscopes," *IEEE J. Solid-State Circuits*, vol. 42, pp. 1790-1802, 2007.

[102]   D. C. Dias, F. S. de Melo, L. B. Oliveira, and J. P. Oliveira, "Regulated Common-Gate Transimpedance Amplifier for Radiation Detectors and Receivers," *in IEEE International Conference Mixed Design of Integrated Circuits and Systems*, 2014, pp. 19-21

[103] B. Viswanathan, R. Pierre, T. Yuksel, F. Anna, and C. C. Enz, "A 0.18um Biosensor Front-End Based on Noise, Distortion Cancelation and Chopper Stabilization Techniques," *IEEE Trans. Biomed. Circuits and Syst.*, vol. 7, no. 5, pp. 660-673, 2013.

[104] A. Khandaker, et.al., "A Low-Power Low-Noise Transimpedance Amplifier for an Integrated Biosensing Platform", *IEEE International Midwest Symposium on Circuits and Systems*, pp. 161-164, 2013.

[105] M. Ingels and M. S. J. Steyaert," A 1-Gb/s, 0.7- m CMOS Optical Receiver with Full Rail-to-Rail Output Swing," *IEEE J. Solid State Circuits*, vol. 34, no. 7, pp. 971-977, 1999.

[106] A. Diaa, "Low Power Transimpedance Amplifier Using Current Reuse with Dual Feedback," *IEEE International Conference on Electronics, Circuits and Systems*, pp. 244-247, 2015.

[107] J. Salvia, P. Lajevardi, and M. Hekmat, "A 56MΩ CMOS TIA for MEMS Applications," *in IEEE Custom Integrated Circuits Conference*, pp. 199-202, 2009.

[108] B. Razavi, "Design of Integrated Circuits for Optical Communications," McGraw-Hill Series in Electrical and Computer Engineering, McGraw-Hill, 2003.

[109] W.Jung, "Op-Amp Applications Handbook," Analog Devices series, Newnes, 2005.

[110] J. Baker, "CMOS circuit design, layout and simulation," New York: Wiley, 2010.

[111] A. S. Sedra, and K. C. Smith, "Microelectronic circuits," New York: Oxford D University Press, 2004.

[112] W. M. C. Sansen, "Analog design essentials," Dordrecht: Springer, 2006.

[113] P.R. Gray, "Analysis and design of analog integrated circuits," New York: Wiley, 2009.

[114] P.E. Allen, and D.R. Holberg, "CMOS analog circuit design," Oxford: Oxford University Press 2002.

[115] L. Haitao, P. Sina, A. Ehsan, et al., "Ultra compact microwatt CMOS current readout with picoampere noise and kilohertz bandwidth for biosensor arrays," *IEEE Trans. Biomed. Circuits and Syst.*, vol. 12, no. 1, pp. 35 – 46, 2018.

[116] K.G. Sara, T. Irene, D. M. Giovanni, C. Sandro, and G. Pantelis, "A differential electrochemical readout ASIC with heterogeneous integration of bio-nano sensors for amperometric sensing," *IEEE Trans. Biomed. Circuits and Syst.*, vol. 11, no. 5, pp.1148–1159, 2017.

[117] Y.S. Sung, W. M. Chen, and C. Y. Wu, "The design of 8-channel CMOS area-efficient low-power current-mode analog front-end amplifier for EEG signal recording," *In IEEE international symposium on circuits and systems*, 2016, pp. 530–533.

[118] H. S. Narula, and J. G. Harris, "VLSI potentiostat for amperometric measurements for electrolytic reactions," *in IEEE Int. Symp. Circuits Syst.*, 2005, pp. 1457–1460.
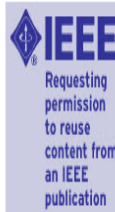
[119] R. F. Turner, D. J. Harrison, and H. P. Baltes, "A CMOS potentiostat for amperometric chemical sensors," *IEEE J. Solid-State Circuits*, vol. 22, no. 3, pp. 473–478, 1987.

[120] S. M. Martin, F. H. Gebara, T. D. Strong, and R. B. Brown, "A low-voltage, chemical sensor interface for systems-on-chip: the fully-differential potentiostat," *IEEE Symp. Circuits Syst.*, 2009, pp. 135–142.

[121] P. A. Boutet, and S. Manen, "Low power CMOS potentiostat for three electrodes amperometric chemical sensor," *in Proc. IEEE Faible Tension Faible Consummations*, 2011, pp. 15–18.

[122] A. B. Islam, F. S. Tulip, S. K. Islam, T. Rahman, and K. C. MacArthur, "A mediator free amperometric bio enzymatic glucose biosensor using vertically aligned carbon nanofibers (VACNFs)," *IEEE Sensors J.*, vol. 11, no. 11, pp. 2798–2804, 2011.

[123] C. Yang, Y. Huang, B. L. Hassler, R. M. Worden, and A. J. Mason, "Amperometric electrochemical microsystem for a miniaturized protein biosensor array," *IEEE Trans. Biomed. Circuits Syst.*, vol. 3 no. 3, pp. 160–168, 2009.

[124] M. Roham, D. P. Daberkow, E. S. Ramsson, D. P. Covey, S. Pakdeeronachit, P. A. Garris, and P. Mohseni, "A wireless IC for wide-range neurochemical monitoring using amperometry and fast-scan cyclic voltammetry," *IEEE Trans. Biomed. Circuits Syst.*, vol. 2, no. 1, pp. 3–9, 2008.

[125] A. J. Bard, and R. F. Larry, "Electrochemical Methods Fundamental and Applications," *John Wiley & Sons Inc.*, 2001, pp. 1-200.

[126] M. M. Ahmadi and G. Jullien, "Current-mirror-based potentiostats for three-electrode amperometric electrochemical sensors," *IEEE Trans. Circuits Syst.*, vol. 56, no. 7, pp. 1339–1348, 2009. .

[127] K. Iniewski, "VLSI Circuits for Biomedical Applications," *1st ed. Norwod, MA, USA: Artech House Inc.*, 2008, pp. 1-150.

[128] S. M. Martin, F. H. Gebara, T. D. Strong, and R. B. Brown, "A fully differential potentiostat," *IEEE Sens. J.*, vol. 9, no. 2, pp. 135–142, 2009.

[129] J. Zhang, N. Trombly, and A. Mason, "A low noise readout circuit for integrated electrochemical biosensor arrays," *in Proc. IEEE Sensors*, pp. 36-39, 2004.

[130] Y. Huang, and A. J. Mason, "A redox-enzyme based electrochemical biosensor with a CMOS integrated biopotentiostat," *in Proc. IEEE Biomedical Circuit & Systems Conference*, 2009, pp. 29-32.

[131] M. M. Ahmadi, and G. A. Jullien, "Current mirror based potentiostats for three-electrode amperometric electrochemical sensors," *IEEE Trans. Circuits Syst.*, vol. 56, no. 7, pp. 1339-1348, 2009.

[132] H.M. Jafari , and R. Genov, "Chopper-stablized bidirectional current acquisition circuits for electrochemical amperometric biosensors," *IEEE Trans. Circuits Syst.*, vol. 60, no. 5, pp. 1149-1157, 2013.

[133] L. Haitao, L. Xiaowen , L. Lin, M. Xiaoyi, G. Roman, and J.M. Andrew, "CMOS Electrochemical Instrumentation for Biosensor Microsystems: A Review," *Sensors*, vol. 74, no. 17, pp. 1-26, 2017.

[134] L. Zuo, S. K. Islam, I. Mahbub, and F. Quaiyum, "A Low-Power 1-V Potentiostat for Glucose Sensors," *IEEE Trans. Circuits Syst.*, vol. 62, no. 2, pp. 204-208, 2015.

[135] V. Shenoy, J. Sungyong, Y. Youngsam ,P. Youngjin, K. Hyoungsoo, and J.C. Hoon, "A CMOS Analog Correlator-Based Painless Nonenzymatic Glucose Sensor Readout Circuit," *IEEE Sensors Journal*, vol. 14, no. 5, pp. 1591- 1599, 2014.

[136] V. Valente, M. Schormans and A. Demosthenous, "An Energy-Efficient 1.2V 4-Channel Wireless CMOS Potentiostat for Amperometric Biosensors," *IEEE International Symposium on Circuits and Systems (ISCAS),* 2018, pp. 1-4,

[137] H. N. Meisam, M. J. Hamed , L. Lian, G. Axel, and G. Roman, "CMOS Neurotransmitter Microarray: 96-Channel Integrated Potentiostat With On-Die Microsensors," *IEEE Trans. Biomed. Circuits Syst.*, vol. 7, no. 3, pp. 338-348, 2013.

[138] P. Sina, L. Haitao, and J. M. Andrew, "Compact CMOS Amperometric Readout for Nanopore Arrays in High Throughput Lab-on-CMOS," *IEEE International Symposium on Circuits Systems*, 2016, pp. 2851- 2854.

[139] J. Guo, W. Ng, J. Yuan, S. Li, and M. Chan, "A 200-Channel Area-Power-Efficient Chemical and Electrical Dual-Mode Acquisition IC for the Study of Neurodegenerative Diseases," *IEEE Trans. Biomed. Circuits and Syst.*, vol. 10, no. 3, pp. 567- 578, 2016.

[140] H. Li, C. S. Boling, and A. J. Mason, "CMOS Amperometric ADC With High Sensitivity, Dynamic Range and Power Efficiency for Air Quality Monitoring," *IEEE Trans. Biomed. Circuits and Syst.*, vol. 10, no. 4, pp. 817-827, 2016.

[141]   R.F.B. Turner, D. J. Harrison, and H. P. Baltes, "A CMOS Potentiostat for Amperometric Chemical Sensors," *IEEE J. Solid-State Circuits*, vol. 22, pp. 473–478, 1987.

[142]   S. M. Martin, F. H. Gebara, T.D. Strong, and R.B. Brown, "A fully differential potentiostat," *IEEE Sens. J.*, vol. 9, pp. 135–142, 2009.

[143]   P. M. Levine, P. Gong, R. Levicky, and K. L. Shepard, "Active CMOS sensor array for electrochemical biomolecular detection," *IEEE J. Solid-State Circuits*, vol. 43, pp. 1859–1871, 2008.

[144]   M. M. Ahmadi, and G.A. Jullien, "Current-mirror-based potentiostats for three-electrode amperometric electrochemical sensors," *IEEE Trans. Circuits Syst. I Regul. Pap.*, vol.56, pp. 1339–1348, 2009.

[145]   I. Bontidean, C. Berggren, G. Johansson, E. Csoregi, B. Mattiasson, J.A, Lloyd, K. J. Jakeman, and N. L. Brown, "Detection of heavy metal ions at femtomolar levels using protein-based biosensors," *Anal. Chem.*, vol. 70, pp. 4162–4169, 1998.

[146]   M. Carminati, G. Ferrari, F. Guagliardo, M. Farina, and M. Sampietro, "Low-Noise Single-Chip Potentiostat for Nano-Bio-Electrochemistry over a 1MHz Bandwidth," *In IEEE International Conference on Electronics, Circuits, and Systems*, 2009; pp. 952–955.

[147]   S. M. Martin, F. H. Gebara, T. D. Strong, R. B. Brown, "A Low-Voltage, Chemical Sensor Interface for Systems-On-Chip: The Fully-Differential Potentiostat," *In International Symposium on Circuits and Systems*, 2004, pp. 892–895.

[148]   E. Lauwers, J. Suls, W. Gumbrecht, D. Maes, G. Gielen, W. Sansen, "A CMOS Multiparameter Biochemical Microsensor with Temperature Control and Signal Interfacing," *IEEE J. Solid-State Circuit*, vol. 36, pp. 2030–2038, 2001.

Appendix A: Copyright Notices

The following copyright notices is for the material in Chapter 2, 3, 4 and 5.

PDF

Help

This paper is part of the JES Focus Issue on Sensor Reviews.

Abstract

Biosensing has capitalized on the excellent characteristics and properties of nanostructures for detecting glucose levels in diabetic patients. In glucose sensing systems, the fabrication of a suitable matrix for immobilizing glucose oxidase (GO_x) has become more interesting for the application of nanofibers in enzymatic electrochemical biosensors. These nanofiber based electrochemical biosensors are superior in manufacturability and performance due to low cost, diversity of materials, ease of miniaturization, response time, durability, and structure versatility. This perspective highlights the latest material integration of various nanofibrous composite membranes of carbon nanotubes, carbon nanofibers, conductive nanoparticles and conductive polymers, that provide large matrix-like, porous surfaces to enhance the immobilization of enzymes, for the fabrication of glucose biosensors.

Export citation and abstract   BibTeX   RIS

License Details

This Agreement between 4202 E Fowler Ave ("You") and Elsevier ("Elsevier") consists of your license details and the terms and conditions provided by Elsevier and Copyright Clearance Center.

Print   Copy

License Number	4845790738624
License date	Jun 11, 2020
Licensed Content Publisher	Elsevier
Licensed Content Publication	Elsevier Books
Licensed Content Title	Advances in Nanostructured Materials and Nanopatterning Technologies
Licensed Content Author	Sylvia W. Thomas,Ridita Rahman Khan,Kavyashree Puttananjegowda,William Serrano-Garcia
Licensed Content Date	Jan 1, 2020
Licensed Content Pages	29
Type of Use	reuse in a thesis/dissertation
Portion	excerpt
Number of excerpts	5
Format	electronic
Are you the author of this Elsevier chapter?	Yes
Will you be translating?	No
Title	Ph.D Student

Permission to reuse SEM images in Chapter 2 is below.

Electrochemical Performance of Electrospun Free-Standing Nitrogen-Doped Carbon Nanofibers and Their Application for Glucose Biosensing

ACS Publications
Most Trusted. Most Cited. Most Read.

Author: Dong Liu, Xueping Zhang, Tianyan You

Publication: Applied Materials

Publisher: American Chemical Society

Date: May 1, 2014

Copyright © 2014, American Chemical Society

PERMISSION/LICENSE IS GRANTED FOR YOUR ORDER AT NO CHARGE

This type of permission/license, instead of the standard Terms & Conditions, is sent to you because no fee is being charged for your order. Please note the following:

- Permission is granted for your request in both print and electronic formats, and translations.
- If figures and/or tables were requested, they may be adapted or used in part.
- Please print this page for your records and send a copy of it to your publisher/graduate school.
- Appropriate credit for the requested material should be given as follows: "Reprinted (adapted) with permission from (COMPLETE REFERENCE CITATION). Copyright (YEAR) American Chemical Society." Insert appropriate information in place of the capitalized words.
- One-time permission is granted only for the use specified in your request. No additional uses are granted (such as derivative works or other editions). For any

A CNTFET based Multi-Stage Transimpedance Amplifier for Blood Glucose Monitoring Systems

IEEE

Requesting permission to reuse content from an IEEE publication

Conference Proceedings: 2018 IEEE 9th Annual Information Technology, Electronics and Mobile Communication Conference (IEMCON)

Author: Kavyashree Puttananjegowda

Publisher: IEEE

Date: Nov. 2018

Copyright © 2018, IEEE

IEEE

Requesting permission to reuse content from an IEEE publication

The design of ultra low noise CMOS transimpedance amplifier for biosensing applications

Conference Proceedings: 2017 IEEE 8th Annual Ubiquitous Computing, Electronics and Mobile Communication Conference (UEMCON)

Author: Kavyashree Puttananjegowda

Publisher: IEEE

Date: Oct. 2017

Copyright © 2017, IEEE

Thesis / Dissertation Reuse

The IEEE does not require individuals working on a thesis to obtain a formal reuse license, however, you may print out this statement to be used as a permission grant:

Requirements to be followed when using any portion (e.g., figure, graph, table, or textual material) of an IEEE copyrighted paper in a thesis:

1) In the case of textual material (e.g., using short quotes or referring to the work within these papers) users must give full credit to the original source (author, paper, publication) followed by the IEEE copyright line © 2011 IEEE.
2) In the case of illustrations or tabular material, we require that the copyright line © [Year of original publication] IEEE appear prominently with each reprinted figure and/or table.
3) If a substantial portion of the original paper is to be used, and if you are not the senior author, also obtain the senior author's approval.

Requirements to be followed when using an entire IEEE copyrighted paper in a thesis:

1) The following IEEE copyright/ credit notice should be placed prominently in the references: © [year of original publication] IEEE. Reprinted, with permission, from [author names, paper title, IEEE publication title, and month/year of publication]
2) Only the accepted version of an IEEE copyrighted paper can be used when posting the paper or your thesis on-line.
3) In placing the thesis on the author's university website, please display the following message in a prominent place on the website: In reference to IEEE

About the Author

Kavyashree Puttananajegowda received the B.E degree in electronics and communication engineering and M.Tech degree in VLSI design and embedded systems from Visvesvaraya Technological University, Karnataka, India, in 2011 and 2014. She joined University of South Florida, Tampa, Florida, USA in 2017 for Ph.D. in electrical engineering. Her research interest includes fabrication and characterization of sensors, low-noise low-power CMOS integrated circuit design for biosensing and RF applications. She received a prestigious Signature Research Doctoral Fellowship from USF graduate studies. She was the Entrepreneurial Lead for USF I-Corps program funded by NSF in 2019.